Cape Peninsula
University of Technology

MODELLING AND SIMULATION OF TIDAL ENERGY GENERATION SYSTEM

Thesis submitted in partial fulfillment of the requirements for the degree of

Master of Engineering in Energy

Faculty of Engineering & the Built Environment

Cape Peninsula University of Technology

by

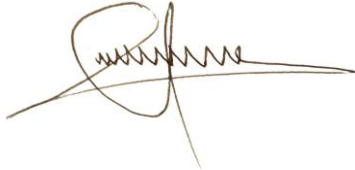**LADISLAS MUTUNDA KANGAJI**

Supervisor:Prof Khaled M. Aboalez

Bellville, April 2022

DECLARATION

I, LADISLAS MUTUNDA KANGAJI, declare that the contents of this dissertation/thesis represent my own unaided work, and that the dissertation/thesis has not previously been submitted for academic examination towards any qualification. Furthermore, it represents my own opinions and not necessarily those of the Cape Peninsula University of Technology.

14/03/2022

Signed   **Date**

ABSTRACT

Nowadays, most of the global electricity generation comes from fossil fuels. With consequent economic burdens and environmental pollution which is caused by the consumption of fuels which creates global warming. Therefore, tidal energy may play a tremendous role in mitigating this carbon dioxide due to its cleanest and most abundant energy source, as well as its cheap price. However, its output power variation with the serious variation of tides causes major power quality problems. This work focused on modelling, simulation and control of tidal energy from a tidal energy generation system in which the power output is challenged by problems such as harmonics, frequency fluctuations, and voltage sags since electricity users can introduce the harmonics onto the supply voltage waveform by non-linear loads. The system has been composed of a 1.5 MW/VDC, a 1.2 MW three-level inverter with a nominal voltage of 600 V, and an inductance (LCL) filter which are connected after inverters receive power from a permanent magnet synchronous tidal generator and connected to a DC load. It has been expected that the inverter will produce harmonic distortion of less than 0,5% and achieve 85%.The same nonlinear controller used in wind turbine applications stand for (PMSG) will be based to adjust the tidal energy system. However, high-speed simulations of circuit-oriented electric and electronic systems have been chosen. The generator power output can be optimised by utilising various control methods that have been proposed to control the voltage and the frequency. The Voltage Oriented Control is a technique that relies on high-level performance DQ-coordinate controllers. This technique for a three-phase boost rectifier has been created and simulated. The system simulation has been executed using the MATLAB /Simulink program. The controller, that is, a current controller and a DC-link voltage controller, has been designed by Internal Model Control method. The presentation of the simulation results has been done and the control evolution of the system performance in response to the load and DC-bus voltage step changes. Two scenarios have been considered relying on the load conditions to analyse the development of the system performance's case, the tidal array energy generation generates less power which did not reach the load demand, then the grid was injecting into tidal array energy generation system. In the last scenario, the tidal array generation is higher than the load, then the surplus of energy has been exported into the grid. Therefore, the intermediate circuit voltage and the high voltage ripple in the input line currents become unacceptable when the control system is not activated.It is demonstrated in this work that the Tidal energy system connected to the grid presents a good performance with a low total harmonic distortion around 0.12% for the voltage and 0.07% for the current. The validity and performance of the preferable control method have been verified by simulation results and correspond with what has been expected. The simulation results demonstrate that the controller can stabilise the constant dc-link voltage under the dynamic and steady-state performance of the system.

ACKNOWLEDGEMENTS

DEDICATION

This thesis is dedicated to the Mutunda Family and Kiboko Family, more particularly my wife Ngcwelekazi Gwegwe – Kangaji and My daughter Favor Mutunda Kangaji, Maman Kabwiza, Maman Mwadi, Pastor Sylvia Kiboko, and My big Brother Willy Mbavu Mutunda. May the Good God continue always to bless you.

TABLE OF CONTENTS

Liste of Figures

List of Table

GLOSSARY

V	Air velocity
A	Angle of attack
$\boldsymbol{\Omega}$	Angular velocity
β	Pitch angle
C	Chord length
$\boldsymbol{\rho}$	Density
E	Energy
μ	Friction coefficient
V_{res}	Local tidal Velocity
M	Pitching moment
C_p	Power coefficient
A	Swept area of the marine turbine
λ	Tip-speed ratio
θ	Yaw angle
MCEDs	Marine current energy devices
PI	Proportional–integral controller
PID	Proportional–integral–derivative controller
SST	Total sum of squares
SVM	Space vector modulation
T.I.	Turbulence intensity
TCCS	Tidal current conversion system
TCS	Transformer-Cable system
TEC	Vertical axis device
HWT	Horizontal axis devices
Tm	Electromagnetic torque
r	Fluid density
V_{tide}	Fluid speed
C	Tide coefficient
$V_{st}(V_{nt})$	Spring (neap) tide current speed
I	Tip speed ratio
s, (r)	Stator (rotor) index (superscripts)
d, q	Synchronous reference frame index
V (I)	Voltage (current)

P (Q)   Active (reactive) power

F   Flux

F_m Permanent magnet flux

$T_{em}(T_m)$ Electromagnetic torque (mechanical torque)

R   Resistance

L (M)   Inductance (mutual inductance)

s   Total leakage coefficient

qr   Rotor position

w (W_s) Rotor electrical speed (electrical synchronous speed)

W_r Rotor current frequency (wr¼ ws – w)

W   Mechanical speed   (W ¼ w/p)

f   Viscosity coefficient

J   Rotor inertia

U   Line voltage

 E   Line voltage

E_g Grid phase-to-ground voltage amplitude

$E_d \; and \; E_q$ dq-coordinates of line or grid voltage (amplitude invariant transformation)

V_{pcc} Voltage at the point of common connection Converter voltage

U_s Converter voltage

 V^* Converter voltage reference from current controller Line-to-Linevoltage

V_{LL} Line-to-Neutral voltage

$V_{LN(peak)}$ Amplitude of Line-to-Neutral voltage

E_m Amplitude of Line-to-Neutral voltage DC-link

DPC   Direct Power Control Initial Condition

IC   Insulated Gate Bipolar Transistor Induction Machine

IGBT   IM Internal Model Control Pulse Width Modulation

IMC   Phase Locked Loop

PWM PLL Permanent Magnet Synchronous Machine

SVM   Space Vector Modulation

VF-DPC   Virtual Flux Direct Power Control

VFOC   Virtual Flux Oriented Control

VOC   Voltage Oriented Control

CHAPTER ONE: INTRODUCTION AND BACKGROUND

1.1 Introduction

Today, most of the global electricity generation comes from fossil fuels. With consequent economic burdens and environmental pollution caused by the consumption of fuels which creates global warming (Melikoglu, 2018). According to several investigations, the effect of global warming is man-made (Shields et al., 2011). However, renewable energy generation systems are in the spotlight of the industry by investors and developers (Amor & Kheldoun, 2018; Hassan, 2016).

The Convention on Climate Change (UNFCCC) adopted the Paris Agreement which recommended that all countries adopt technologies and strategies to contain the increase in global temperature to 2°C (Hillis et al., 2020). South Africa, with its tidal potential, which is the largest in Africa, can be used to produce clean and renewable energy. However, a major exception is the potential for electricity generation from tides and resulting from tidal generating forces that are generated by the coupled Earth-Moon system (Neill et al., 2018). Tidal power has a great advantage over the ocean and solar power of being the most predictable renewable energy (Neill et al., 2018). It is worth noting that tidal energy technology has a period of its development, optimising these devices for their location, to improve the efficiency of the extraction of kinetic energy from free-flowing water. Being submerged in Tidal Stream Turbines (TSTs) is inherently much less intrusive than containment plans and minimises impacts on the marine environment (Morris et al., 2016). The basic operating conditions for tidal turbines are based on a free flow velocity of 2m/s and 3 m/s and a depth of 20 and 30 m, at least for early implementation with deeper water designs (> 40 m) (Morris et al., 2016). Furthermore, it is very important to mention that the continuous submarine operation requires that tidal system works reliably with high availability because at certain locations tidal currents can offer very high energy density which can lead to large amounts of power. This involves the strategies to reduce the visits of site to a minimum, as tidal devices are usually installed in places with strong tidal currents in high flow speeds (M.C. Sousounis et al., 2016). Other advantages are linked to tidal networks which feature energy transport very close to shore and offshore substations and high voltage submarine transport will not be necessary components installed at sea to finally minimise maintenance at sea. It was therefore proposed to use tidal power developers who could extend the availability of their systems by moving the power electronics from the nacelle to the shore. This will also limit site visits as the frequency of power converter failures may be higher depending on the data from onshore wind turbines. However, it is not a question of making a total conversion of tidal energy due to Betz's law and mechanical losses in turbines (Angeloudis et al., 2017).

This work focused on the simulation, planning, and control of tidal energy. Overall, the literature review illustrates that scalable programs are chosen over the more simplistic analysis method

and even linear programming methods due to their ease of implementation and application and many variables. . The systematic review of the literature carried out shows that numerical modelling, experimental investigations, and multi-criteria decision analysis are very essential to calculate a turbine adapted to the parameters of the site and the given quantities of flow. Moreover, the speed of the tidal current is so sensitive to the sudden variations which are the reasons for the creation of the pulsations on the tidal current turbines. However, pulses have detrimental effects on the fatigue and the final load of the tidal turbine and operation of the transmission, which leads to the oversizing of the device and costly maintenance.

Normally, the control strategy is based on changing the maximum power point tracking reference speed so that the generator absorbs less energy from tidal currents during a sudden increase in flow speed and increases the production of energy when the flow velocity decreases. This project aimed to model, simulate and control the three-phase network of the tidal network connected to the network, which was installed in a network of fixed-pitch tidal turbines at variable speed.

The tidal turbine was used to supply electricity to a coastal town, with the grid supply of electricity in South Africa. The entire simulation system included models of tidal turbine systems, a converter, a DC / AC inverter, and a grid voltage monitoring unit.

Therefore, the main objectives of this study were :

      a. To develop mathematical and simulation models,

      b. To verify the model through a case study simulation of the tidal system.

1.2. Background

Fossil fuels represent more than 80% of all the primary energy used for power generation in 2014, the amount of greenhouse gas produced by coal, natural gas, and oil in the power system industries was around 44%, 20%, and 35% respectively(Borthwick, 2016). Therefore, the deployment of clean technologies on a big scale needs to be part of the solution for greenhouse gas mitigation (Pegels, 2010).

South Africa although its coastal reserves areas, many remote areas are still without electricity, an average of 28% of South African households, that remains the development barrier. However, tidal power energy is a huge and reliable energy source because its turbine has the benefit of high efficiency and its predictability quality place it as a reliable renewable energy over other renewable energy (wind, solar, etc.). However, its implementation requires a lot of money compared to other renewable energy sources (Hwang et al., 2009).

Additionally, putting aside the similarity harnessing technique, the power energy output of a horizontal axis tidal turbine compares to one of the wind turbines shows that the horizontal tidal turbine has a higher energy output with the same quantity of fluid flow velocities because water

density is 800 times bigger than air when the tidal current energy compare to wind and wave energy is an eco-friendly energy source (Grogan et al., 2013; Li et al., 2016).

Relatively few investigations have been carried out on the technical potentials of different ocean energy technologies and such potentials may change depending on future technological evolution. The ocean power energy sectors are still in the development stages, with less than 3 MW of total capacity energy production for both wave power and energy from tidal currents during the period 2004 – 2009 (Schumann et al., 2019).

Marine energy extraction utilizing Marine current energy devices (MCEDs) has emerged as a sustainable alternative to the energy from fossil sources due to its huge advantage of being predictable (Rourke et al., 2010). However, the biggest challenge of tidal power generation system is that the Tidal Current Conversion System (TCCS) efficiency which is just under 40% and its costly construction and maintenance, due to the offshore nature of the tidal energy (Eddine et al., 2007).

In South Africa, Eskom operates the national transmission line and owned the majority of the energy sector with 95% capacity production and only 2 % of energy is produced by private industries. The South African government has targeted to implement the use of renewable energy sources to cover the energy shortage and reduce the carbon dioxide production from fossil fuel energy and at the same time gradually replace the dependence of the energy from coal. The government with the independent power producer (IPP) procurement program wants to co-generate renewable energy to achieve 3725 megawatts for the improvement of socio-economic and environmentally sustainable growth (Pegels, 2010; Loots et al., 2015). This is the motivation the worldwide marine renewable sector is focused on harnessing wave and tidal energy and carrying out research and feasibility study assessing the potential of the marine renewable sector as an alternative source of energy (Benelghali et al., 2010).In South Africa, it is also very clear that Eskom currently has a growing interest in generating marine renewable energy resources from the Agulhas Current (Reinecke, 2013).

1.3.Statement of Research Problem

Tidal energy has the potential to generate carbon dioxide-free energy with significant predictability over long period scales due to its tide's regularity than solar and wind energy, which mainly depends on the weather conditions. Additionally, compared to wind turbines, the tidal turbine horizontal axis has a higher energy output with the same quantity of fluid flow velocities due to the water density which is 800 times bigger than air.

Though the energy developers have improved energy extraction devices to tidal arrays, the investigation into the accurate tidal system prototype is still ongoing. Moreover, harnessing the kinetic energy of tides possess many sets of technical challenges, because the amount of water, which is direct to the tidal turbine array, has only impacts on some blades surfaces,

meaning the tides energy transformation is just part and the increased variation of speed tides can create the increase of electric power output of the generator which will have consequences of the spike of DC-link voltage rise, therefore to solve these problems LCL filters are connected after inverters to eliminate harmonics resulting from inverters.

1.4.Research question

The research questions emanating from:

a) How can the Independent Power Producers (IPPs) in collaboration with the utility company (Eskom) enhance the South African ocean potentiality energy to produce efficient electricity?

b) How can the control of the tidal speed influence positively the cost of tidal enhancement and can it motivate the electricity users to shift to renewable energy from the ocean?

c) How can tidal energy generation be more available to reduce carbon dioxide?

1.5.Aims and Objectives.

This project aimed to model, simulate and control the tidal array grid system connected, tidal turbine array using a control design for a three-phase PWM rectifier and LCL filters are connected after inverters receive power from a permanent magnet synchronous tidal generator and connected to a DC load. The tidal array turbine was used to provide electricity to a coastal city, with mains electricity supply in South Africa. The whole simulation system consisted of tidal array turbine system models, converter, DC/AC inverter, and grid voltage monitoring unit. Therefore, the primary objectives of this study were :

a) To develop mathematical and simulation models,

b) To verify the model through a case study simulation of the tidal system,

c) To optimise and maximise the tidal energy system

d) To perform a techno-economic analysis on the optimal model.

These will assist to controlling different parts of the system such as PSMG, closed-loop control technique of back-to-back two-level VSC used to regulate the DC link voltage. To model and simulate the control system. The power performance of direct-driven, fixed-pitch, variable-speed tidal turbines with PMSG and the mathematical model of all principal devices block such as rectifier, inverter, converter, were presented with their mathematical modelling is presented in detail. The whole blocks system was modelled using MATLAB/Simulink software 5 (Figure 23,24).

1.6.Significance of the Research

The optimisation of renewable power generation using power electronics converters in many studies. In this case of tidal power generation, these converters may contribute significantly to the reliability of the tidal energy system while improving the availability of the tidal turbine energy system underwater because the energy production depends on the operation time of the tidal turbine underwater, to ensure great power quality. Furthermore, this research study modelling will improve the efficiency of tidal plants while minimising the maintenance cost to ensure that the system becomes cost-effective. Additionally,it will make tidal energy utilisation a better alternative since its pollution-free, reliable and always predictable compared to solar and wind energy systems. Therefore, the modelling and simulation of the tidal power generation system, as well as the energy optimisation of the system output energy, could provide significant value to the field. Thus, an increase in the design of tidal return projects has sparked the desire to develop simulation modelling tools for the optimisation of tidal energy to reduce uncertainties by giving an overview of their potential and their impacts.

1.7.Delineation of Research

Several previous works focused on different aspects of tidal energy extraction techniques, such as the main modes of operation of tidal power plants, as well as algorithms to regulate their timing. This dissertation focussed on complementary modelling and carrying out proper simulations of the entire system, and also discussed associated uncertainties. Initially, numerical simulations are used more in the study of the effect of various parameters on the production of electricity. However, the fundamental problem of evaluating optimal operating parameters may require great precision (Angeloudis & Falconer, 2017). At present, developers of tidal turbines have not yet decided on the optimal Tidal Current Conversion System (TCCS), which justifies several model designs for tidal energy extraction. While most designs feature a bottom mount with low resistance blades and horizontal axis rotors, the generator side also contains several different techniques used in generator technology. However, the dominant combination of components is a function of the generators that are directly driven or the synchronous generators with permanent magnets with gears and squirrel cage induction generators (SCIG). The output power limit is set using the fixed or variable pitch blades. As other studies were done on a TCCS with long-distance drives, they used a low voltage LV generator. In this study, a control scheme for a three-phase PWM inverter LCL Filter, converter, DC/AC inverter was developed for tidal arrays energy generation. The topology for the system consists of a rectifier receiving AC power from a 1.5 MW permanent magnet synchronous generator at 951 V. The control scheme was be designed to maximise circuit efficiency.. The control scheme adopted in this study is based on a voltage-oriented control

strategy to maximise circuit efficiency. The modelling and simulation were performed using Matlab/Simulink environment.

1.8.Dissertation structure

The layout of the remainder of this study is as follows:

Chapter 1: The chapter has provided the introduction and background around renewable energy and tidal energy.Chapter 2: this chapter,   focused on different aspects of the project in their entirety. The tidal resources, the description of the tidal energy systems, the different types of tidal turbines, and control methods investigated.

Chapter 3: focuses on some of the classical (PI) designs of wind turbines that have been exploited for tidal turbine control. This chapter also provides insight into modelling, simulation, and control of the tidal array grid system grid connected 3-phase, which was fitted in a fixed-pitch variable-speed tidal turbine array.

Chapter 4: Explored how the system was constructed. Further factors were also decided on such as the mathematical model of the whole simulation system that consisted of the tidal current turbine with permanent magnet synchronous generator connected to the grid using inverter LCL Filter, converter, DC/AC inverter, and grid voltage monitoring unit.

Chapter 5: Showed the results and discussed whether the project simulation and control have been successful. It also touched on possible limitations, positive and negative aspects of the project**,** and also shed light on , unexpected findings .

Chapter 6: The last, but not least, conclude by summarising the main points of the dissertation and also make some recommendations of possible future research topics.

1.9.Publications

The publications below have evolved from the master's research:

Ladislas Kangaji , Efe Orumwense, Khaled Aboalez, Modelling and Performance Analysis of Grid-connected PMSG based Tidal Generation System AIUE Proceedings of the 2nd Energy and Human Habitat Conference 2021 https://dx.doi.org/10.2139/ssrn.3901370.

Ladislas Kangaji , Efe Orumwense, Khaled M. Abo-Al-Ez.2021. Tidal Stream Energy; Control optimisation; Hydrodynamic modelling; Tidal turbines efficiency; Tidal Energy Modelling. Energy for Sustainable Development. Review Article(it is submitted).

CHAPTER TWO: LITERATURE REVIEW

2.1 Introduction

This chapter provides an understanding of different aspects of the project in their entirety. Firstly, the site where the project was operated, and Secondly, the general presentation of different parts of the tidal turbine energy system. Many tidal current devices were presented, as some characteristics of tidal current devices are different depending on the designs model. As described in the following section the European Marine Energy Centre (EMEC) has collected and grouped all the available concepts that utilise tidal streams to generate electricity. In addition, the breakdowns of the electrical architecture of the tidal current conversion systems has been described and the type of generator combined with the associated controllers and location of power electronics.

2.2 Tidal energy resources

The tides are created by the gravitation pull of terrestrial planets, whereby the sun and moon are the key factors for the tidal forces on planet earth as illustrated in Figure 2-1. The impacts of tidal energy are transmitted as crustal rocks in the seawater which flow in an up and down motion due to gravitational pull (Lumpkin & Johnson, 2013; Ghefiri; et al., 2017).
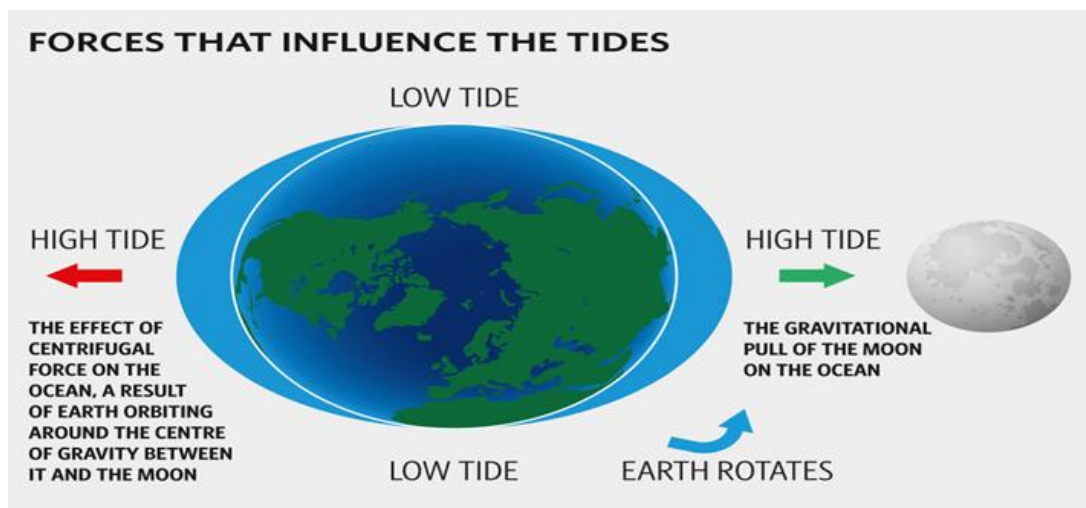
Figure 2—1:The gravitational attraction tidal bulge from of Earth, Moon, and Sun (Rassooll, 2014).

2.2.1 The tidal current resource in South Africa

The investigations have shown that the tidal energy potential (tidal stream and tidal range) is 26000 (TWh) of which is about 8800 (TWh). Tidal dissipation is comparable to the 3.5 TW of global electric generating capacity projected for 2004 (Borthwick, 2016).
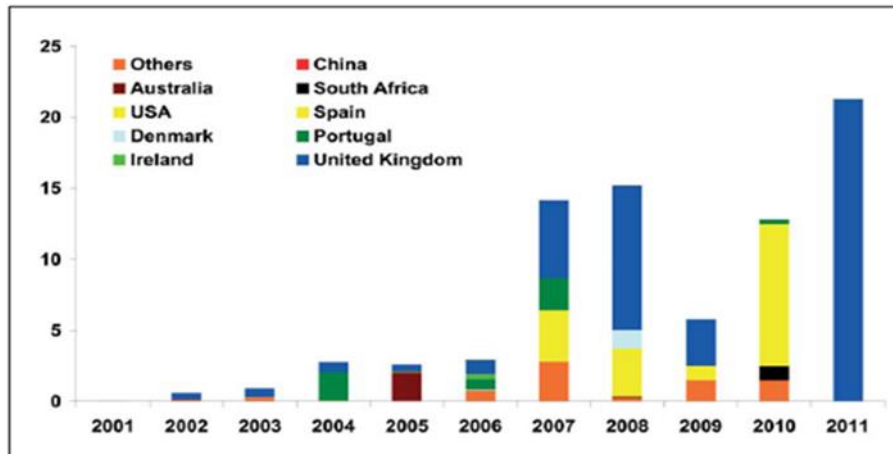
Figure 2—2:Wave and tidal energy worldwide capacity forecast by country (2001-2011(Laws & Epps, 2016).

The South African coastline has approximately 2 798 kilometers large. This is a huge advantage for the country and the African continent to experience tidal energy generation especially for the coastal towns as they can be powered by the ocean surrounding them (Reinecke, 2013; Lumpkin & Johnson, 2013). However, marine energy (wave, tidal, etc.) needs to be localised. The localised fraction of marine energy could still significantly contribute to the electricity supply.

Table 0—1: South Africa's natural resources (Reinecke, 2013).

Location		Water depth				
		100m	200m	300m	500m	1000m
Richards Bay	Distance offshore (Km)	0.7	0.8	0.9	1.0	1.1
	Current speed (m/s)	20	23	25	26	38
Durban	Distance offshore (Km)	-0,1	-0,1	-0,01	0,6	1
	Current speed(m/s)	9	12	14	35	60
Port Edward	Distance offshore (Km)	1.3	1.5	1.5	1.5	1.4
	Current speed (m/s)	11	12	14	17	20
East London	Distance offshore (Km)	1.2	1.4	1.4	1.3	1.2
	Current speed(m/s)	21	24	26	30	34
Port Elizabeth	Distance offshore (Km)	0.8	1.2	1.2	1.1	1.2
	Current speed(m/s)	9	44	46	55	58

The surface current core (>1.2 m/s) off Richards Bay lies inshore of the 1000 m isobaths.
The surface current core (>1.1 m/s) off Durban lies inshore of the 1000m isobath.
The surface current core (>1.5 m/s) off Port Edward is located at water depths of between 300 m - 1000 m. The surface current core (>1.3 m/s) off East London lies inshore of the 1000 m isobaths.
The constant lines speed in m/s within the Agulhas Current off the southeast coast .

2.2.2 South Africa Ocean regions

In the African continent, South Africa has the largest cost line. South Africa has located on the southern tip of the African continent (Figure 2.3), with a total amount of 2 798 km of its borders, namely, the Indian Ocean located to the southeast and the Atlantic Ocean to the west. There is a jet then separations, with one side flowing southward to reach the Agulhas flowing back current and the other flowing westward to reach with the southward-flowing the Agulhas has time-mean velocities of 60 –150 cm, with the greatest velocities found from 32.5S, 29E to 34.5S, 25.5E (Reinecke, 2013; Lumpkin & Johnson, 2013). These numerous currents were called rivers in the ocean, and transport massive volumes of sea water, it attains up to **100 x 106 m^3/S.** The current velocities in the core of the largest western limit's currents are approximately reached more than 1 m/s, and often over 2 m/s, with the width greater than 100 km and depths more than 2000 m (Schumann, 2013a).

The gravity, wind, and sunshine determined tidal wave and thermal power potentiality has been evaluated approximatively around 22,000 and 87600 TWh/year (Khan et al., 2017; Borthwick, 2016).
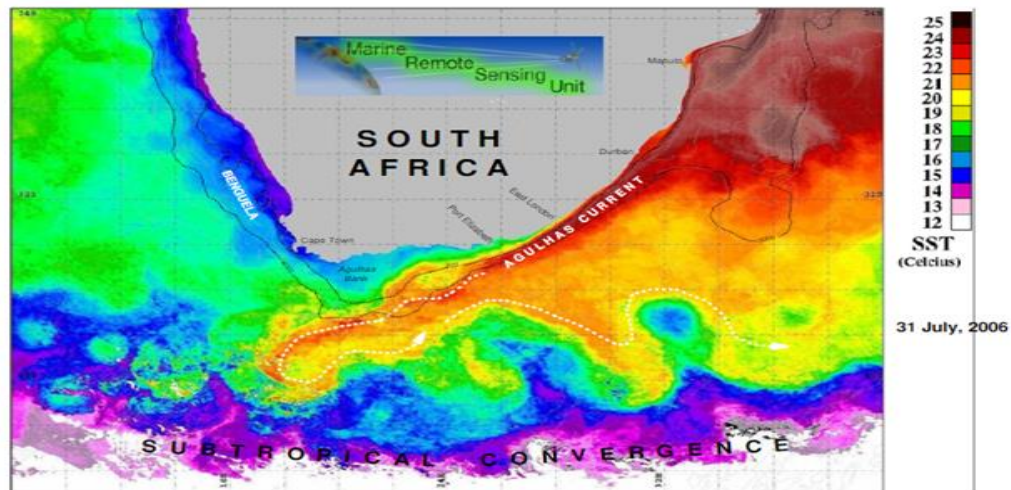
Figure 2—3:A composite false colour satellite picture has been captured on 31 July 2006, indicating SST on the determined scale (Schumann, 2013a),(Schumann, 2013a).

Among the great cities in South Africa, East London is medium in size compared to Johannesburg, Durban, and Cape Town. It is situated along the shores of the Eastern Cape, (Figure 2- 3). The city has a modest climate which plays a tremendous role to wave energy and marine conditions. The rain levels are estimated at 593mm per year, throughout the year

but mostly it is the summer season with the most rainfall. The daily maximum temperature varies between 20°C in July to 26°C in February. July is one of the coldest months in winter when the mercury drops to 9.3°C on average during the night. The tidal difference between low and high tides can be as high as 2 m but the lowest is 0.5 m. The height of waves ranges from 4 m to 5 m, depending on the wind (Reinecke, 2013; Schumann, 2013a).

2.2.3. Tides

Tides are predictable due to the earth's rotation which constantly occurs 24 hours (a solar day) that make it a reliable renewable energy option as shown in Figure 2-9. The advance 50 minutes every single day of the tides due to the moon rises. The cycle of lunar also changes in the height between high and low tides; the maximum difference of the heights between high and low tides is 'spring tide', and the minimum tidal range is 'neap tide'(Jian Zhang et al., 2014). The Tides around South Africa have been described as semidiurnal micro-tidal, which shows M2 tide domination, and the amplitude has been generally less than 2m. In fact, concerning high spring tides the amplitude can reach up to 2m, but at neap tides, it is as small as just 0.5m. This indicates that Cape Town's main sites are further eastwards, although the difference in the period is generally less than 30 minutes. The speed measurement of tides has been generally around less than 5 cm/s (Schumann, 2013a). The expected current maximum lies approximately along the 200 m isobaths, indicated by the dotted line in Figure 2-4. Of interest is the increase in current speed with distance southwards, and the local maximum speed found off the East London area.
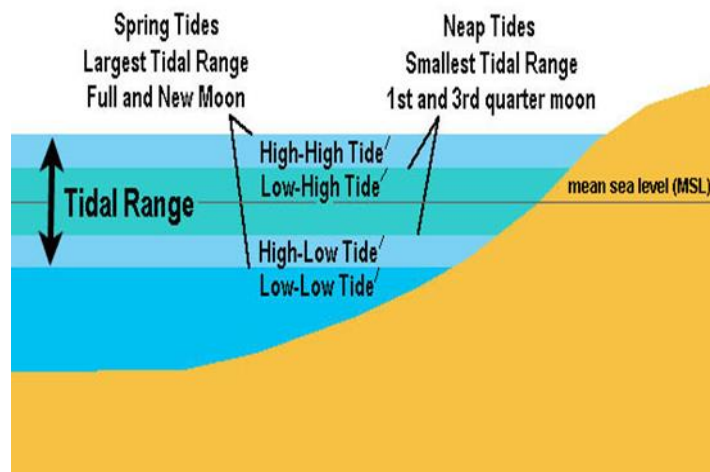
Figure 2—4:Tidal range is the distance between average highest and lowest tides (Jian Zhang et al., 2014).

The amplitude rises northwards into the Mozambique Channel. The South Africa marine measurements of tidal currents have indicated that they are small with Schumann and Perrins (1982) indicating the speeds were about less than 5 cm/s (Reinecke, 2013; Schumann, 2013a). During the examination of values achieved from the statistical analysis, Cape Morgan and East London locations were demonstrated to be prominent sites (Table 2 -1). The position of these two locations can be seen in Figure 2-3. It is clearly stated that the East London location could will also be the better choice in respect to proximity to the nearest substation. Figure 2-4 also shows protected marine areas (Schumann, 2013a).

2.3. Tidal stream and ocean current

2.3.1. Introduction

The seawater density is much bigger than the air density (approximately 832 times much bigger) (Liu et al., 2011). Thus, the power energy output from a tidal is higher than a wind turbine of similar sizes if it assumed fluid speeds are the same. Nevertheless, regarding energy harnessing, all of them use direct usage of the kinetic energy of pushing water to power turbines (Liu et al., 2016). However, tidal energy is predictable compared to the wind which relies on weather conditions (Laws & Epps, 2016).

2.3.3. Tidal stream

There are two ways in which tidal power energy can be generated: The tidal stream generator and tidal barrages, but this study only focused on the tidal generator stream. This design model is located at Pentland site Firth between the North of Scotland and the Orkney Islands. The two turbines have two 20 m rotors, with a capacity around 1 – 2 MW which is proportional to the speed current, and operate in 30 – 50 m water depths. Each rotor runs in clean water upstream of its support arm. The seabed anchorage is now shown with a gravity base, and the swinging arm ball joint is attached to the base by a three-axis swivel assembly.

Additionally, there are two forms of water stream turbines; horizontal axis and vertical axis turbines. The generation of tidal energy from the up and down of the tides were harnessed on a commercial scale (Hwang et al., 2009; Schumann, 2013b). The tidal turbine array is so far the most promising technique for harnessing tidal energy on a large scale(Faudot; & Dahlaung, 2011). However, the extraction of tidal stream energy can have an impact on the surrounding hydrodynamic environments as shown in Figure 2-5. The shifting of hydrodynamic developments can further impact the transport of sediment, water quality (Faudot; & Dahlaung, 2011; Li et al., 2016).
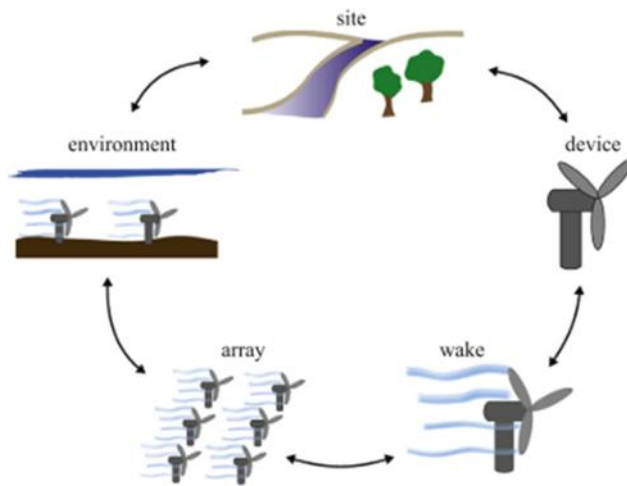
Figure 2 —5:The tidal stream hydrokinetic energy conversion systems (Laws & Epps, 2016).

The tidal turbine array has been so far the most important method for large-scale tidal stream energy extraction (Lin et al., 2016). The tidal stream turbine is indicated in Figure 2-6.
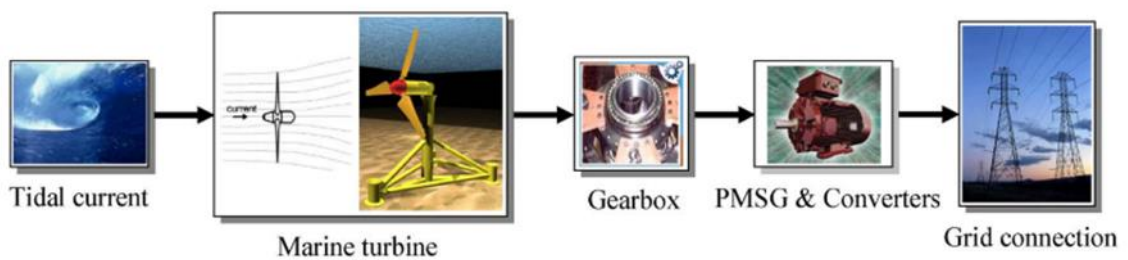
Figure 2—6:Tidal current turbine global block diagram (Benelghali et al., 2011).
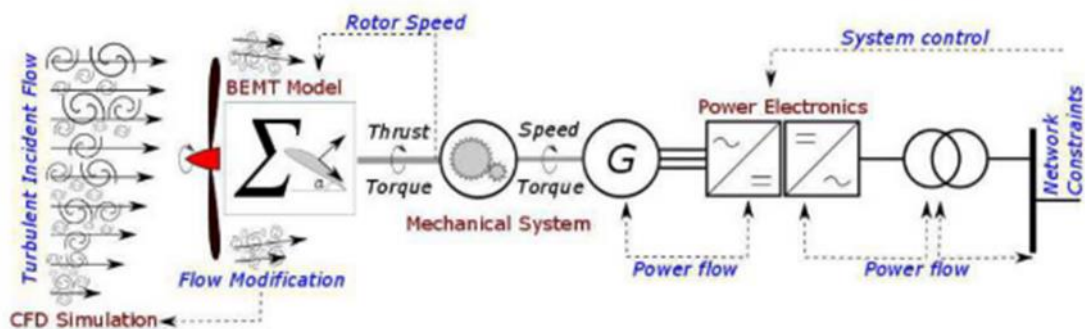
Figure 2—7:Tide-to-wire model for a basic tidal turbine(European Commission, 2019).

Hydrokinetic power relies on the velocity of the river, ocean, or tidal current. The minimum operation requirement of the tidal turbine is a minim water speed and water depth with the average 2–4 knots (1–2 m/s) of minimum speed, even 1 knot (0.5 m/s) can still be harnessed depending on the particular technology approach because the optimum speeds are around the 5–7 knot in Figure 2—7 (1.5– 3.5 m/s) (Johnson & Pride, 2010). The list concerning the stream

energy extraction prototype devices that have been working and/or undergoing sea tests is presented in Table 2-2.

Table 0—2: The Stream Energy extraction prototype devices(Johnson & Pride, 2010).

Type	Name	Capacity	Test Location	Designer	Year
Axial flow	AR1000	1 MW	UK	Atlantis	2011
Axial flow	Sea Flow	300 kW	UK	Marine current turbines	2003
Axial flow	Sea Gen	1.2 MW	UK	Marine current turbines	2008
Axial flow	Alstom1 MW*	1 MW	UK	Alstom	2013
Axial flow	HS1000	1MW	UK	ANDRITZ HYDRO Hammerfest	2011
Axial flow	HyTide 1000	1MW	UK	VOITH HYDRO	2013
Axial flow	Haineng II	200 kW	China	Harbin Engineering University	2013
Axial flow	ZJU 60 kW*	60 MW	China	Zhejiang University	2014
Axial flow	OUC 50 kW*	50MW	China	Ocean University of China	2014
Axial flow	NENU 20 kW	20 kW	China	Northeast Normal University	2013
Cross flow	TidGen	150kW	USA	Ocean Renewable Power	2012
Axial flow	Haineng I	300kW	China	Harbin Engineering University	2012
Crossflow	Haineng II	600 kW	China	Harbin Engineering University	2013
Crossflow	DUT 15 kW*	15 kW	China	Dalian University of Technology	2013

2.3.2.1. Tidal turbine technologies and concepts

The energy harnessing of a tidal flow occurs with the kinetic energy transformation during displacement of the fluid, within the mechanical motion system, which can then spin a generator. Therefore, different characteristics of the devices are presented in the following section:

2.3.2.2. Vertical axis tidal turbine

The vertical axis tidal turbine is rotating around a vertical axis, composed of a gearbox and a generator located above or below the seawater level. This tidal device rotates in both directions of flow current Figure 2-8a). The average power from TEC devices is around 50 to 250 kW range (Laws & Epps, 2016).
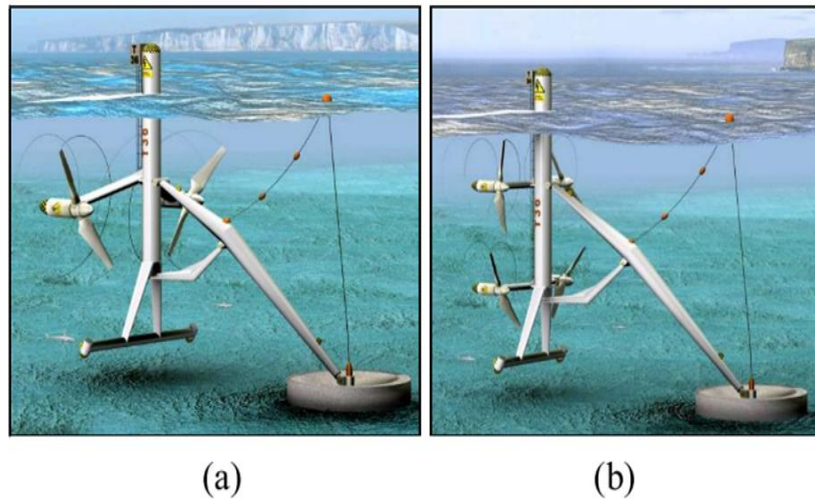
Figure 2—8: The Tidal Stream concept (Benelghali et al., 2010)

2.3.2.3. Darrieus tidal turbine

The darrieus device is a flowing cross machine, which is the rotation of its axis that attains the operating flowing of the fluid at accurate angles. This technology uses an orientable vertical rotor that can communicate the torque straight to the water surface.(Johnson & Pride, 2010; Elghali et al., 2007)It also requires a complex transmission system or an underwater, these devices are shown in Figure 2-9 (a) Kobold turbine (b) Floating plat form (Schumann, 2013a; Jian Zhang et al., 2014; Laws & Epps, 2016).

2.3.2.4. Horizontal axis tidal turbine

The Horizontal axis tidal turbine rotates around a central hub, with a propeller that works as a blade (see Figure 2-8, above), composed of a gearbox and a generator coil located above or below the seawater level. This device technology needs a self-adjustment design of orientation for the speeds direction variation which represent an important feature of their development, the average power out is around 1 – 2 MW (Daborn, 2012). The rim of the generator design pattern eliminates the bulky central core, due to symmetrical aspects that allow the device to operate in two different directions without realignment. These systems have a bell-shaped entrance (a 'duct' or 'shroud') that allows the acceleration of the flow of sea water through the generator to improve the efficiencies and for more power (Lin et al., 2016).

2.3.2.5. Lunar turbine

This device is designed for the 1MW out generation (a) Lunar turbine, (b) Lunar farm(Johnson & Pride, 2010; Elghali et al., 2007). Thus, these smaller turbine capacities are working depending on the power out already set. However, a big amount of energy can be produced

by a device which the blade diameter has been given. All these tidal turbines operate according to a symmetrical design model and operate in both two directions.

Figure 2—9:The tidal and sea water current devices (Benelghali et al., 2010; Johnson & Pride, 2010; Borthwick, 2016; Sousounis & Shek, 2017).

2.3.3. Electric generators topologies

The wind topologies are slightly the same as the tidal turbine; that's the reason the mathematical parameters differ on the coefficient of density (Eddine et al., 2007). The electrical machine is the principal element in the electrical interface sub-system. Other peripherals have been composed of power electronic devices, transformers, transfer switches, and protection equipment. In the tidal current devices, the input mechanical torque drives the rotary machines (Khan et al., 2009). The General Electric architecture is indicated in Figure 2-11:(a) and Figure 2-15. The tidal power system is composed of:

A. Collection: This is the portion of the TCCS with the cables that bring together the power from the generator to the hub or the shore rely on the electrical architecture, and it contains the rectifier.

B. Aggregation: The TCCS portion where the power from many devices is collected. To be feasible the devices must be electrically linked and based on the same voltage and stable frequency in AC structures or a communal DC link.

C. Transmission: At this TCCS level, the voltage coming from all devices part which makes the tidal array is stepped up for grid connection (Sousounis, 2018).
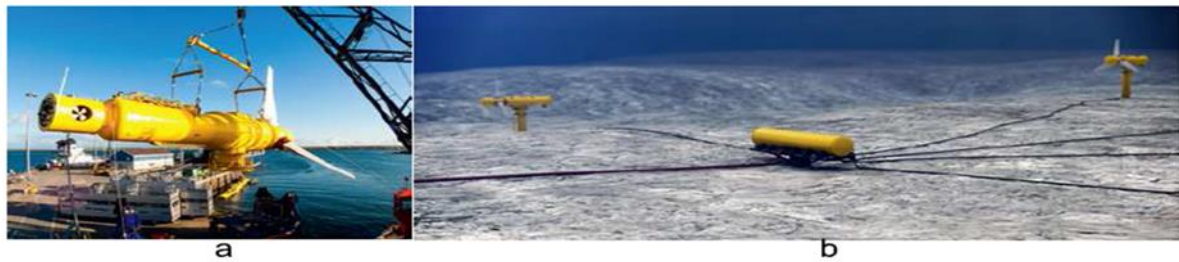
Figure 2—10: (a) GE 1MW tidal stream device. (b) Artist impression of the GE tidal array electrical hub (Sousounis, 2018).

The transmission of the medium voltage of the generator output to shore has been done by long three-phase subsea cables indicated above Figure 2-10 (a) and (b), in low voltage by an onshore transformer. The filters of the voltage source converter(VSC) are installed to convert the AC to DC and vice versa as shown in Figure 2-15 (Johnson & Pride, 2010). At the grid side, the inverter low voltage output is firstly filtered and then a step-up transformer is used accurately to satisfy the grid high voltage (Sousounis et al., 2014).

2.3.3.1. Hydrofoil blades

The hydrofoil blades use a hydrodynamic lift principle that provokes the turbine foils to displace accordingly faster than the velocity current of the surrounding sea water (Tarafdar et al., 2013). The Gorlov Helical Turbine (GHT) is indicated in Figure 2-11 (Johnson & Pride, 2010). The turbine has one or several long helical blades that run along a surface cylindrical. Generally, the GHT starts itself and can generate energy from sea water speeds flow even low at 1.5 m/sec with the rise of the power depending on the sea water velocity cubed (Chen et al., 2013).
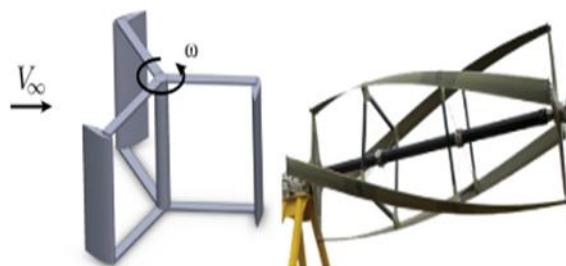
Figure 2—11:straight-blade and helical-blade cross-flow turbine (Laws & Epps, 2016).

There are various concepts of operation of cross-flow turbine, which are relying on wind operational basic principle. Darrieus and Gorlov turbines are more popular concepts design of cross-flow turbines in the marine industries (Figure 2-12) (Zanette et al., 2010).
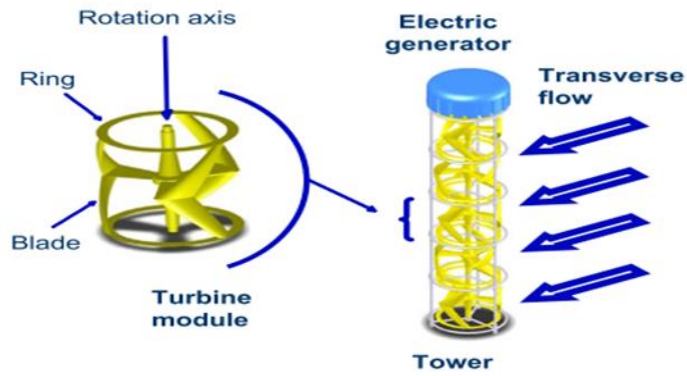
Figure 2—12:Darrieus and Gorlov turbines(Laws & Epps, 2016).

The oscillating hydrofoil devices and vortex-induced vibration devices are commonly used. There are two types of devices of oscillating configurations the first one, is an oscillating-hydrofoil device - driving an arm to displace with the lift force act upon a hydrofoil and transform the energy into electricity through a hydraulic system Figure 2-13 (a) (Lin et al., 2016),The second device is the vortex-induced vibration devices Figure 2-13 (b) that use the alternative shedding vortices downstream of a bluff body exposed to the flow, which is a very popular concept flow-induced principle called Karman Street (Lin et al., 2016).

(a)

(b)
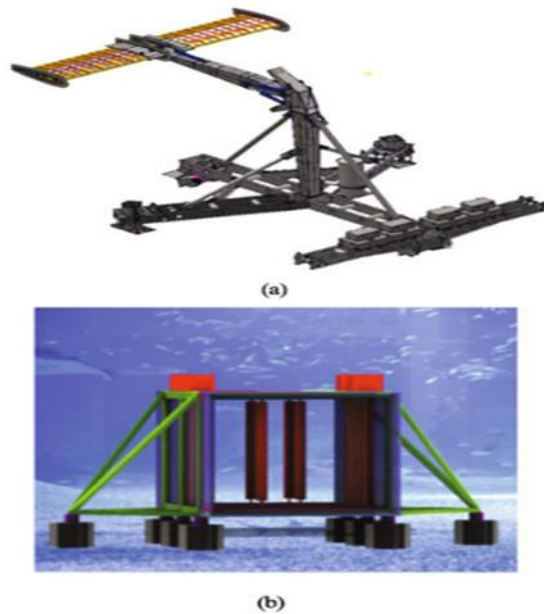
Figure 2—13:Oscillating tidal stream energy converters(Lin et al., 2016).

2.3.3.2. The prototype SR2000

The prototype SR2000 floating tidal turbine (Figure 2-14) contains two 1MW horizontal-axis tidal current devices that work at variable velocities but with a stable pitch blade. The power take-off structures are linked to a transportation vessel that is 6m larger. Apart from the single mooring structure of Oceade [Figure 2- 14 (a)], the developer designed a subsea hub to connect and transmit the energy from tidal arrays. This is a second tidal current turbine developed by Nautricity, called Cormat [Figure2-14 (b)]. The Platform for ocean energy (PLAT-O) is a submerged taut moored, buoyant, subsea reaction sub-system, which acts as a support structure for tidal which is designed by the sustainable marine energy (SME) which has been moored using an anchor (Chica et al., 2015).

.

a   b
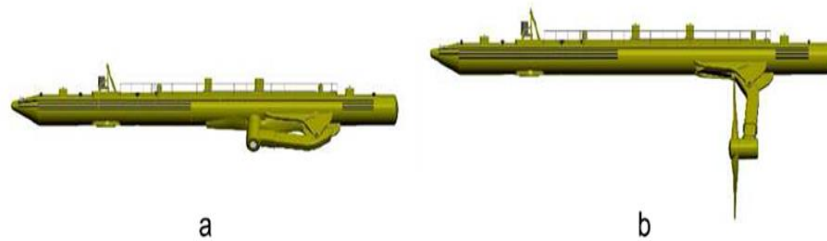
Figure 2—14:Artist impression of the SR2000 at transportation/survivability (Sousounis et al., 2014).

2.3.3. Tidal turbine topology

Tidal current   Marine turbine   Gearbox   PMSG & Converters   Grid connection
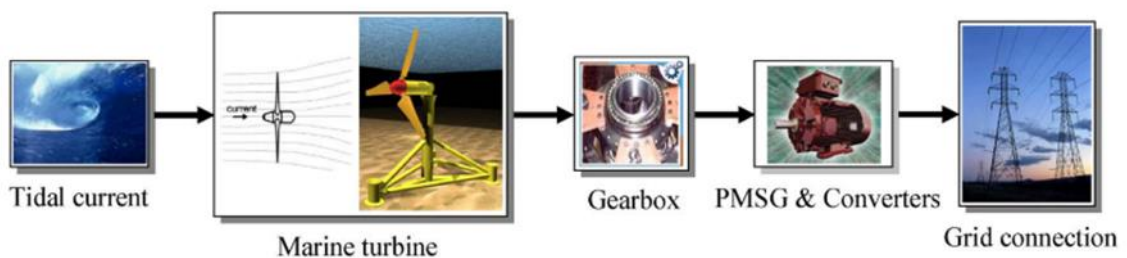
Figure 2—15:Tidal current turbine global block diagram (Benelghali et al., 2011).
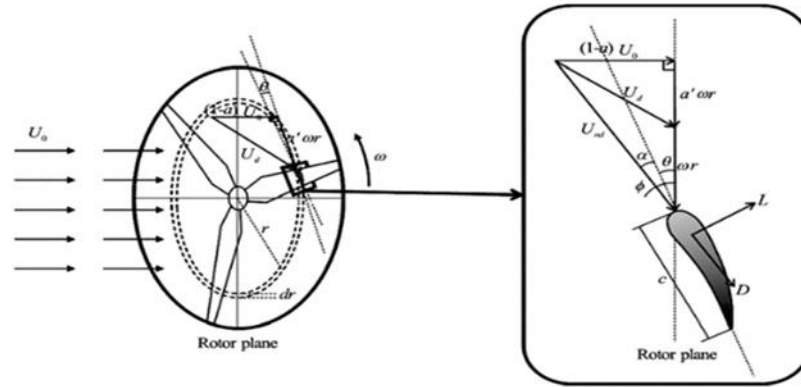
Figure 2—16:The basic ideas of blade element momentum method (W. Li et al., 2016).

2.4. Mathematical representation of a tidal energy system

The first parameter when designing sizing is the rotor. Preferably it is ideal to have a bigger size of the rotor but not too long, as the cost is the function of the rotor measure (Chica et al., 2015).The power energy outlet (**P**) of the horizontal axis hydrokinetic turbines shown in Figure 2-16 with the density of the fluid (**ρ**), surface swept by the blade of a rotor $A = \pi R^2$, (R as the angle of the blade radius or tip radius), the speeds of the sea water (**V1**), the power coefficient (C_p) and the drive train efficiency (generator, gear, etc.) (η), which is assumed to be 70% for a small turbine of electric production (Chica et al., 2015). The tidal blade turbines receives hydrokinetic energy, which then gets transformed into mechanical and then electrical forms. Generally, the kinetic energy is accompanied in the seawater stream with a mass (**m**) and a speed(V) which is given as.

$$E = \frac{1}{2}mV^2 \tag{2.1}$$

For a rotor of a turbine of the tidal rotor with the cross-sectional surface (A) exposed to tidal stream as indicated in Figure 2-17, the kinetic energy is expressed as:

$$E = \frac{1}{2}\rho v V^2 \tag{2.2}$$

Where ρ is the density of the water and v is the parcel volume of water available into a rotor. The interaction between the tides parcel and the rotor per unit time has a cross-sectional area equal to that of the rotor (A) and thickness equal to the water velocity (V). Hence the kinetic energy per unit time equation (2.2), power, can be expressed as:

$$P = \frac{1}{2}\rho v V^3 \tag{2.3}$$

Therefore, the potential power energy available in the water stream is proportionally dependent on the water density, the surface of the tidal rotor, and the water velocity. The effect of the water speed is very important due to its cubic relationship with the power. it is assumed that the disk slows the tidal current equally at each radius (Tarafdar et al., 2013).
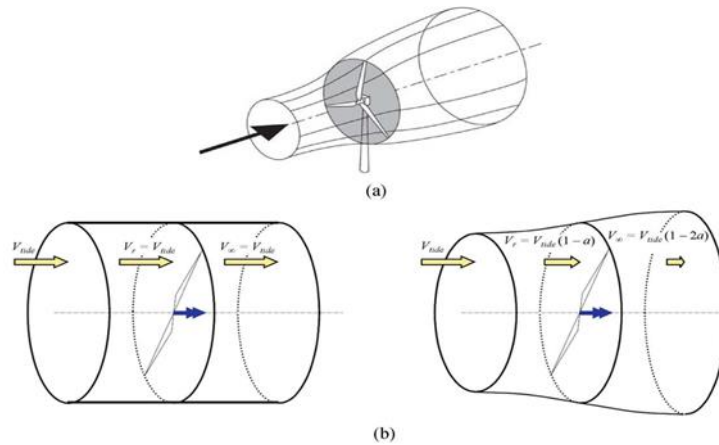
Figure 2—17:Actuator-disk model. (a) Energy extracting stream tube of a wind/marine turbine. (b) marine turbine with (right) and without (left) loading (Tarafdar et al., 2013).

2.4.1. Power Absorption by a Turbine

The tidal turbine can absorb a part of the tidal power energy available as indicated in Figure 2-17 (Tiwari & Babu, 2016). This amount of power relies on the kind of turbine and the efficiency. The coefficient must be significantly smaller than one and is named the power coefficient C_p. So, the power which the tidal turbine extract from tides can be expressed as follows:

$$P = \frac{1}{2} C_p A \rho V^3 \qquad (2.4)$$

In practice, the typical power coefficient is 35 – 45%. A tidal energy plant with a rotor, transmission line, generator, maximum power tracking (MPPT), and other devices, which all have the maximum efficiency lower compared to one of the entire systems, only I deliver between 10 – 30% of the original energy available in the tides (Ghefiri et al., 2015).

2.4.1.1. Power coefficient

The C_p coefficient power determines the extraction of power efficiency of a tidal turbine (Figure 2-18). The tip ratio of the speed of a tidal turbine is the ratio between the bordering angle blade velocity and the tidal speed shown in Figure 2-19, and it is expressed as

$$\lambda = \frac{R\omega}{V} \qquad (2.5)$$

Where R is the tidal turbine radius, ω is the angular velocity of the tidal turbine and V is the tidal velocity (Sousounis et al., 2014).
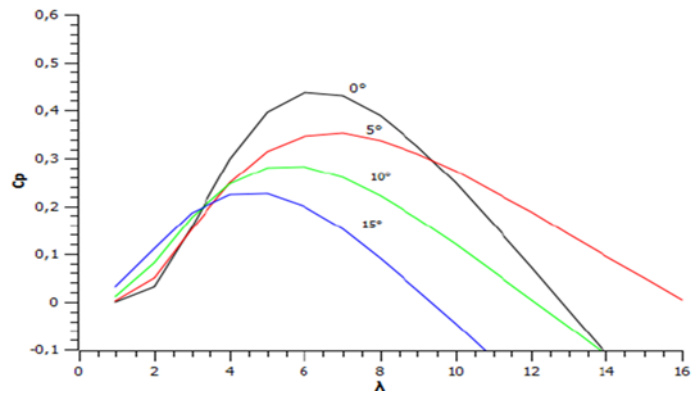
Figure 2—18:C_p as a function of the angle velocity ratio(λ) with pitch(θ) angle as factors (Sousounis et al., 2014; Chica et al., 2015).

$$P = \frac{1}{2}\rho A V^3 C_p \eta \qquad\qquad (2.6)$$
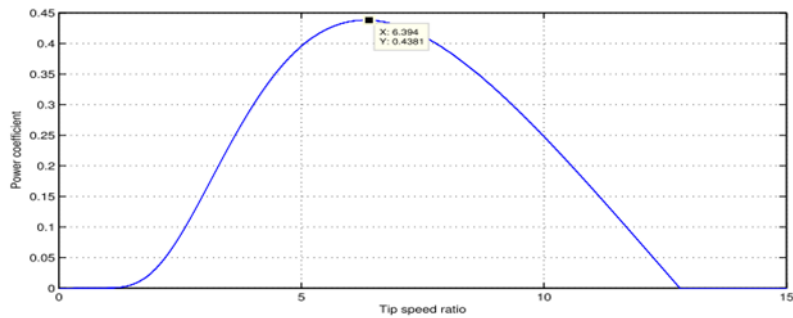
Figure 2—19:Power coefficient curve (K. Ghefiri et al., 2017).

2.4.1.2.The hydrodynamic behaviour of a tidal turbine

Some studies focus on the assessment of the hydrodynamic behaviour of a tidal turbine utilizing the Rankine–Froude actuator disk design (Tarafdar et al., 2013).. This design focus on changing the rotor with a theoretic actuator disk, which is a surface form of a circle of zero thickness that can resist a pressure difference, and thus decelerate the tidal current through the disk. The main goal of the actuator disk design model is to obtain a first wake-induced flow estimation and the total induced power loss.
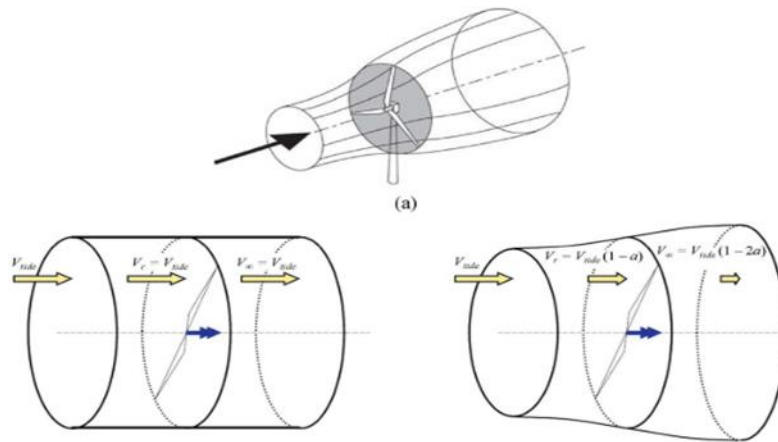
Figure 2—20:Tidal turbine with(right)and without (left)loading. The actuator disk model(Tar afdar et al., 2013)..

A uniform thrust load in turn depends on the indefinite number of rotor blades. Figure 2-20 shows a one-dimensional flow of liquid in the direction perpendicular to the plane of the actuator disk for an unloaded and loaded turbine. For example, for an unloaded machine that is at zero loads, the speed of the current in the direction of the plane of the rotor (V_r) is equivalent to the speed of the tidal current which is not disturbed (V_{tide}); in contrast to that of the loaded machine, the speed of the rotor current decreases. When e considering that in the case where the induced speed is reduced by the rotor is **V**, then the speed at the disc is represented by $V_{tide}, V^{\frac{1}{4}}, V_r$, and far downstream, the slowing down of the current was pronounced up to the speed **V**. The deviation between the axial component of the current velocity and that of the axial velocity of the flow in the direction of the plane of the rotor is called the induced velocity. Thus, the disk speed is the average of the upstream and downstream speeds. The description of an axial induction factor, a, as the fractional reduction in the speed of the current between the free flow and the direction of the plane of the rotor is inquired by (2.7).

$$a = \frac{V}{V_{tide}} \tag{2.7}$$

The results in (3.36):

$$\begin{cases} V_r = V_{tide}(1 - a) \\ V_\infty = V_{tide}(1 - 2a) \end{cases}$$

For $a = 0$, when there is no current and deceleration, they will be no extraction of power, whereas, for $a = 0.5$, the far wake velocity disappears, and the lack of flow behind the turbine, no power is produced. The extraction of power from the tidal current by the rotor is indicated by Equotion (2.12).

$$P = \frac{1}{2}\rho A V_r (V - V_\infty)(V - V_\infty) \tag{2.8}$$

Substituting V_r and V_∞ from (2.8), it has been shown that,

$$P = \frac{1}{2}\rho A V_{\text{tide}}{}^3 4a(1-a)^2 \tag{2.9}$$

A power coefficient C_p is then described as

$$C_p = \frac{P}{\frac{1}{2}\rho A V_{tide}{}^3} = 4a(1-a)^2 \tag{2.10}$$

Where the denominator illustrates the global kinetic energy of the free-stream current is circulating in a stream tube with a surface equal to the disk area. The extraction of the power is represented by (2.11).

$$P = \frac{1}{2}\rho A V_{\text{tide}}{}^3 \tag{2.11}$$

The theoretic maximal amount of the power coefficient C_p occurs when a=1/3.

Hence $C_{pmax} = \frac{16}{27} = 0.59259, \frac{2}{3}V_{tide}$ and $V_\infty = \frac{1}{3}\ V$ $\tag{2.12}$

Thus, the theoretic maximal value of extracted energy equals the $\frac{16}{27}$ the portion of the kinetic energy.

This constraint is relative to the Betz limit, or precisely with the Lanchester-Betz limit. Practically this limitation cannot be achieved and the maximum amounts of the C_p of real turbines are usually around 0.4 – 0.5 range.

The C_p variations depend on the pitch angle of the blades (β) and the tip-speed ratio λ, defined as the ratio between the rotor tip-speed and the tides velocity. A $C_p(\lambda, \beta)$ the curve illustrated in Figure 2-21. This is a basic model that provides the details of the turbine behaviours. There is a model which is easier to utilise that can rely on the blade element momentum (BEM) theory, which is the most popularly used method for the calculation of the induced velocities on wind turbine blades. This theory is a continuity of the actuator disk theory (Odgaard & Stoustrup, 2015) used for each blade section.
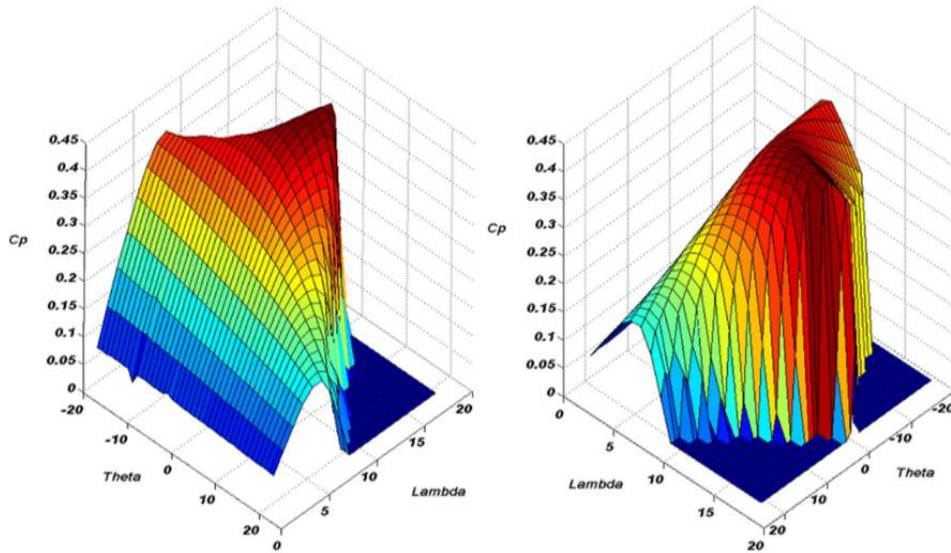
Figure 2—21:Power coefficient surface (Habibi et al., 2017)

2.4.1.4. Electrical architecture options for tidal current conversion systems
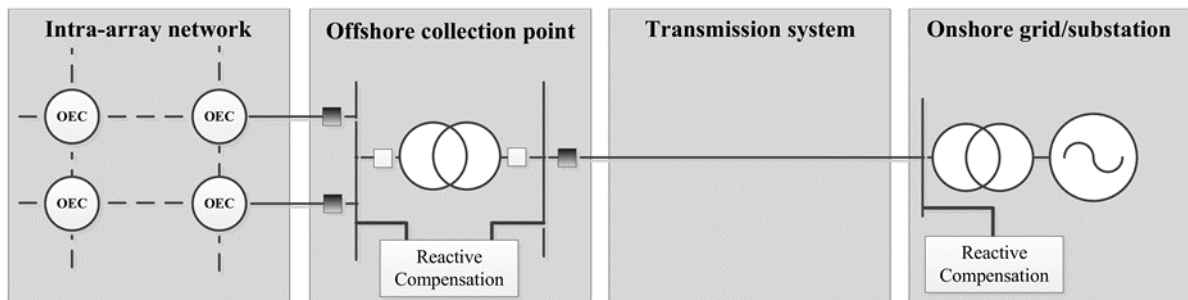
Figure 2—22:Simplified electrical network for offshore arrays (Muljadi et al., 2016; Collin et al., 2017).
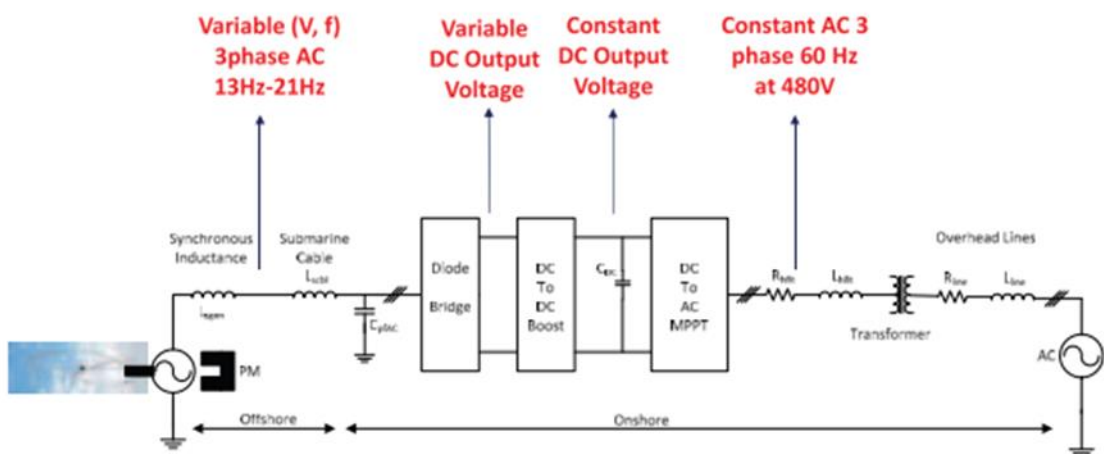
Figure 2—23:The simplified electrical system (Muljadi et al., 2016).

An offshore grid can be grouped into four subsystems such as the intra-array grid, which connects the ocean energy converters (OEC), the offshore collection points, the transmission system, and the grid link point. Onshore, with common coupling (PCC). A simplified diagram of the subsystems is shown in Figure 2-22. The main electrical components of the electrical network are subdivided into six different sub-groups as shown in Figure 2-23 and Table 2-4. The collection and transmission of the power and communication signals in the network are done by cables, and the connectors facilitate a non-permanent connection of different electrical subsystems. The increase, as well as the reduction of voltage levels for power transmission purposes, is done using transformers; the main role is to increase the voltage at the device level from low voltage (LV, <1 kV) to medium voltage (MV, 1–35 kV) and also in the offshore collection point to increase the high voltage (HV,> 35 kV) to transport it to the shore (Collin et al., 2017).

Table 0—3: Electric component composition of auxiliary of the tidal energy system

Category	Components
Cables	Static, dynamic
Connectors	Wet-male, dry-male, T-off
Transformers	Power, grounding, auxiliary, and measurement
Switchgear	Circuit breakers, relays, fuses, and disconnectors
Power quality	Reactive compensation, flexible AC transmission system, and harmonic filters
Collection points	Hubs, substation

2.5. Generator choice

The mounting of the generator on the turbine shaft for the conversion of the mechanical power produced by the turbine blades into electrical energy is one of the most important energy parameter.   The similarities between tidal current turbine technologies and wind turbine technologies. Therefore, the concept of wind turbine generators could be used for tidal current turbines (J. Zhang et al., 2014).

2.5.1. Squirrel Cage and Wound Rotor Induction Generator

The induction generators are classified into two groups, those with squirrel cage (SCIG) and those with wound rotor (WRIG). These two types are the most used ones because they are affordable, robust and require little maintenance (Jian Zhang et al., 2014). Figure 2-24 (a)

shows the topology of the fixed speed tidal generator with a multi-stage gearbox and a SCIG connected to the grid using a flexible stator and a transformer. WRIG has a similar composition. The difference is in the control of the rotor as indicated in Figure 2-24 (b). However, both SCIG and WRIG always draw reactive power from the grid, so they still need a compensator. To avoid the problem of the compensator and the flexible stator, the use of a generator with a reducer and full-scale power converter has been proposed as indicated in Figure 2-24 (a),(b),(c) (Rafiei et al., 2019).
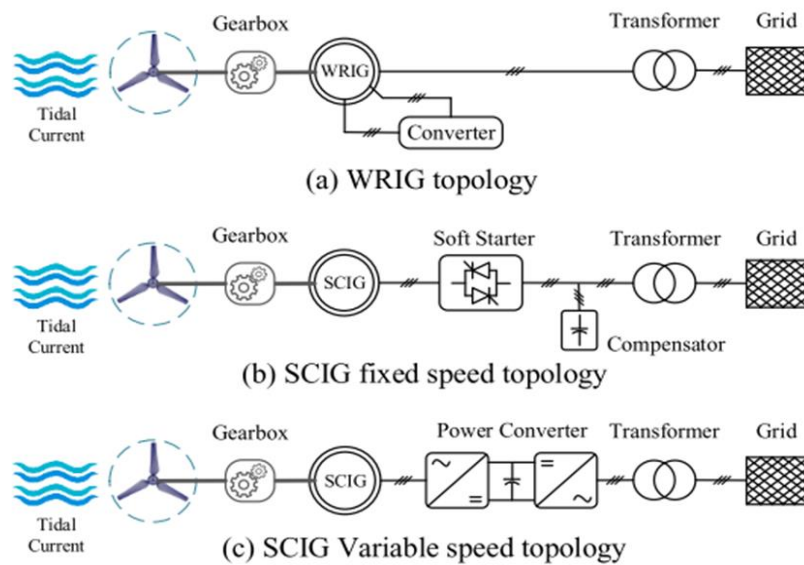
Figure 2—24:Induction generator structure (Rafiei et al., 2019).

2.5.2. Doubly Fed Induction Generator

Figure 2-25 shows the topology of DFIG, where the stator is directly connected to the network, while the wound rotor is connected by using an electronic power converter. The variable speed range is approximately ± 30% around the synchronous speed (Rafiei et al., 2019). The nominal power of the electronic power converter is only 25 - 30% of the generator capacity; this concept is very economical (Benelghali et al., 2012).
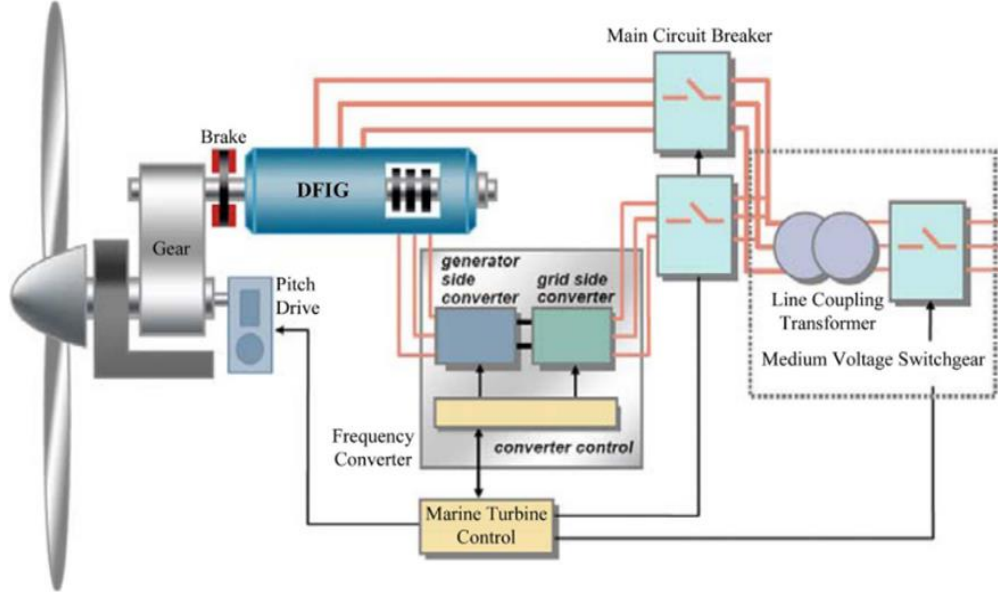
Figure 2—25: DFIG topology (Benelghali et al., 2011).

2.5.3. Permanent Magnet and Electrically Excited Synchronous

The direct drive train applications with full-scale power converter connected to the grid typically use PMSG and EESG, as shown in Figure 2-25., The highest potential of PMSG topology for tidal current turbines due to its reduced downtime, increased power output, and reliability. In general, the construction of the EESG should be done with a rotor that is connected to a field converter. The stator is very similar to machine induction. The EESG does not present any risk of demagnetisation compared to the permanent magnet (Rafiei et al., 2019; Benelghali et al., 2012).
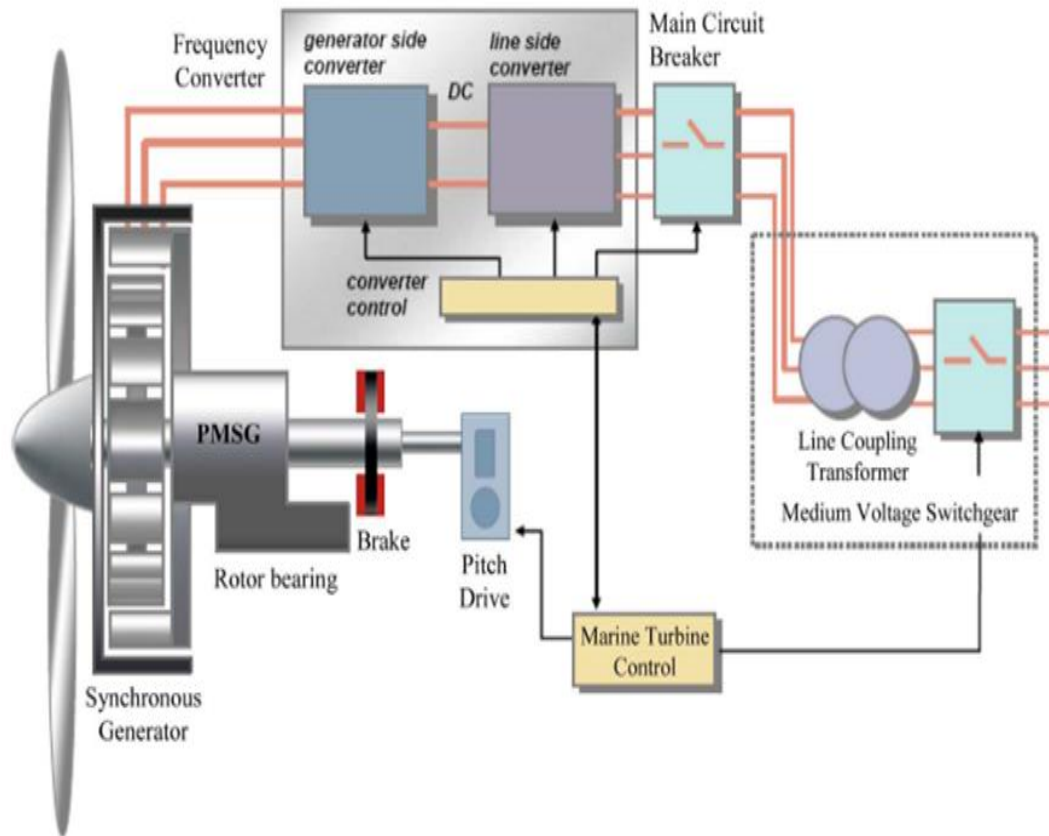
Figure 2—26:Synchronous generator topology (Benelghali et al., 2011).

Reducers are used in the new generation electricity market. However, in a direct drive concept, the low rotational speed characteristic leads to a larger pole pair generator system in volume and mass. To reduce the size and mass of the design, a gearbox may be in the dotted line indicated in Figure 2-26. Especially for floating platform turbines, this is the current choice even though the gearbox concept requires higher maintenance costs. For direct-drive and oscillating hydrofoil designs, especially horizontally piped turbines, PMSGs are most preferred. The design of many converters is preferable in a renewable energy system (Blaabjerg & Ma, 2013; Rafiei et al., 2019). The diagram with all the possible electrical architectures is shown in Figure 2-23.

2.5.4. Permanent magnet synchronous generators in tidal current systems

The performance of the state of the art of Marine Tidal Turbines (MCT) depends primarily on the nature of the resource (current speed) (Odedele et al., 2014). The characteristics of the turbine such as the blade's number, the fixed or variable pitch, the horizontal axis, as well as the vertical axis. The different characteristics of the generator such as the permanent magnet synchronous, the wound synchronous, the doubly-fed induction, the squirrel cage induction, and the associated power electronics are the technologies choices. For instance, some generators are preferable to others, in some cases, the use of the direct-drive solution with a

permanent magnet synchronous (PMSG) and an IGBT PWM back to back converter presents more advantages for an MCT when compared to the usage of an induction generator (Odedele et al., 2014). In the field of tidal energy generation, the PMSG model in tidal current systems is preferable in comparison to other types of generators (Odedele et al., 2014). This design model is composed of two sets of contra-rotating blades which are driven by a PMSG directly Figure 2-27:(a) and (b))(Ugalde-Loo et al., 2014). There are many types of generators and converter designs, but according to surveys, it has been found that using a PMSG with active PWM vector control is one of the most efficient and reliable solutions (Amézquita-Brooks et al., 2015).
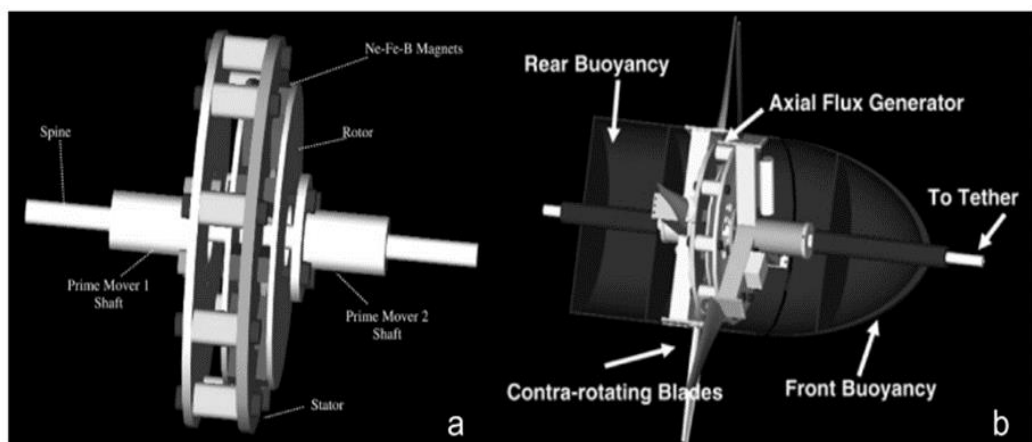
Figure 0—27: (a) CAD design of contra-rotating axial-flux PMSG. (b) Contra-rotating generator prototype (Clarke et al., 2010).

The PMSG design topology for tidal current applications is presented in Figure 2-27. Its commercialisation design model form is used by Open Hydro is relied on turbines that are openly at the centre and the conversion is reached by PMSG that is mounted on the rim and is directly driven by the turbine illustrated in Figure 2-8a and Figure 2-8b (Clarke et al., 2010).

2.6. Tidal energy transmission to shore
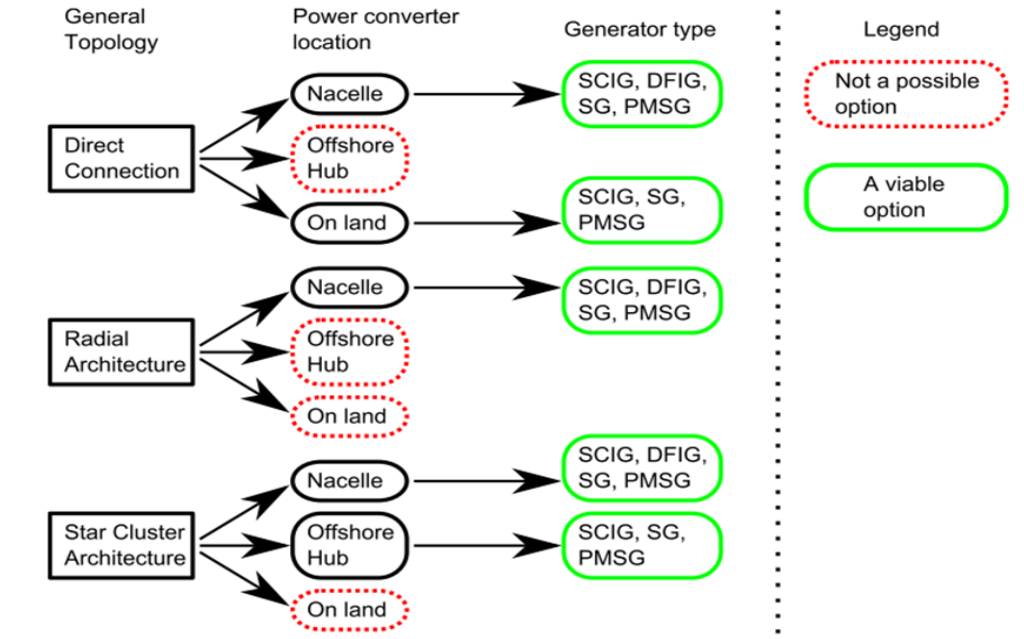
Figure 2—28:Block diagram of all the possible AC options of an electrical architecture for a tidal array (Sousounis, 2018).

Using a direct connection to shore, the power electronics can only be placed in the nacelle or on land. However, to put the power electronics on land requires long cables operating in variable frequencies making the use of a DFIG impossible. In this study , the electrical topology of direct connection to shore with power electronics in the nacelle or on land was made possible with the use of SCIG and PMSG as indicated in Figure 2-28. The radial architecture is usually implemented in a ring topology. Each turbine has fully-rated BTB power converters and a step-up transformer in the nacelle or enclosed in a separate subsea structure next to the turbine. A high voltage cable, 33kV in AC or ±7.5 kV in DC, connects several turbines based on the rated power. In this thesis, the radial architecture was implemented for a system of up to 16 tidal turbines with a 33kV cable (Sousounis, 2018).

2.7. Universal bridge topology

The system of the device is integrated by a permanent magnet brushless generator include a passive three-phase (3Φ) rectifier to convert voltage to DC and a resistor bank to determine the load on the DC link (Baker et al., 2014).

Figure 2-29 illustrates the fundamental diagram of the three-phase boost converter. UL indicates the line voltage and the bridge converter voltage controllable from de the dc-side. The general phasor diagram and diagrams for both rectification and regeneration operation can be drawn at unity power factor (UPF) (Wang et al., 2018).
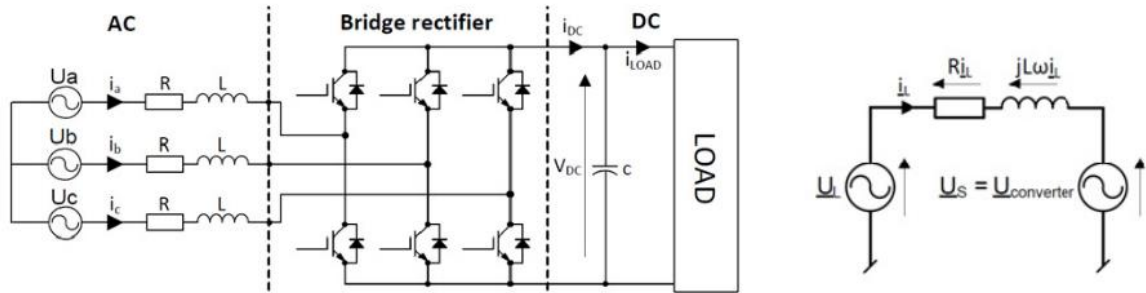
Figure 2—29:Three-phase rectifier topologies (Wang et al., 2018).

The line current iL is controlled by the voltage drop across the inductance L connecting both voltage sources (line and converter) shown in Figure 2-30. When the phase angle ε and the amplitude of converter voltage Us has been controlled (Wang et al., 2018), automatically the phase and amplitude of the line current are also controlled indirectly. Thus, the average value and sign of the DC is an issue that needs to be controlled as it is proportional to the active power conducted through the converter. The reactive power has been controlled separately with a shift of the basic harmonic current IL, on regulating the voltage UL.

a) General phasor diagram   b) Rectification (at UPF)   c) Regeneration (at UPF)
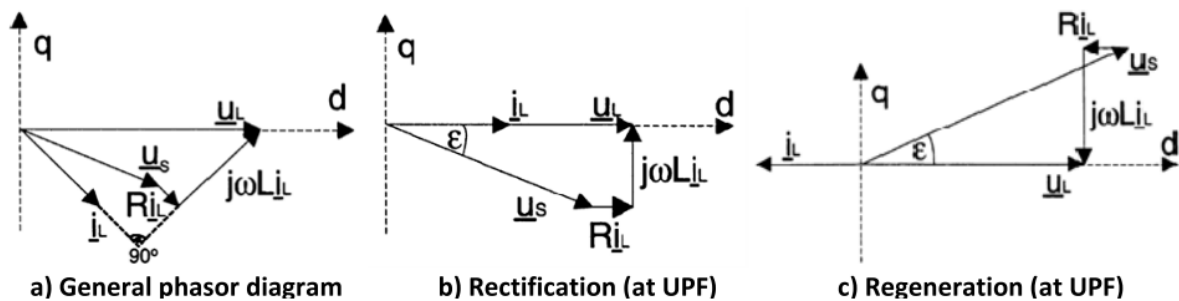
Figure 2—30:Phasor diagrams.

2.8. Cable tidal systems

The modelling of longer submarine cables by the π section network allows precise and uniform distribution of RC cable resistance, LC inductance and capacitance CC (Li et al., 2017). The essential similar sections π to model with more precision the frequency transients are proposed by the following equation.

$$N = \frac{8.t_{c.f_{max}}}{v_c} \qquad (2.13)$$

Where V_c is the travelling speed of the waves in the cables, it is indicated in Equation (2.14)

$$V_c = \frac{1}{\sqrt{L_c.C_c}}$$ (2.14)

The cable length was chosen after studies carried out by ANDRITZ Hydro Hammerfest estimated at around 3.5 km with low frequencies estimated at around (f_{max}) 5 kHz. The characteristics of the π cascade network are presented in Table 2-5. The modelling was based on the Pirelli cable which was used at the East London site in South Africa, the 11 kV Pirelli submarine cable, three conductors, insulated in ethylene-propylene rubber, intended for alternating current. The modelling was also composed of an optical fibre, three $2.5mm^2$ copper signal cables and a two-wire shield (Li et al., 2017). Since two π-sections cannot represent the frequency range of 5000 Hz, a three π-sections was chosen which indicated as f_{max}.

Table 0—4: Submarine cable network(Marios C Sousounis et al., 2016).

Symbol	Quantity	Value
R_c	Cable resistance	0.197Ω/Km
L_C	Cable inductance	0.742 mH/Km
C_c	Cable capacitance	0.310 µF/Km
$|Z_c|$	Cable characteristic impedance	52.5708Ω
l_c	Cable length	3.5Km
N	Number of π sections	2.12
N'	Number ofπ sections chosen	3
f_{max}	Maximum accurately indicated frequency	$7000H_z$

The passive filters are included in the power generation systems to suppress harmonic currents and reduce the voltage distortion which occurring in sensitive parts of the system,and the improvement at generator side depends on the second-order LCL filter to minimise the surges present at depth for a converter-cable-generator device (Kuschke et al., 2012; Marios C Sousounis et al., 2016). In this case, the purpose of modelling the LCL -filter is to minimise the overvoltage across the generator terminals and reduce the resonance effects in the cables on the other side, the single tuned filter, tuned to the switching frequency of the controller, and reduce harmonics produced by the VSC which regulates the generator (Li et al., 2017). Figure 2-31 illustrates the generator side of the TCCS with different technical filtering characteristics. The LCL filter elements are shown in Table 2-6 (Marios C Sousounis et al., 2016).
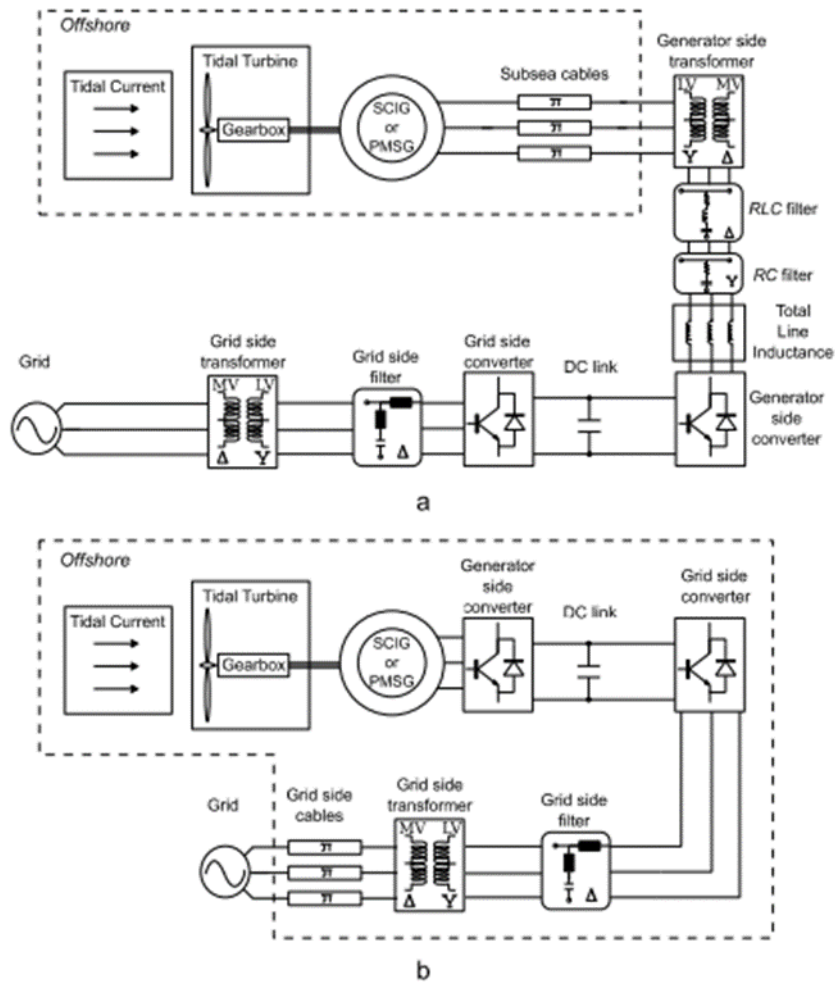
Figure 2—31:Block diagram of the single TCCS with long-distance controls and the associated control blocks (Marios C Sousounis et al., 2016; European Commission, 2019).

The practical structure of the generator side of the TCCS device without filters b device with an LVLCR filter c Device with an LCL filter and a single tuned filter.

Table 0—5: LCL Filter

Symbol		Quantity	Value
R_{filter}		Filter resistance	0.1915Ω
L_{filter}		Filter inductance	0.2728 mH
C_{filter}		Cable capacitance	84.6701µF
$t_{critical}$		Critical rise time	0.7962 m/s

The rotation ratio must be taken into consideration. On the other hand, the final filter components must be related to the primary winding of the transformer. More details regarding

the filter modelling equations for the Figure 2-31 LCL filter and the single tuned filter are presented in Equation (2.15) R_{filter} .

$$R_{filer} = 2.\sqrt{\frac{L_{filter}}{C_{filter}}} = |Z_c| \tag{2.15}$$

$$\sqrt{L_{filter}C_{filter}} \geq$$

$$t_{critical} \tag{2.16}$$

$$t_{critical} = 15.l_c\sqrt{L_cC_c} \tag{2.17}$$

Table 0—6: Inverter parameters

Parameters	Value
DC power	1.5 MW
DC-Link Voltage	1400 V
Active power	1.400 MW

Table 0—7: Tidal generation system parameters involved in the modelling process

Parameters	Value
Line voltage after filter	600 V
Current after filter	1200 V
Power factor	0.85
PWM carrier frequency	2000Hz
Grid frequency	50 Hz
Modulation range	0.7
Attenuation factor	20%
Acceptable maximal power factor variation	5%
Inverter configuration	Three-phase

2.9. Grid side Systems connected

The power generated by the TCCS is fed to the grid using the VSC. The grid-connected inverter is connected to the grid by a line choke to minimise line current distortion, a filter that minimises harmonics and a 600 V to 11 kV step-up transformer. The inverter is regulated via PWM scheme which is dubbed as voltage-oriented control with decoupled controllers which boost a constant DC link voltage of 1100 Vdc, a constant frequency output of 50 Hz on the AC side and control on the reactive power value.

2.9.1. Tidal turbine Grid-connected

The tidal power turbines generation tied to the grid do not require energy storage devices as the grid may supplement any deficit of power to meet the load demand when the system generates a small amount or does not generate power. In case the local load is lesser than generated power, the excess power can be sold to the grid (Tiwari & Babu, 2016).

Several works in the literature focus on different aspects of tidal energy extraction techniques that are based on the main modes of operation of tidal power plants as well as algorithms to regulate the timing of the simulation. One such method analysed the variation in performance of a central vertical axis device (TEC) when the table is filled row by row. There is an increase in the design of tidal return projects that has sparked the desire to develop simulation modelling tools for the optimisation of tidal energy to reduce uncertainties by giving an overview of potential benefits and corresponding impacts (Angeloudis et al., 2016). Additionally, in energising the modern tidal power system, the control of generation and frequency are the most challenging issues required for effective operation. The control of charging frequency plays an important role to maintain the regulation of the synchronism of the electricity production systems which has a diversification of sources by regulating the real powers (TPP) (Kumar; Shankar; Gauri, 2018). However, present a systematic literature review that has been examined certain types of complementary modelling detailing the simulations carried out to properly analyse the influence of these various methods on the tidal energy output.

The modelling and simulation of tidal energy generation are gaining more attention among researchers although tidal turbines are yet to have an optimal tidal current conversion system (TCCS), which justifies several model designs that have been proposed for tidal energy extraction. While most designs feature a bottom mount with low resistance blades and horizontal axis rotors, the generator side also contains several different techniques used in generator technology. However, the dominant combination of components is a function of the directly driven generators or the synchronous generators containing permanent magnets with gears and squirrel cage induction generators (SCIG). Some of the studies investigated the running costs and grid connection costs or installation costs indicated a lack of effective tools for these types of studies, hence the reason for estimation of results. However, this studies succeeded in establishing a simulation model of operational costs and device availability to solve this problem. During the analysis, different costs were considered such as the costs of the positions offshore, cable costs, maintenance costs and energy loss costs. This is evident from the improvement of the simulations that were made for large scale conditions using CFD simulations which is using a geometry-driven full-scale tidal current turbine. The clarification of the performance of the tidal turbine, and the focus was at blade forces that occurred during rotation in a high shear speed profile. The MATLAB-Simulink model for a tidal current turbine system through the modelling of the source attracted more research interest and numerous

publications are observed in this field. The investigations on tidal energy applications about the power output had a substantial increase. However, recent researchers (Uihlein & Magagna, 2016) reviews were based on running costs, grid connection costs, or installation costs which came to pinpoint a lack of operational experience which leads to an estimate of operational costs. They succeeded in establishing a simulation model of operational costs and device availability to solve this problem. During this analysis, several different costs were considered such as the costs of the positions offshore, cable costs, maintenance costs, and energy loss costs (Uihlein & Magagna, 2016). Additionally, in energising the modern tidal power system, the control of generation and frequency are the issues most necessary for its reliable operation. Of these two, the control of charging frequency (LFC) plays an important role in maintaining in synchronism the electricity production systems which have a diversification of sources by regulating the real powers (TPP)(Kumar; Shankar; Gauri, 2018). The limits of modelling and the strategies of simulations analysed were qualified and possible solutions to overcome them were proposed.

Despite the numerous running costs, grid connection costs, or installation costs and using CFD simulations which is using a geometry-driven full-scale tidal current turbine. There is fewer projects assessment that deals with a comprehensive comparison between all of these strategies from different points of view. These assessment articles revealed that there are only a few related studies targeting grid integration of modelling, simulation, and control of the tidal array grid system connected. In the few studies already conducted, most tend to focus on harmonics are generally which is caused by nonlinear loads that draw nonsinusoidal current from sinusoidal voltage sources due to their benefits, including their ability to operate under varied voltage ranges and the fact that the topology decouples the output from the inverter output, reducing AC power ripple. Despite these drawbacks, the current study focuses on tidal turbine array using a control design for a three-phase PWM rectifier and LCL filters connected after inverters received power from a permanent magnet synchronous tidal generator and connected to a DC load. Due to its cost-effectiveness in achieving low harmonic distortion and high efficiency.

Summary

This chapter reviewed the tidal power system structure and the tidal current resource in South Africa. According to the literature review, there are two ways in which tidal power energy can be generated: The tidal stream generator and tidal barrages, but this study only focused on the tidal generator stream. The tidal turbine array has been so far the most important method for large-scale tidal stream energy extraction. The actual principles and new trends in terms of functionality such as the electrical architecture options for tidal current conversion systems of a tidal stream connected to the grid can be grouped into four subsystems such as the intra-

array grid, the offshore collection points, the transmission system and the grid link point, Permanent Magnet and Electrically Excited Synchronous. The key drivers for the development of tidal energy systems include elements such as, the direct drive train applications with full-scale power converter connected to the grid typically use PMSG, and the system of the device integrated by a permanent magnet brushless generator includes a passive three-phase (3Φ) rectifier to convert voltage.

CHAPTER THREE: CONTROL SYSTEMS

3.1. Introduction

This chapter focuses on the modelling of the grid-tied tidal energy system. The components modelled include the generator, the filter, the power converter and the control systems. Some of the classical PI designs of wind turbines are also discussed because they were used for tidal turbine control. Some studies examine the concept of control of the Marine current system and show a strong interaction as a solution between the type of control modelling used and the optimal geometry of the device, with optimal energy capture as a finality. Hence, for cases that focus on ocean energy, control modelling suggests performance benefits. Assuming the main power converter is designed first, adding a control suggests a significant optimisation of power capture. Despite this, the implementation of the tidal turbine control application has not yet been achieved, but there is a great similarity between the control of wind turbines and tidal turbines, with the density difference estimated to be 1000 times higher in the application of tidal turbines (Goleman et al., 2019). Analyses were also done to see if improving a control system could drive the system more aggressively to add energy capture, which might lead to a reduction in travel time.

Generally, tidal streams begin power generation at 2m/s to 6cm/s which deferent from the wind speeds of about 6.7 mph (3 m/s). The use of a drive amplifies the motion of an alternating wave energy device, which could have a dramatic effect on the movement of the device. Therefore, the balance between increased power consumption and increased device wear (cost) needs to be analysed in depth (Ghefiri et al., 2015). While potentially disrupting the more aggressive movement of the system, several control features can be used as a designer in the practical area. In addition, most optimal control developments that facilitate an explicit arrangement between control action and the main objective (e.g. traceability of the point of recipient energy maximisation, etc.), offers a handle of the modelling of the system on the level of aggressiveness of the command (Goleman et al., 2019).
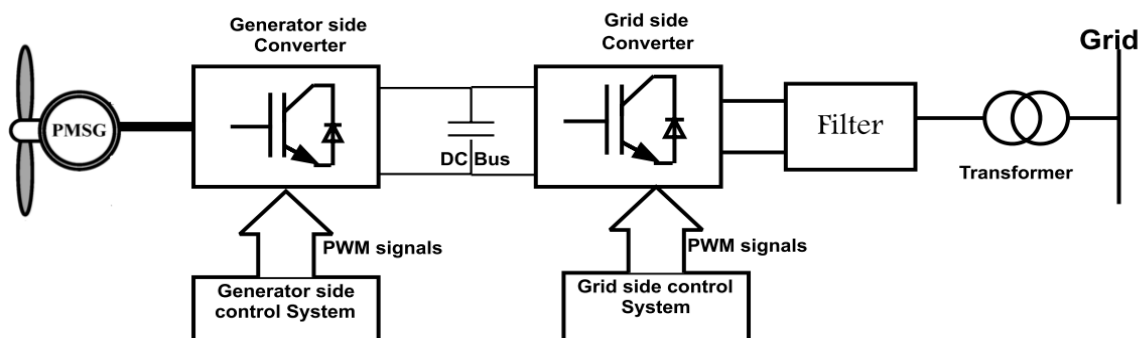
Figure 3—1: The design of the TST topology (Tripura, 2019).

Figure 3-1 below indicates a grid in direct connection to the drive turbine with a Permanent Magnet Synchronous Generator (PMSG)(Tripura, 2019).Full-rated back-to-back converters connected PMSG is also presented with the grid side control setup of generator side and grid side converters usage (Elzalabani et al., 2015; Allmark, 2017). The turbine setup operates for variable speed turbine control designs, such as optimal lambda control, which could be reached by controlling the generator feedback torque. Furthermore, the turbine driveshaft is directly connected to the turbine rotor on one side and the generator rotor on the other. Many technologies have been developed to harness the tidal energy from the seawater, such as the horizontal axis tidal turbine and the vertical axis tidal turbine which is rotating around a vertical axis (Rourke et al., 2010; Chica et al., 2015). The tidal turbine rotation must be kept parallel to the current direction and its rotor need to be controlled to follow the current direction, to improve the harnessing power energy efficiency (Zanette et al., 2010).

It has been noted that the tidal current turbines allow the extraction of the energy from the kinetic movement of water much as wind devices do extract energy from the air. As indicated schematically in Figure 2-31, The mechanical drive train and the generator play a key role to convert the kinetic energy of the tidal currents into mechanical energy shown in form of mechanical torque T_m that controls the drive train with the generator angular speed ω_r generating electrical torque ω_m that drive the generator and rotor angular speed ω, R controlling the tip speed ratio of the turbine (Allmark, 2017).

Hydrokinetic devices are ideally located at the place where there is stable flow throughout the year and are not exposed to great flood events, turbulence (Johnson & Pride, 2010). The power available in the displacement of tides is the kinetic energy of seawater motion. Finally, it has been suggested that different "levels" of control may be important in the field of tidal energy as indicated below **(**Figure 3-2). There is a higher level of supervisory control which assists in the assessment of the incident of energy resources and could hamper the operation of the device in the face of excessive situations. Such a decrease could be a recommendation to keep the device properly, to reassure itself of self-operation, as in the case of wind turbines. For the application of tidal power (as opposed to wind power), the extremes of current flow are well known, and the tidal current device was designed to operate in an energy capture system over this relatively narrow working range. For instance, the speed controller is allowed to compare the optimum generator speed, $\omega_{opt} \, Gen$ and actual generator speed, $\omega_{mec} \, Gen$, which is measured, in order to produce a reference signal for the electromagnetic torque of the generator. The reference signal of the electromagnetic torque T_{e^*}, is used as input to the generator controller ZDC SVM (Sousounis & Shek, 2019; Sousounis et al., 2019).

52
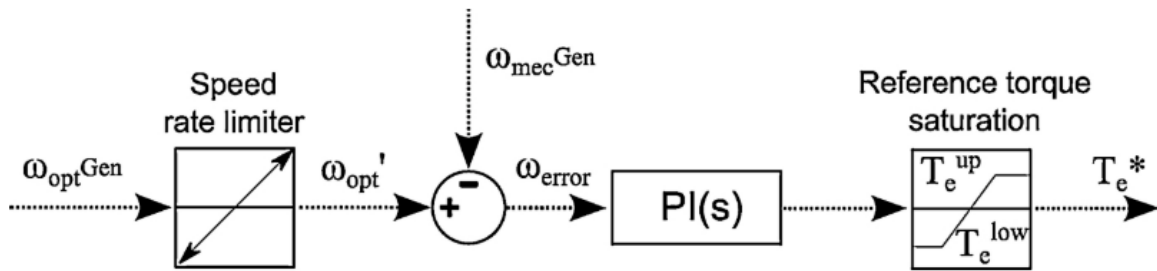
Figure 3—2: Typical tracking speed problem for a control system(Sousounis et al., 2019).

3.2. Control of tidal systems

Figure 3-3 presents the power extracting strategy for a tidal turbine system. It is an ideal power strategy that is generally utilised as the fundamental parameter of control strategies that allow harnessing the energy from tidal turbines. The tidal turbine does not operate below a pre-defined cut-in tidal velocity V_c (Nanos et al., 2015). As the tidal velocity V rises above the turbine's cut-in speed, the power supplied by the generator augments proportionally to the cube of the tidal velocity by following an MPPT strategy. When the tidal velocity achieves the rated tidal speed V_R, the generator/converter set is suppling as……….
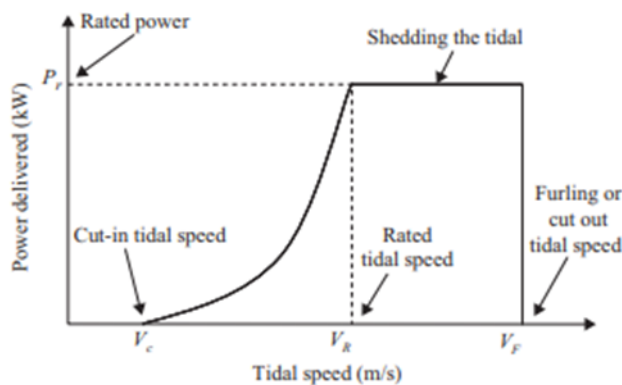
Figure 3—3: Idealized power curve of power.

The tidal turbine is designed for some speeds range and the power must be limited. The reason some parameters must be controlled such as the generator speed, blade angle adjustment.

During the operation of the tidal turbine, the power output remains constant as the tidal velocity increases above the rated velocity (Nanos et al., 2015). The strategy used for MPPT and the power constraint is shown in Figure 3-4   pitch control.
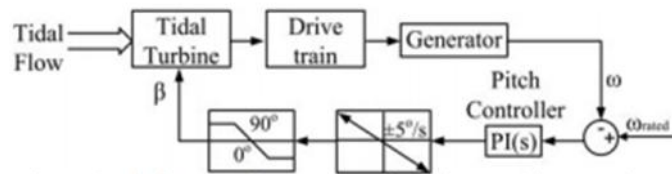
Figure 3—4: Pitch controller structure based on turbine speed (Sousounis et al., 2014).

3.2.1. Control of tidal current system Electrical generators

This part of the work presents the modern power electronic controller method which can establish a complete variable speed control. Firstly, the field and voltage-oriented controllers were developed, followed by proportional-integral (PI) . Finally, some problems concerning power converters reliability were developed as well.

3.2.2. Control of back-to-back converters in full-converter variable speed configurations

This part indicates how controlling the variable speed with back-to-back converters can increase the performance of tidal power generation take-off systems. This section provides a control program for a variable speed solution with a complete- converter design and a PMSG. A field-oriented control (FOC) program for the generator-side converter and a voltage-oriented control (VOC) for the grid which is in connexion with the converter is analysed.

3.2.3. Generator-side power converter control

The generator-side power converter controller adjusts the speed and/or torque of the electric generator in reference t FOC vectors parameters evaluated by a higher-level controller. Figure 3-5 below classified the variable frequency control techniques into different categories (Esmaeilian et al., 2014). These control techniques can be grouped into two categories such as scalar and vector controls. Regarding the control, only some parameters were determined such as the magnitude and frequency of the voltage, current, and flux linkage vectors. Thus, the control system is not applied to the space vector localisation during transients (Wang et al., 2018). On the contrary, the vector control depends on a relationship that is verified for an effective transient, also the instantaneous voltage position, current, and flux space vectors are controlled. Therefore, the control of the system is adjusting the space vectors' position and

ensure g the accurate orientation for both steady-state and transients. The VOC vs FOC vectors control is one of the most techniques, which utilises current control loops in a synchronous reference framework. The V FOC presents some advantages over VOC because it offers improved conditions of the rectifier control under non-ideal line voltage (Sanjuan, 2010). The repetition of the speed variation is an arbitrary way to maintain system acceleration, the SCIG was controlled using onshore VSC also using DTC-SVM. DTC-SVM model includes the closed-loop torque and flux control in well-structured stator flux has been implemented. The DTC SVM process control system design is presented in Figure 3-5 and Figure 5—6.
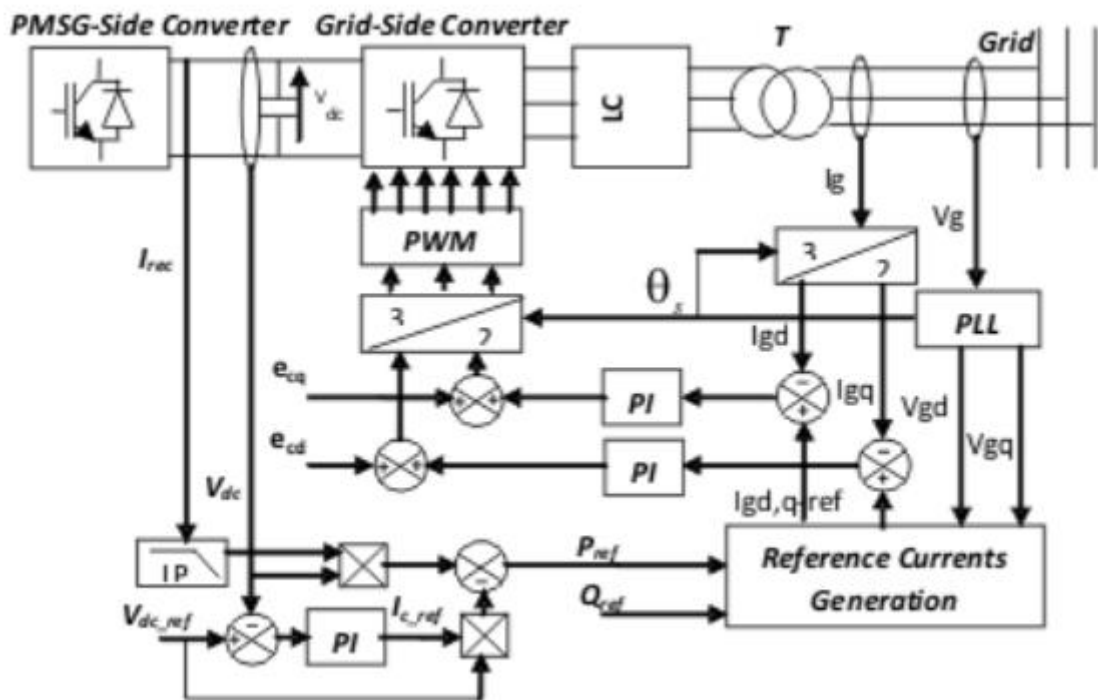
Figure 3—5:Block diagram of the voltage-oriented control technique (Allagui et al., 2014).

The FOC vectors are regulating the controlled variables i_{1d}, i_{1q} and W_m shown in Figure 3-6, it is indicated that the controlled block diagram has two nested control loops; an exterior PI controller adjusts the generator mechanical rotational speed and the two interior PI controllers that regulate the DQ stator currents (Sanjuan, 2010). In addition, decoupling terms to make the PI regulators immune to the effects of the coupling terms of the system are also included. Assuming that the internal control loops are much faster (at least five times faster).
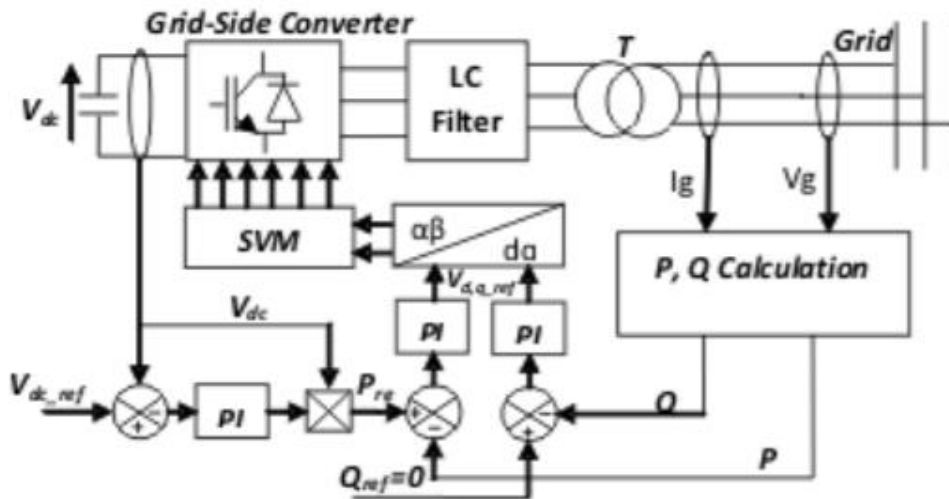
Figure 5—6: Illustration of PMSG model block diagram (Allagui et al., 2014).
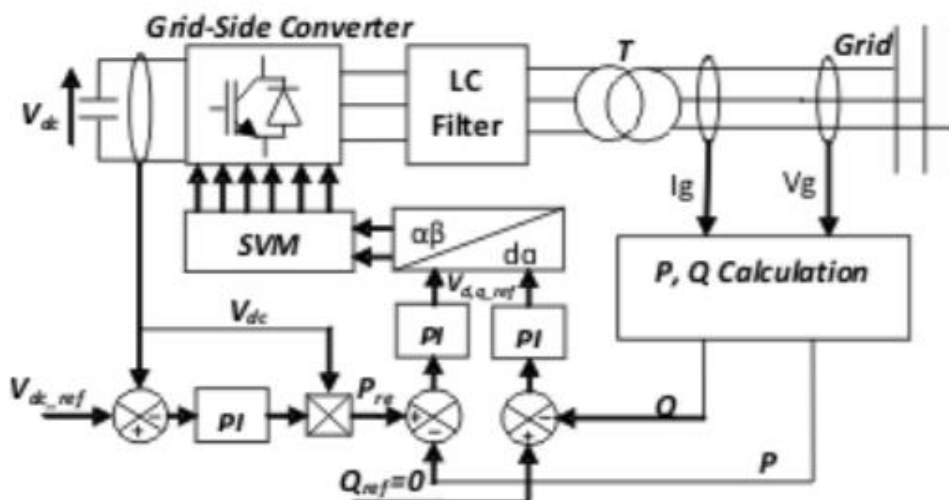
Figure 5—7: Block diagram of the direct power control technique (Allagui et al., 2014).

The zero-pole cancellation method described is used after decoupling the current loops while the transfer functions affecting the active and reactive components of the current are simplified to a first-order system as shown in Figure 3-7.

3.4. Power energy limitation control system

The tidal turbine speed needs to be controlled to enable the limitation of power output. The turbines regulation of the pitch has variable pitch blades that can feather if the turbine speed is in higher rated speed. However, the stall regulation of turbines regulation has fixed pitch blades and utilize the characteristic blade configurations to limit the speed of the turbine at rated levels. The stall regulation of the turbines produces a huge load on the blades and needs a more complex control system configuration.

3.4.1. Variable-speed fixed-pitch turbine.

The main objective of the regulation of the variable-speed fixed-pitch turbine is to adjust the power harnessed from the tidal currents using the generator speed variation. While the use of the control aims to capture the maximum available power from the tidal stream. For a tidal velocity smaller than V_R corresponds to an optimum turbine rotational speed which generates a maximum power coefficient C_p as represented in Figure 3-8 (Garcia-rosa et al., 2015). When the tidal velocities are bigger than V_R, the rotational speed is selected to maintain the turbine's output power to the rated power of the generator and drive set. In this case, the reference speed is selected to be bigger than the speed which corresponds to the maximum amount of C_P to maintain the torque value and allow it to operate in a power curve stable area (Nanos et al., 2015).
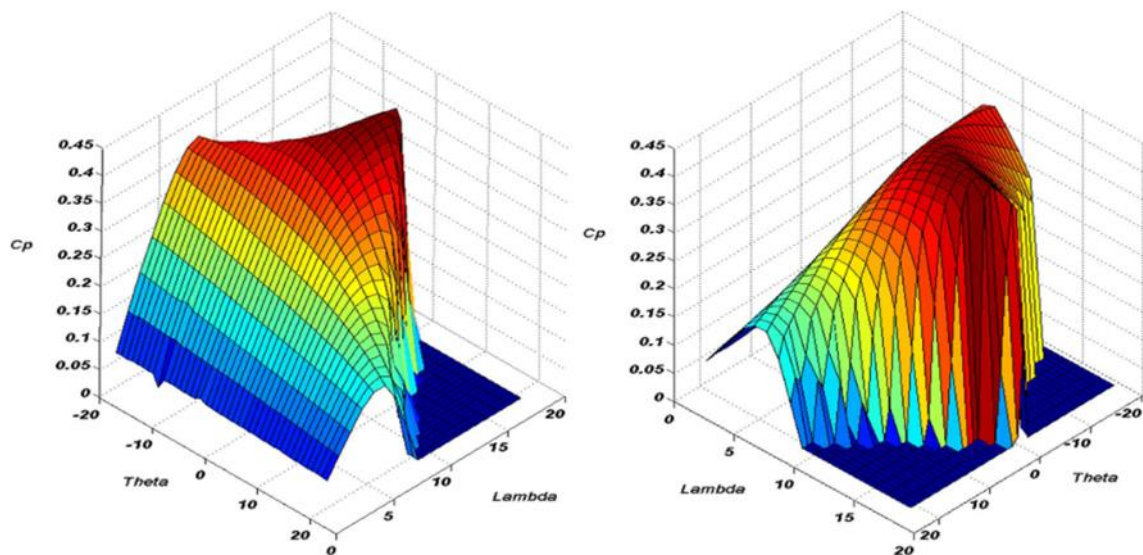
Figure 5—8: $C_p(\lambda, \beta)$ curves (Benelghali et al., 2011),(Habibi et al., 2017).

The reference indicated in Figure 3-9 and above is the reference of speeds (depending on the tidal velocity amount) that constitutes the optimal regimes configurations (ORC) (). The operation points of the turbine around the ORC ensures an optimal constant-state regime. In this condition, the capturing of power is the availability maximum of the tidal stream. This is equivalent to keeping the TSR at its optimal value l_{opt} for $V < V_R$ (Figure3-40(b)). Keeping constant TSR at its optimal value can be reached by using the turbine at variable tidal speed. This mode of operation is possible only when the generator and drive combined can control the speed in the corresponding range (Nanos et al., 2015).
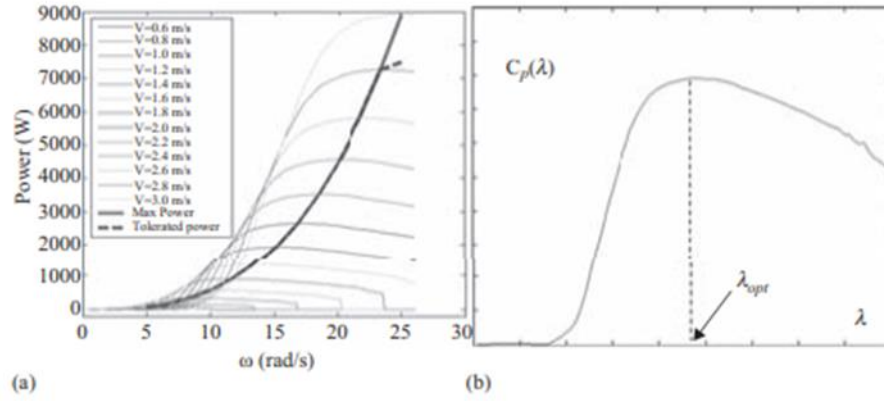
Figure 5—9: (a) Power curves for different tidal current speeds; (b) power coefficient curve.

Generally, the control approaches change by assumptions regarding the known models/parameters, the seize determination of variables, and the tidal turbine model usage. The tidal turbine model characteristics (torque and power), the optimal control of a variable speed fixed-pitch turbine is relying upon the following strategies, when $V = V_R$.

3.4.2. Shaft rotational speed optimal control using a setpoint from the turbine data.

This approach is applicable in the case where the optimal value of the TRS_{opt} is available. Utilising a setpoint from the tidal turbine data. This solution can be used whether the optimal value of the $TRS\lambda_{optimal}$ is available. The tidal turbine is operating on the ORC.

$$\lambda(t) = \lambda_{optimal} \tag{3.1}$$

This means that the shaft rotational speed is closed-loop maneuverer. To achieve its maximum value:

$$\Omega_{ref} = \frac{\lambda_{optimal}}{R} V(t) \tag{3.2}$$

3.4.3. Active power optimal control

Utilising a set-point from the shaft rotational speed data

The usage of this technique when both $\lambda(\mathbf{optimal})$ and $C_{pmax} = C_p(\lambda optimal)$ are available (Zhang et al., 2014). So, in the case where the extraction of the power can be presented as

$$\partial P_{TURB} = \frac{1}{2} C_p(\lambda)\rho\pi R^2 v^3 \tag{3.3}$$

$$= \frac{1}{2}\frac{C_p}{\lambda^3}P\pi R^5 v^3 \tag{3.4}$$

By changing $\lambda\left(\mathbf{optimal\ and\ C_{pmax} = C_p}\right), (\lambda_{\mathbf{optimal}})$, one results in the power reference for the second portion of the power tidal speed curve.

$$P_{TURB} = P_{ref} = k\omega^3_{ref} \tag{3.5}$$

Where $K = \dfrac{1}{2}\dfrac{C_{p(optimal)}}{\lambda_{optimal}}\rho\pi R^5$ (3.6)

This method assumes an active power control loop being utilised; whose reference was determined from Equation (3.6). This approach is generally applied, particularly for power wind turbines, and can still be employed for tidal turbines (Ngancha et al., 2017).

3.4.4.1. Tidal torque control loop

Following the procedural rules to make the power energy generation more efficient and optimised the capturing of energy, the rotor turbine needs to function at the maximum achievable power. This is made possible by fixing the electromagnetic torque (T_{ref}) which is equivalent to the tidal torque relating to the maximum possible power. The turbine operates at maximal efficiency when it is turning at optimal TRS_{lopt}, then the maximal power is proportional to the cubed rotational speed equations (3.7) and (3.8) (Garcia-rosa et al., 2015).

$$T_{ref} = \eta k\omega^2_{ref} \tag{3.7}$$

If the condition $V > V_R$ is satisfied, so the reference torque needs to be constrained to

$$T_{ref} = \frac{P_r}{\omega} \tag{3.8}$$

Additionally, the turbine control configuration enables the tidal speed to be tracked within acceptable mechanical loads limitation, but this approach can only be used for a slow tidal speed change. However, in the case of a strong turbulent tidal current, filtering is important to make sure a sufficient slow closed-loop changes.

3.4.4.2. Speed control loop

The controller architecture depends on the turbine linearised simulation. The basic closed-loop configuration is presented in Figures 3-10. An ascending gain, k_p, consequently, guarantee an improved tracking performance. Even though, one needs the inclusion of control effort (torque) constraints, so k_p values need also be restricted at some limit. Although the constant-state speed error is estimated to be zero, there will every time be nonzero forceful errors because of a significant adaptable reference signal W_{ref}. The imposing of the closed-loop performances is ensured for the selection of the working point. Both the gain and the time steady of the torque.
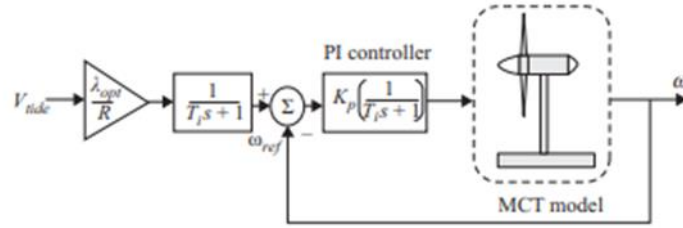
Figure 3—10:Turbine PI control configuration (Benelghali et al., 2012).

In this case, the peed control loop case-controlled system around a certain constant-state working point based on that working point (through tidal velocity and rotational speed) represent in Table 0—1.

Table 0—2: The hydrodynamics of tidal turbine parameters.

Parameters	Value
Nominal mechanical out power	1.5. e6
The base power of the electrical generator	1.2
Speed of water	12
Base rotational speed (pu of the base generator)	35000

3.4.4.3. Power control loop

The electromagnetic torque is the system input, and the generation of active power P is the output. The controller structure depends on the parameters of the system response at step variations in the generator torque for a set tidal speed. The contrast between the tidal torque and the electromagnetic torque causes the change of the rotational speed, such that the power augments gradually according to the tidal speed dynamically until it achieved a new constant-state value (Nguyen et al., 2015; Elzalabani & Nafeh, 2015; Benelghali et al., 2012). The control system is defined in the synchronous d-q frame. For the proposed control strategy, the permanent magnet synchronous generator dynamic model is written in the s-domain with the stator voltage given by (Ghefiri; et al., 2017)**:**

$$\begin{cases} -(R + L_{ds})i_d = V_d - \varphi_s\omega_s \\ -(R + L_{ds})i_q = V_q - \varphi_s\omega_s \end{cases}$$ (3.9)

The mechanical equation is expressed by.

$$T_{gen} - T_{em} = (J_s + h)\Omega_{gen} \tag{3.10}$$

Where $\Omega = \frac{\omega_s}{P}$ is the mechanical speed and $\boldsymbol{T_{gen}}$ is the mechanical torque provided by the gearbox or directly by the turbine (in a directly driven system) to the generator shaft.

The electromagnetic torque $\boldsymbol{T_{em}}$ is defined by the turbine as:

$$T_{em} = \frac{3}{2}P(\phi_d i_d - \phi_q i_d) = \frac{3}{2}[\phi_m i_q + (L_d - L_q)i_d i_q] \tag{3.11}$$

$$\text{With} \quad \begin{Bmatrix} \phi_d = L_d + \phi_m \\ \phi_q = L_q i_q \end{Bmatrix} \tag{3.12}$$

The generator chosen for simulation is a surface-mounted permanent magnet synchronous generator. (Sanjuan, 2010). Therefore, there are no saliency effects and $\boldsymbol{L_d = L_q}$ so the electro magmatic torque $\mathbf{T_{em}}$ can be simplified as:

$$\mathbf{T_{em}} = \frac{3}{2}P\phi_m i_q \tag{3.13}$$

An incorporated loop is a must for the current (torque) control. Then an external loop can be utilised to regulate the tidal turbine shaft speed. As indicated in Figure 3-10 above the PMSG rotor speed can be manoeuvred through the rotor current $\mathbf{I_q}$ which is relative to the torque. It is noted that in the case of a fixed-pitch turbine, the limit of power can be reached via an over-speed process (the generator and the converter set need to be structured to be regulated in the matching speed range).To demonstrate how the control is behaving, the PMSG-based turbine is simulated for a changing tidal speed (Paz, 2020).

3.5. Control scheme

The control scheme chosen in this case study is the voltage-oriented control techniques illustrated in Figure 3-12. The system has a fast dynamic response and consists of controlling the output DC voltage through a double loop structure of the current. The outer loop is a DC-link voltage control producing the inner current references (Wang et al., 2018).
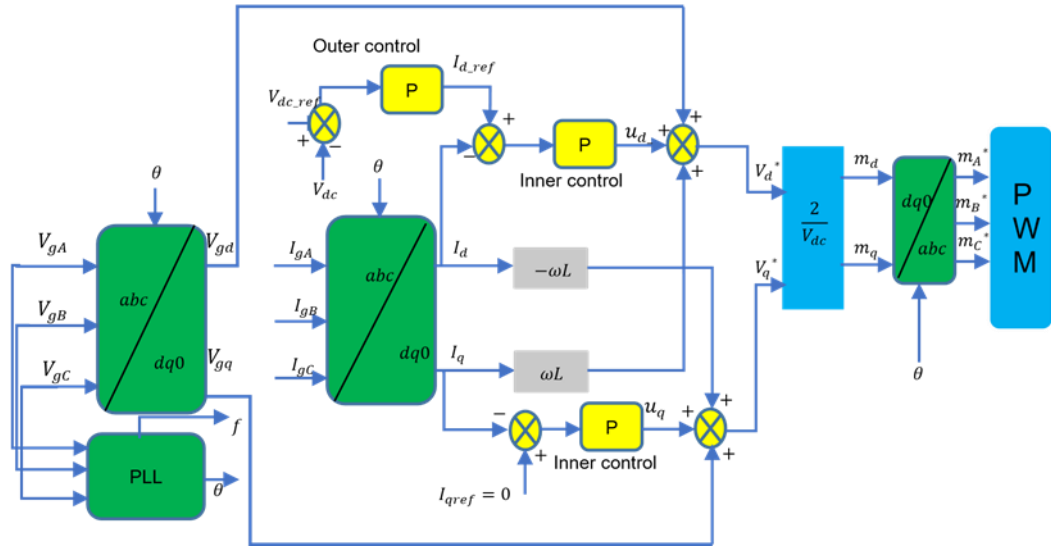
Figure 3—11: PWM rectifier control scheme (Esmaeilian et al., 2014).

3.5.1. Outer loop control

The converter is controlled using an outer voltage control loop and an inner current control loop. The DC-link voltage is evaluated and compared against a voltage set point. The error signal is converted to a d-axis current setpoint using a PI regulator. The circuit is managed to reach a unity power factor by setting the q-axis current setpoint to zero. The dq-current setpoints is will be fed to a current controller (Wang et al., 2018). The outer loop control keeps constant the DC-link voltage value near to a set DC reference voltage, which needs to be much higher than the generator peak voltage to maintain the converter's diode blocked. When the condition satisfaction is achieved, the DC-link voltage is evaluated and compared to the set DC reference. The error resulting from the comparison is used to produce the reference id current for the current loop through a PI controller. The transfer function of the outer loop controller is illustrated below (Benelghali et al., 2012; Teodorescu et al., 2011):

$$TF_v = k_{pv} + \frac{k_{pv}}{sT_{iv}} \tag{3.14}$$

Where the tuning parameters can be estimated as bellows (Teodorescu et al., 2011):

$$\begin{cases} k_{pv} = 0.12 \frac{C_{dc}}{T_s} \\ T_{iv} = 17T_s \end{cases} \tag{3.15}$$

Where k_{pv} shows the proportional gain, T_{iv} the time integrator in the outer voltage loop, T_s is the sampling period representing as below:

$$T_s = \frac{1}{f_s} \tag{3.16}$$

3.5.3. Inner Loop Control

Within the inner loop, the current id and iq resulted through the dq0 generator transformation of the current I_a, I_b and I_c are in comparison respectively using the i_{d-ref} generated at the outer loop and i_{q-ref} which is set to zero. The transfer function of the inner loop controller is indicated below (Esmaeilian et al., 2014):

$$TF_i = k_{pi} + \frac{k_{pi}}{sT_{ii}} \tag{3.17}$$

Where k_{pi} and T_{ii} are estimated with the equation below (Teodorescu et al., 2011):

$$\begin{cases} k_{pi} = \frac{L_s}{3T_s} \\ T_{ii} = \frac{L_s}{R_s} \end{cases} \tag{3.18}$$

Where k_{pi} represents the proportional gain and T_{ii} indicates the integration time constant of the inner loop control.

Table 0—3 illustrates respectively the tuning parameters of the outer and the inner loop controls.

Table 0—4: Rectifier control design parameters

Control loop parameters	
Outer loop	
K_{pv}	133.5
K_{iv}	133500
Inner loop	
K_{pi}	3.24
K_{ii}	50.625

3.5.4. Modulation control
The modulation signals md and mq are used to generate the PWM signals to drive the rectifier switches based on the following equation (Esmaeilian et al., 2014):

$$\begin{cases} m^*{}_d = \frac{2}{V_{dc}}(V_{gd} + L_s\omega I_d + u_d) \\ m^*{}_q = \frac{2}{V_{dc}}(V_{gq} - L_s\omega I_q + u_q) \end{cases} \tag{3.19}$$

Where V_{dg} and V_{gq} are the disturbances from input power transmission, ud and uq are the current errors output signals.

Summary

The control of the tidal systems, which includes different major components such as Blackbox modelling, and the simulation plays a key role in improving the performance and economic viability of tidal power systems. While the more traditional control issues for energy generation regulation is more present to a large extent in applications of marine currents energy, some of

the basics problems such as the conversion of energy at maximum level. However, there are other different aspects of control technology which does not apply to marine energy systems. It can be noted that the fault-tolerant control technology can be used to control the arrays of tidal turbines to maintain grid compliance and smooth energy output of a tidal power systems farm. While the voltage-oriented control techniques applied to the tidal system possess a fast dynamic response and consist of controlling the output DC voltage through a double loop structure of the current.

CHAPTER FOUR: MATHEMATICAL MODELLING OF A TIDAL ENERGY SYSTEM

4.1 Introduction

This chapter deals with the mathematical modelling of each tidal power system connected to grid components. These components include the Drive train, permanent magnet synchronous, LCL filter, filter capacitor, back-to-back converters, such as DC to DC boost converter, DC-to-DC buck converter and voltage source inverter. The control designs of power electronics converters devices mentioned are illustrated in Figure 4—1.
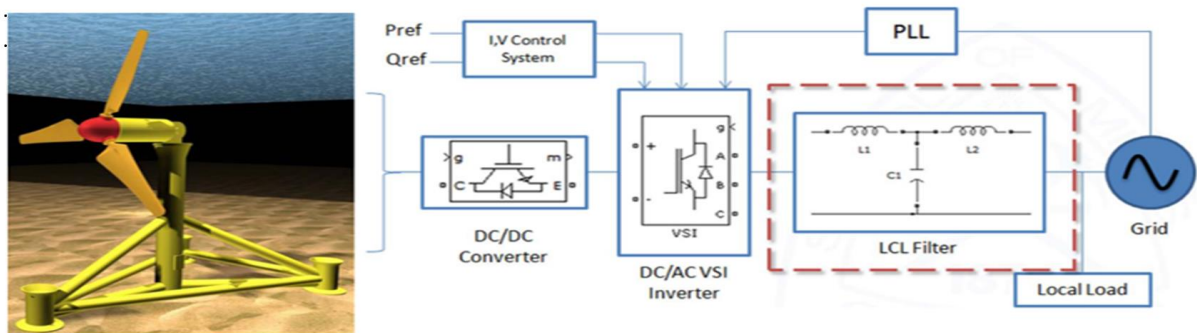
Figure 4—1: General schematic for grid-interconnected dc power source

4.2. Drive train modelling

The mechanical model is part of the dynamical system of the tidal current turbine that allows the interaction with the grid side but particular attention will be given to the drive train because this part of the tidal turbine structure is very important due to its impact on the power fluctuations (Jahromi et al., 2013). The mechanical drive train can be represented as a two-mass model, a large mass describing the rotor, and a smaller mass shown in Figure 4-2 (Habibi et al., 2016). The rotation of masses contains the inertia T_{gen} and T_{gen}. The connection of the (low speed) rotor shaft to (high-speed) generator shaft using a 1: N gearbox. The low-speed shaft is modelled using a stiffness k and a damping coefficient c, while the high-speed shaft is assumed stiff (Khan et al., 2010). The drive train is transferring the dynamical rotor torque water, T_{rot}, into weak speed shaft torque T_{gen} (Khaoula Ghefiri et al., 2017; Habibi et al., 2017). The mechanical modelling dynamical definition is illustrated by the following equation (4.37).

$$\begin{cases} \dfrac{d\Theta_{rot}}{dt} = \omega_{rot} \\ \dfrac{d\Theta_k}{dt} = \omega_{rot} - \dfrac{\omega_{gen}}{\omega_{gear}} \\ \dfrac{d\Theta_{rot}}{dt} = \dfrac{(T_{rot} - T_{gen)}}{J_{rot}} \end{cases} \qquad (4.1)$$

With $\mathbf{q_k}$ which is the angular difference between the two extremes of the flexible shaft. In an easy way, $\mathbf{q_k}$ can be taken as an invariable parameter and the drive train modelling can be simplified as indicated in Figure 4-2.
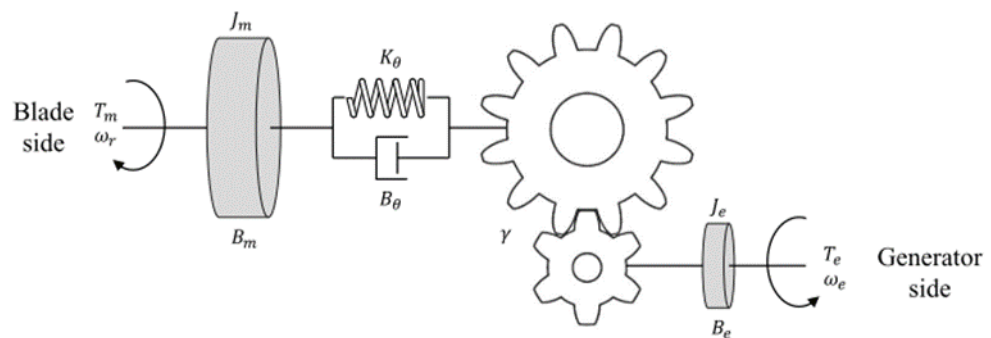
Figure 4—2:The Drive train rotational modelling(Habibi et al., 2017; Biweta & Mamo, 2017; Nanos et al., 2015).

For instance, the simulation model results use BEM theory, for a provide three-blade turbine, indicated in Figure 4-2, illustrates the rotor power coefficient C_p according to the variation of the pitch angle variation of the blades β and the speed ratio λ (Jahromi et al., 2013).

4.3. Modelling of permanent magnet synchronous of tidal generator

Various types of generators can be employed in tidal power systems as the induction generators are classified into two groups, those with squirrel cage (SCIG) and those with wound rotor (WRIG), Figure 2-25 and Figure 2-26. However, in this study, the adopted type of generator was the permanent magnet synchronous generator.

4.3.1. Modelling of permanent magnet synchronous

In this work, the PMSGI   was taken into account as shown in Figure 4-3, tidal generation system due to many advantages such as higher efficiency, its simple structure, its capability of function at slow speed, itself-excitation ability leading to high power factor and high-

efficiency operation (Benelghali et al., 2010). Moreover, the fact that the PMSG is constructed without a gearbox, and it contains the variable speed control improved the availability of the system; reduced its active weight, and mitigated the frequency of maintenance. The design of (Elzalabani & Nafeh, 2015). Two power conversion stages are indicated in Figure 4-4: the ac/dc and dc/ac stages. In grid-connected systems, two important topologies such as ac/dc power conversion which is used: diode-bridge passive rectifier and the one that contains the boost converter or a three-phase full-bridge active rectifier (back-to-back converter) (Ikni et al., 2014).
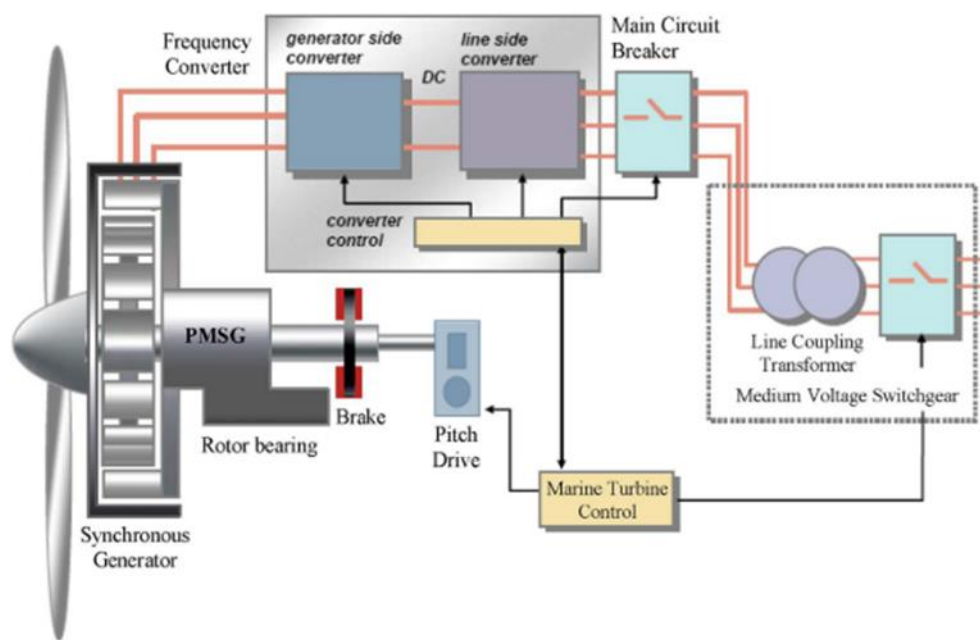
Figure 4—3:Schematic diagram of a PMSG-based generation system (Benelghali et al., 2011).

The wind energy technology extraction is similar to one of the tidal energies. Thus, most of the extraction wind generator topologies model can be applied in tidal energy harnessing (Zhou et al., 2015). This part focused more on the PMSG model associated with back to back IGBT converter (Khaoula Ghefiri et al., 2017). According to the PMSG, the stator voltage equations in fixed reference structure are presented as follows equation (4.2).

$$[V_{abc}] = [R][i_{abc}] + [L]\frac{d(i_{abc})}{dt} + \frac{\lambda abc}{dt} \qquad (4.2)$$

Where $[L] = \begin{bmatrix} L_{xx} & M_s & M_s \\ M_s & L_{xx} & M_s \\ M_s & M_s & L_{ss} \end{bmatrix}$

The PMSG is modelled in a simplified assumptions way.

        A.   sinusoidal distribution of stator winding,

        B.   electrical and magnetically symmetry,

C. almost inexistence iron losses and unsaturated magnetic circuit.

Considering these assumptions, the generator model in the constant-state (or stator) coordinates all its conditions (Sanjuan, 2010).

From equation (4.2), a simplified model suitable for simulation modelling and control can be evaluated in d-q rotor coordinates. Conversion between (a, b, c) and d-q coordinates can be $J_{rot}, T_{rot}, T_{gen}$ low-speed shaft gearbox high-speed shaft generator θ_{rot} 1: η gear, θ_{gen} (Zhou et al., 2015). Figure 4-2 a simple drive train model 310 Electric design for tidal energy structure implemented using the classical park transform. Utilising this transform, the d-q PMSG voltages and fluxes are obtained as shown by equation below (Nguyen et al., 2015):

$$\begin{cases} V_d = R_{id} + L_d \frac{di_d}{dt} - L_q i_q \omega_s \\ V_q = Ri_q + L_q \frac{di_d}{dt} + (L_d i_d + \phi_m)\omega_s \end{cases} \qquad (4.3)$$

The electromagnetic magnets torque is presented as follows:

$$T_{em} = \frac{3}{2} P(\phi_d \cdot i_d - \phi_q i_d) = \frac{3}{2} P[\phi_m i_q + (L_d - L_q)i_d i_q] \qquad (4.4)$$

Whether the permanent magnets are mounted on the rotor surface, then $L_d = L_q$ and the electromagnetic torque is obtained as:

$$T_{em} = \frac{3}{2} P \phi_m i_q \qquad (4.5)$$

In the assumptions the mounting of permanent magnets on the rotor equation of rotating parts (generator, rotor, drive train, turbine) (Zhou et al., 2015). For instance, for a direct drive system, the mechanical equation is.

$$T_{gen} - T_{em} - T_I = J \frac{d\Omega}{dt} \qquad (4.6)$$

Where T_{gen} is described as a mechanic torque that is generated by the gearbox or directly from the tidal turbine (Jahromi et al., 2013). These are input parameters for the generator. The assumptions of the torque can be done from the gearbox configurations, the tidal turbines power curves, the flow speed and the tidal turbine rotational speed is a torque that describes the mechanical and iron losses. T_I is a torque which describes the mechanical and iron losses (Zhou et al., 2015; Khaoula Ghefiri et al., 2017). As the main generator electric parameters are provided (L_d, L_q, ϕ_m), (The mechanic parameters of the generator) in equations (4.3), (4.4) and (4.5) can be utilised for the simulation of the electro-mechanic behaviour of the generator. It can be noted that the nominal magnetic flux ϕ_{nom} into the round rotor PMSG is indicated as shown by equation below (Caixeta et al., 2014).

$$\phi_{nom} = \frac{\sqrt{6V_{nom}}}{3\omega_{nom}} \qquad (4.7)$$

Where $\mathbf{V_{nom}}$ is the nominal voltage, ω_nom is the angular velocity of the generator, and ϕ is the magnetic flux.

The linkage magnetic flux ϕ can be determined utilising equation 4.44 below:

$$\phi = \phi_{pu} X \phi_{nom} \tag{4.8}$$

Where $\phi_{\mathbf{pu}}$ is the magnetic flux per unit value, and $\phi_{\mathbf{nom}}$ indicates the total flux of the magnet.

The nominal power $Pnom$ of a round rotor PMSG is indicated by the equation:

$$P_{nom} = \sqrt{3}\ V_{nom}I_{nom}\cos\varphi \tag{4.9}$$

Where $\mathbf{V_{nom}}$, $\mathbf{I_{nom}}$ and $cos\varphi$ are respectively the nominal voltage, current, and power factor.

The nominal impedance $Znom$ of a round rotor PMSG is evaluated as follows:

$$Z_{nom} = \frac{V_{nom}}{I_{nom}} \tag{4.10}$$

The stator resistance Rs is determined by the following equation:

$$R_s = R_{pu}Z_{nom} \tag{4.11}$$

Where $\mathbf{R_{pu}}$ represents the resistance per unit value, and $\mathbf{Z_{nom}}$ indicates the nominal impedance. The nominal inductance $\mathbf{L_{nom}}$ of around rotor PMSG is evaluated as follows:

$$L_{nom} = \frac{Z_{nom}}{\omega_{nom}} \tag{4.12}$$

Where ω_{nom} represents the angular velocity.

The inductance of a round rotor PMSG $\mathbf{L_{dq}}$, $\mathbf{dqo}$ frame can be evaluated as follows:

$$L_{dq} = L_{dq-pu}L_{nom} \tag{4.13}$$

Where $\mathbf{L_{dq-pu}}$ is the inductance per unit value.

The moment of inertia J of a round rotor PMSG is determined by the following equation 4.14 (Wang et al., 2015):

$$J = \frac{2N_p{}^2 HP_{nom}}{\omega_{nom}} \tag{4.14}$$

Where $\mathbf{N_p}$ is the number of pole pairs and H represents the inertia constant. The electromagnetic torque is the system input, and the generation of active power P is the output. The controller structure depends on the parameters of the system response at step variations in the generator torque for a set tidal speed in Figure 4-4 (Garcia-rosa et al., 2015). The contrast between the tidal torque and the electromagnetic torque Figure 4-5 causes the change of the rotational speed, such that the power augments gradually according to the tidal dynamic speed until it achieves a new constant-state value (Benelghali et al., 2011).
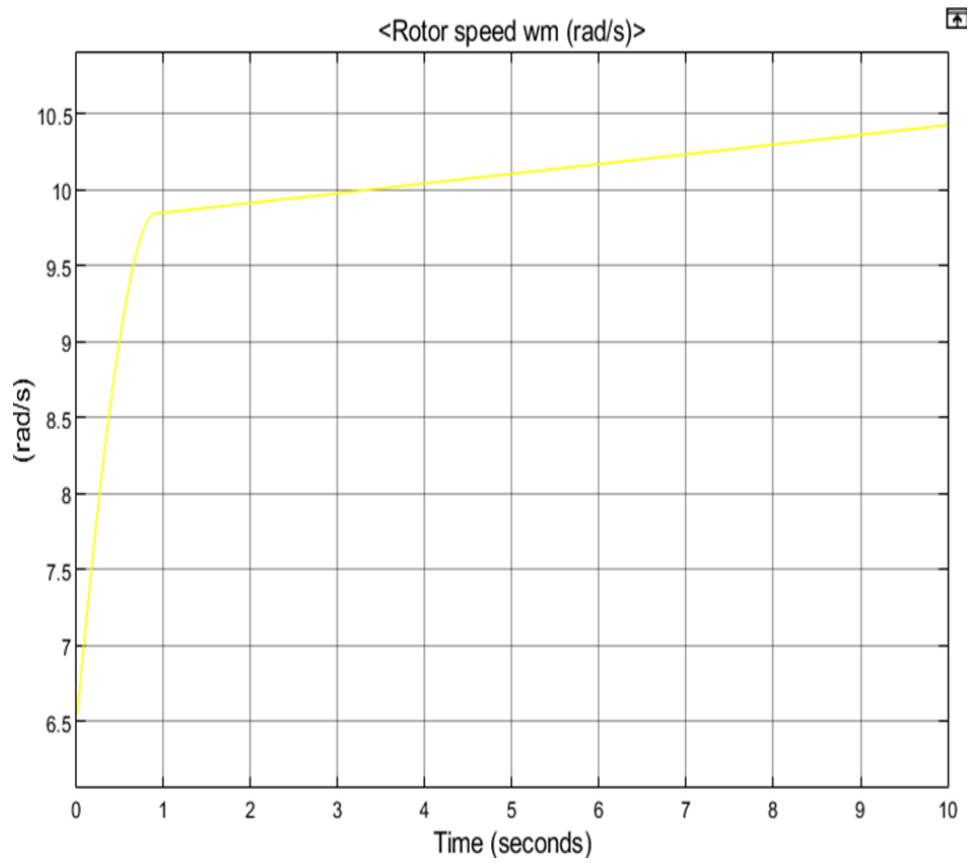
Figure 4—4: Rotor speed.
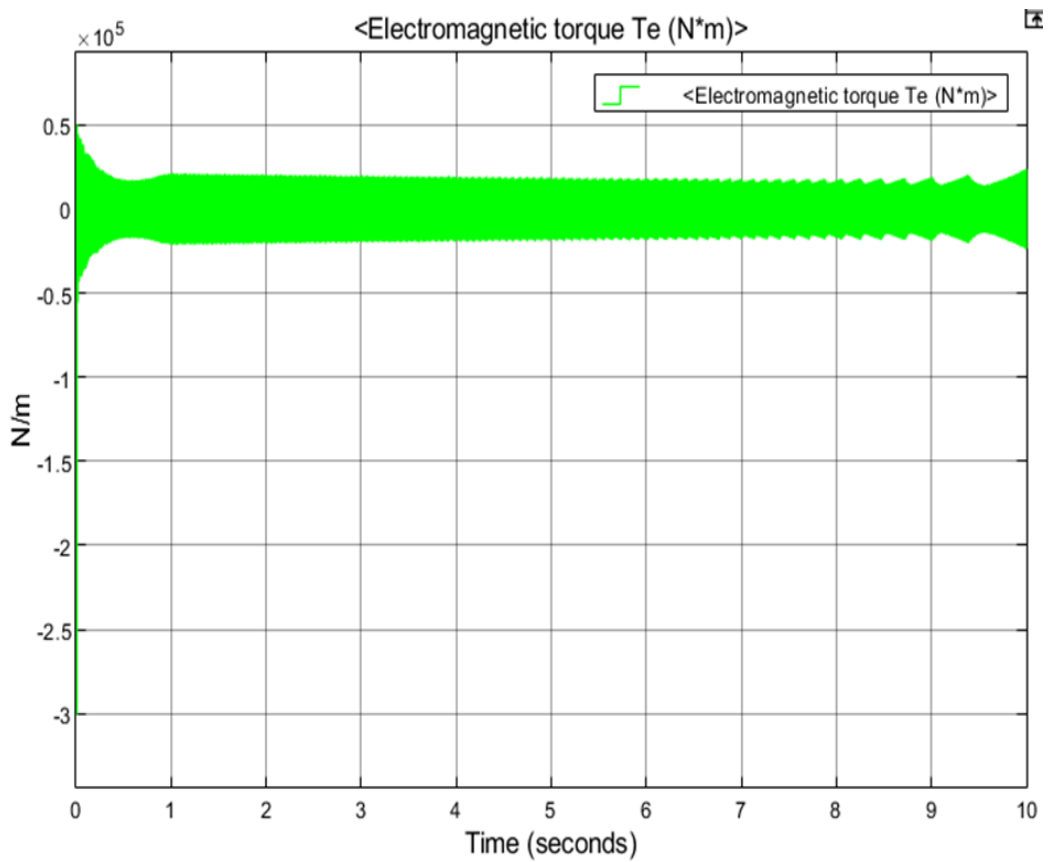
Figure 4—5: The tidal torque and the electromagnetic torque.

As an example, an optimal control based on a PI speed controller has been simulated using a dedicated MATLAB/Simulink library with a variable speed and fixed-pitch turbine-driven PMSG (Nguyen et al., 2015). The control system is defined in the synchronous d-q frame. For the proposed control strategy, the permanent magnet synchronous generator dynamic model is written in the s-domain with the stator voltage as shown below (Khaoula Ghefiri et al., 2017):

$$\{-(R + L_{ds})i_d = V_d - \phi_q \omega_s\} \tag{4.15}$$

$$\{-(R + L_{ds})i_q = V_q + \phi_d \omega_s\} \tag{4.16}$$

The mechanical equation is expressed by.

$$T_{gen} - T_{em} = (J_s + h)\Omega_{gen} \tag{4.17}$$

Where $\Omega = \frac{\omega_s}{P}$ is the mechanical speed and $\boldsymbol{T_{gen}}$ is the mechanical torque provided by the gearbox or directly by the turbine (in a direct driven system) to the generator shaft.

The electromagnetic torque $\mathbf{T_{em}}$ is defined by the turbine as.

$$T_{em} = \frac{3}{2}P(\phi_d i_q - \phi_q i_q) = \frac{3}{2}\left[\phi_m i_q + (L_d - L_q)i_d i_q\right] \tag{4.18}$$

$$\text{With } \begin{Bmatrix} \phi_d = L_d + \phi_m \\ \phi_q = L_q i_q \end{Bmatrix} \tag{4.19}$$

The generator chosen for simulation was a surface-mounted permanent magnet synchronous generator. Therefore, there are no saliency effects and $\mathbf{L_d = L_q}$.

Then the electro magmatic torque $\mathbf{T_{em}}$ can be simplified as

$$T_{em} = \frac{3}{2}P\phi_m i_q \tag{4.20}$$

To demonstrate how the control is behaving, the PMSG-based turbine is simulating for a changing tidal speed (Paz, 2020). The parameters that were used to model the permanent magnet synchronous tidal generator are provided in Table 4-1.

Table 4—1: Tidal generator modelling parameter

Parameters	Values
P_{nom}	1.5 MW
V_{nom}	600 V
R_s	0.006
L_{dq}	0.3e-3
ϕ	1.48
J	35000
Viscous Damping	0.01
Friction	0
N_p	48

4.3.2. Modelling of LCL Filter

The three-phase LCL filter modelling using inverter rated of power P_n, the DC-link voltage VDC, the frequency of the grid f_g, the frequency of switching f_{sw}, and the frequency of sampling f_{samp}, as well as the voltage of the grid as input parameters. The LCL filter parameters are provided in Table 4—2, and the execution of its features is made possible through the following equations:

4.3.3. The Filter capacitor

The impedance Z_b and base capacitance C_b respectively, are provided by the equations below (Tarasantisuk et al., 2016):

$$Z_b = \frac{U_n^2}{P_n} \tag{4.21}$$

$$C_b = \frac{1}{W_g Z_b} \tag{4.22}$$

Where U_n represents the voltage of the grid voltage and W_g the frequency of the grid in rad per second.

The LCL filter capacitor Cf is estimated around 5% of the base capacitanc indicated in equation 4.23 (Mahlooji et al., 2018):

$$C_f = 0.05 C_b \tag{4.23}$$

4.3.4. Current ripple

The maximum current ripple at the inverter output is represented by the equation (4.24) below (Reznik et al., 2014):

$$\Delta I_{Lmax} = \frac{2V_{DC}}{3L_i}(1 - m)mT_{SW} \tag{4.24}$$

L_i **represents** the inverter side inductor, while the T_{SW} shown the switching period, and **m** indicates the inverter modulation index provided in this investigation estimated around $m = 0.57$ (Sen et al., 2014). It is indicated that the inverter side current ripple needs to be fixed around 10 − 25% of the maximum current (I_{max}), so ΔI_{max} is given as…….. (Mahamat et al., 2017):

$$\Delta I_{Lmax} = (1\% - 5\%)I_{max} \tag{4.25}$$

During this assessment, the percentage is around 1% to remain at ΔIL_{max} =0.01L_{max}, where

$$I_{max} = \frac{P_n\sqrt{2}}{3V_{ph}} \tag{4.26}$$

where V_{ph} represents the line to ground voltage. From Equation (4.26), L_i is determined as follow (Sen et al., 2014):

$$L_i = \frac{0.49V_{DC}}{3\Delta I_{Lmax} * f_{SW}} \tag{4.27}$$

The CLL filter is designed to mitigate all the predicted current estimated around 20%, resulting in an output current ripple evaluated at about 2%. Equations (4.27) and (4.28 relate to the harmonic current (Reznik et al., 2014):

$$L_g = \frac{\sqrt{\frac{1}{K_a^2}+1}}{C_f \omega_{SW}^2} \tag{4.28}$$

With K_a represents the preferable attenuation, ω_{SW} has shown the frequency of switching which is determined in rad per second, and r represents the ratio between the inverter side and the grid side inductances (Benzazah et al., 2016):

$$L_i = rL_g \tag{4.29}$$

The resonant frequency ω_{res} in rad per second, and the damping ratio (ζ) of the LCL filter is expressed in equations (4.30) and (4.31), respectively.

$$\omega_{res} = \sqrt{\frac{L_i+L_g}{L_i L_g C_f}} \tag{4.30}$$

$$ç = \frac{C_f \omega_{res} R_d}{2} \tag{4.31}$$

where R_d represents the damping resistor parameter.

Finally, the control of the resonant frequency is the last key point in the design of the system. The resonant frequency needs to be approximatively sized half of the switching frequency due to the filter requirement such as sufficient attenuation in the converter switching frequency. It can be noted that the resonant frequency for the LCL filter can be evaluated as follows (Benzazah et al., 2016):

$$f_{res} = \frac{1}{2\pi}\sqrt{\frac{L_i + L_g}{L_i L_g C_f}} \tag{4.32}$$

$$10f_g < f_{res} < 0.5f_{SW} \tag{4.33}$$

It is required to verify that the resonant frequency satisfies Equation (4.33). In contrast, the parameters should be re-evaluated. The damping resistor value can be determined using Equation (4.34) as seen in (Hamad et al., 2019):

$$R_d = \frac{1}{3\omega_{res}C_f} \tag{4.34}$$

Table 4—3: LCL Filter parameters

Parameter	Value
Inverter side inductor ((L_i)	0.9 mH
Grid side inductor(L_g)	0.072mH
Capacitor filter (C_f)	531µF
Damping Resistor (R_d)	0.118Ω
Resonant frequency (f_{res})	845 Hz
Inductor resistances ($R_i = R_g$)	0.00761 $\varOmega$
Sampling frequency f_s	10,000 Hz
Crossover frequency (f_c)	254Hz

4.3.5 Modelling of back-to-back converter

The full-scale back-to-back converter allows the link between the PMSG and the load. The converter is configured by the generator side converter and the load-side converter. The load-side inverter ensures the conversion of the DC voltage to the AC voltage and the LC filter reduces the output voltage harmonics (Biweta & Mamo, 2017). The composition of back-to-back converters linked to PMSG WECS is indicated in Figure 4-3. Using a supplementary inverter, with PMSG can provide ac power with constant frequency and voltage to the grid (Tripura, 2019).
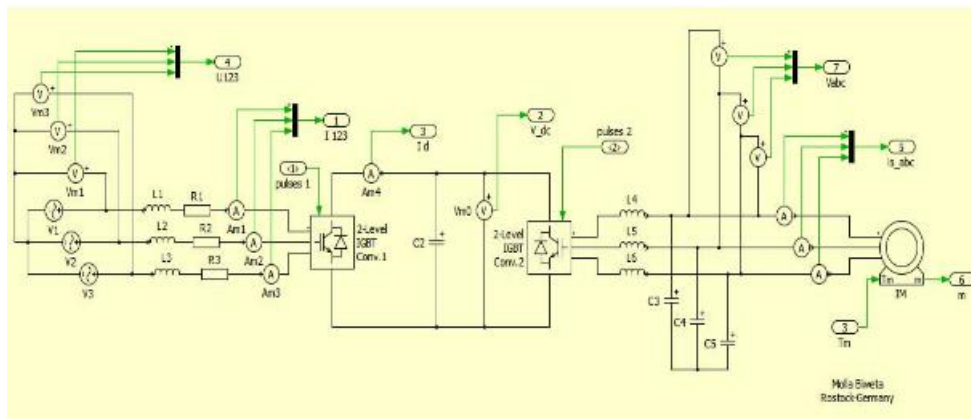
Figure 4—6:Generic Three-phase VSC electrical topology (Biweta & Mamo, 2017).

The system arrangement is indicated in Figure 4-6. The main electrical circuit model composed of a three-phase voltage source with line inductance and resistance linked to the AC-side of a back-to-back, 2-level IGBT converter (Tripura, 2019). The DC side of the converter is linked to a load, designed as an induction machine, via a DC-link capacitor (Biweta & Mamo, 2017). The tidal turbine drives a PMSM which produces an AC with variable frequency and amplitude. An active rectifier converts this 'wild' ac into a dc (Baker et al., 2014). It is a voltage source rectifier that is configured using a line inductance on the AC side (Ls, Rs), six individual IGBT switches, and a DC-link capacitor C on the DC side. The active rectifier is a three-phase IGBT

voltage source converter controlling the generator current by getting the AC power from a balanced three-phase voltage source(V_a, V_b, V_c) and the current provided are (I_a, I_b and I_c). The DC output of the rectifier supply current I_{dc} to a load RL (Baker et al., 2014). The voltage of a three-phase voltage source PWM rectifier in **abc** coordinates is indicated below (Brito et al., 2015):

$$
\begin{bmatrix} L_s \dfrac{dI_{ra}}{dt} \\ L_s \dfrac{dI_{rb}}{dt} \\ L_s \dfrac{dI_{rc}}{dt} \end{bmatrix} = \begin{bmatrix} -R_s & 0 & 0 & 0 \\ 0 & -R_s & 0 & 0 \\ 0 & 0 & -R_s & 0 \\ S_a & S_b & S_c & -1 \end{bmatrix} \begin{bmatrix} I_{ra} \\ I_{rb} \\ I_{rc} \\ I_L \end{bmatrix} + \begin{bmatrix} V_a - V_{ra} \\ V_b - V_{rb} \\ V_c - V_c \\ 0 \end{bmatrix} \tag{4.35}
$$

Where V_{ra}, V_{rb} and V_{rc} are the rectifier parameters input voltages indicated as a function of switching devices, and S_a, S_b and S_c are the switching functions, either 0 (switch is off) or 1 (switch on):

$$
\begin{cases} V_a = V_m sin\theta \tag{4.36} \\[2mm] V_b = V_m \left(\theta - \dfrac{2\pi}{3} \right) \tag{4.37} \\[2mm] V_c = V_m \left(\theta + \dfrac{2\pi}{3} \right) \tag{4.38} \end{cases}
$$

Considering Clarke's transformation, the dynamic modelling of the PWM rectifier is expressed by:

$$
\begin{bmatrix} V_\alpha \\ V_\beta \end{bmatrix} = L_s \begin{bmatrix} \dfrac{dI_\alpha}{dt} \\ \dfrac{dI_\beta}{dt} \end{bmatrix} + \begin{bmatrix} R_s & 0 \\ 0 & R_s \end{bmatrix} \begin{bmatrix} I_d \\ I_q \end{bmatrix} + \begin{bmatrix} V_{rd} \\ V_{rq} \end{bmatrix} \tag{4.39}
$$

Where V_α and V_β, $V_{r\alpha}$ and V_{rd}, andV_{rq} ,I_α and I_β are the voltage V_a, V_b and V_c the voltage V_{ra}, V_{rb}, V_{rc} and the current I_{ar}, I_{br} and I_{cr} in $\alpha\beta$ frame, respectively (Sanjuan, 2010).

In the same way, using Park's transformation, the modelling of the PWM rectifier equation is given by:

$$
\begin{bmatrix} V_d \\ V_q \end{bmatrix} = L_s \begin{bmatrix} \dfrac{dI_d}{dt} \\ \dfrac{dI_q}{dt} \end{bmatrix} + \begin{bmatrix} R_s & -\omega L_s \\ \omega L_s & R_s \end{bmatrix} \begin{bmatrix} I_d \\ I_q \end{bmatrix} + \begin{bmatrix} V_{rd} \\ V_{rq} \end{bmatrix} \tag{4.40}
$$

Where V_d and V_q, V_{rd} and V_{rq}, and I_d and I_q are the voltage V_a, V_b and V_c, the voltage.

V_{ra}, V_{rb} and V_{rc}, and the current I_{ra}, I_{rb} and I_{rc} in d-q frame respectively, and $\theta = \omega t$ is the angle between the d-axis and q-axis. By using the transformation of 4.76 into d-q rotating reference frame, the Equation was expressed as shown below (Chen & Jin, 2007).

$$
\begin{cases} V_d = L_s \dfrac{dI}{dt} + \omega L_s i_q + u_d \\[2mm] 0 = L_s \dfrac{dI}{dt} - \omega L_s i_d + u_q \end{cases} \tag{4.41}
$$

Where the resistance value is not considered because it is very small and $V_q = 0$

4.3.6. Modelling of line inductance

The inductance plays a key role in the rectifier operation. It produces an induced voltage that enables the voltage source rectifier to function in boost mode and the same time facilitates the DC-link voltage to be higher than the magnitude of the input voltage is blocking the diodes for the system's proper operation (Brezina et al., 2011). In addition, the inductance function as a filter to mitigate the current ripple and reduce the rectifier's operation range (Chen & Jin, 2007). The voltage decreases across the inductance that controls the current, and this voltage is controlled by the rectifier, although its highest value is limited by the DC link voltage (Marian et al., 2002). The inductance can be evaluated using Equation 4.42 below (Wang et al., 2013):

$$L_S \geq \frac{(V_{dc} - 3E_m)E_m T_s}{2V_{dc}\Delta I_{max}}$$
(4.42)

Where ΔI_{max} denotes the maximum ripple current generally is evaluated around 20% of the maximum current, E_m represents the peak voltage of the AC generator, and T_s indicates the sampling period.

4.3.7. Modelling of DC-link voltage

The specific operation of the rectifier relies on the minimum DC-link voltage, which is evaluated by the peak of line-to-line voltage as shown in equation 4.43 (Marian et al., 2002):

$$V_{(DC-min)} > \sqrt{2}\sqrt{3}V_{LN(rms)} = \sqrt{3}E_m$$
(4.43)

Where $V_{(DC-min)}$ is the minimum $DC-Link$ and $VLN_{(rms)}$ is described as the line to ground voltage. However, generally, the DC-link voltage relies on the PWM method, in this , study, the minimum DC-link voltage was evaluated using Equation (4.44). Considering the maximum reference voltage as $\frac{V_{DC}}{2}$, Equation (4.45), (Brezina et al., 2011):

$$V_{(LNpeak)} = \frac{V_{DC}}{2}$$
(4.44)

$$\frac{\sqrt{2}}{\sqrt{3}}2V_{LN(peak)} = \frac{V_{DC}}{2}$$
(4.45)

$$V_{(DC-min)} > 2V_{LN(peak)} = \frac{2\sqrt{2}}{\sqrt{3}}V_{LN(rms)} = 1.663VLL(rms)$$
(4.46)

However, in this , study, the DC link voltage was taken as not conforming with Equation (4.47). The DC-link capacitor was evaluated using the equation below:

$$C_{DC} = \frac{P}{2\pi f V_{DC}\Delta V_{DC}}$$
(4.47)

Where ΔV_{DC} represents the maximum ripple DC voltage, and it is around 5% of the supply voltage, V_{DC} as the DC bus voltage, P indicates the active power and f as the generator frequency.

Table 4—4: PWM regenerative rectifier modelling parameter

Parameters	Values
V_{dc}	1500 V
V_{ll}	600 V
C_{DC}	0.04 Farad

4.3.8. Modelling of Phase Locked Loop (PLL)

In this study, the Phase-Locked Loop (PLL) method was used to generate the phase angle for the transformation. A typical PLL circuit was composed of different components such as the phase detector, the loop filter, and the voltage-controlled oscillator (Behera & Thakur, 2016). The closed-loop transfer function of a PLL (Figure 4-7) is given by the equation below (Dong et al., 2011):

$$G_{PLL}(s) = \frac{\theta^*}{\theta} = \frac{K_{1s} + K_2}{S^2 + K_{1s} + K_2} \tag{4.48}$$

Where k_1 is the PI loop filter proportional and k_2 is the proportional corresponding integral gain.
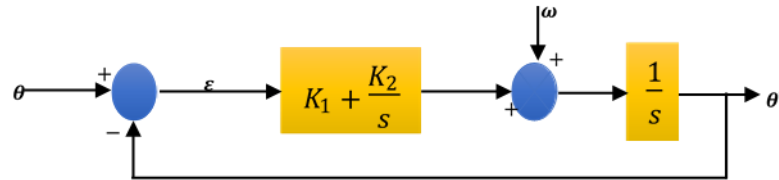
Figure 4—7: Small-signal model (Behera & Thakur, 2016).

The parameters k_1 and k_2 of a PLL can be obtained via the following equation (Teodorescu et al., 2011):

$$\begin{cases} \omega_{n-PLL} = \sqrt{K_2} \\ \xi_{PLL} = \frac{K_1}{2\sqrt{K_2}} \end{cases} \tag{4.49}$$

Where ω_{n-PLL} is the natural frequency and ξ_{PLL} is shown the damping ratio.

Table 4-4 presents the results values of K_1 and K_2.

Table 4—5: Phased Locked loop parameters.

PLL parameters	
K_1	9.7
K_2	22045.45

Summary

This chapter evaluated the mathematical modelling of each tidal power system connected to grid components. These components include the drive train, permanent magnet synchronous, LCL filter, filter capacitor, back-to-back converter, such as DC to DC boost converter, DC-to-DC buck converter and voltage source inverter. The control design of power electronics converters devices mentioned above is also illustrated.

CHAPTER FIVE: RESULTS AND DISCUSSION

5.1. Introduction

This chapter focused on results and discuss in more detail the poor power quality can cause grid disturbance and serious economies losses. It is necessary for grid connected distributed units to meet the grid codes and standards governing their operation. The total harmonics distortion (THD) is one the parameters consider in power quality study. The IEE and IEC standards set the harmonic distortion limits for currents and voltage in power system based on the currents level and voltages levels.Voltages raging from 1 and 68 KV ,the THD must not exceed 5% THD,and the currents greater than 1000A should have no 20% THD. The system is presented in Figure 5-1. MATLAB Simulink is employed to provide an environment for modelling, simulation, and analysis of power system networks using the Voltage Oriented Control method for a three-phase boost rectifier will which be designed and simulated. Moreover, an implementation of the system will be started.

5.2. Modelling of the tidal current conversion systems of electric mode

The tidal turbine shaft is connected to the PMG rotor with a full-scale power converter connected to the grid typically using PMSG. The transmission of the MV generator output (6.6 kV) is carried out by land way through long three-phase submarine cables. Generally, the MV is transformed into LV (690 V) using an onshore transformer. The filters are placed between the voltage source converter (VSC) and the step-down transformer. However, the variable speed regulation of the PMG is using the controller of the generator side.

On the network side, the first step is filtration by the filter, the converter and rectifier have been included in the system in Figure 5-2. The filter, rectifier, converter, has been incorporated into the tidal energy system in a voltage wave at the generator limits. When the tidal conversions systems have been simulated in combination with these additions' systems part. Then, after the simulation of the entire system, the results are provided for the modelled tidal conversion system running for a half-tide cycle, which is around 10 min in this study.

The back-to-back energy converter (B2B) or the generator excitation can be used as control actuators for the torque handled. However, it can also be noted that if the tidal turbine reaches its nominal power, it must be "devoid of power" to avoid exceeding the nominal conditions. In this situation, maximising power conversion is not recommended, and for variable pitch turbines, the blade pitch can be controlled to stop power conversion but the pitch angle was considered fixed in this case study. Many of these control wind systems can be used in the control of tidal turbines. Tidal current turbulence and characteristic system drift due to system wear can directly impact the dynamic performance of a tidal turbine. For this reason, various control methods suitable for any specific turbine design can be used. In general, classic PI or PID control is the most used. The grid-connected tied power system was modelled and

simulated using the MATLAB/Simulink software to evaluate the system operational performance using the design parameters shown in (Tables 4-1, 4-2,4-3,4-4 and 4-5). The simulation results are given in three sections: the result of the generator-side characteristics, the control system results, and the results expressing the inverter output performances.
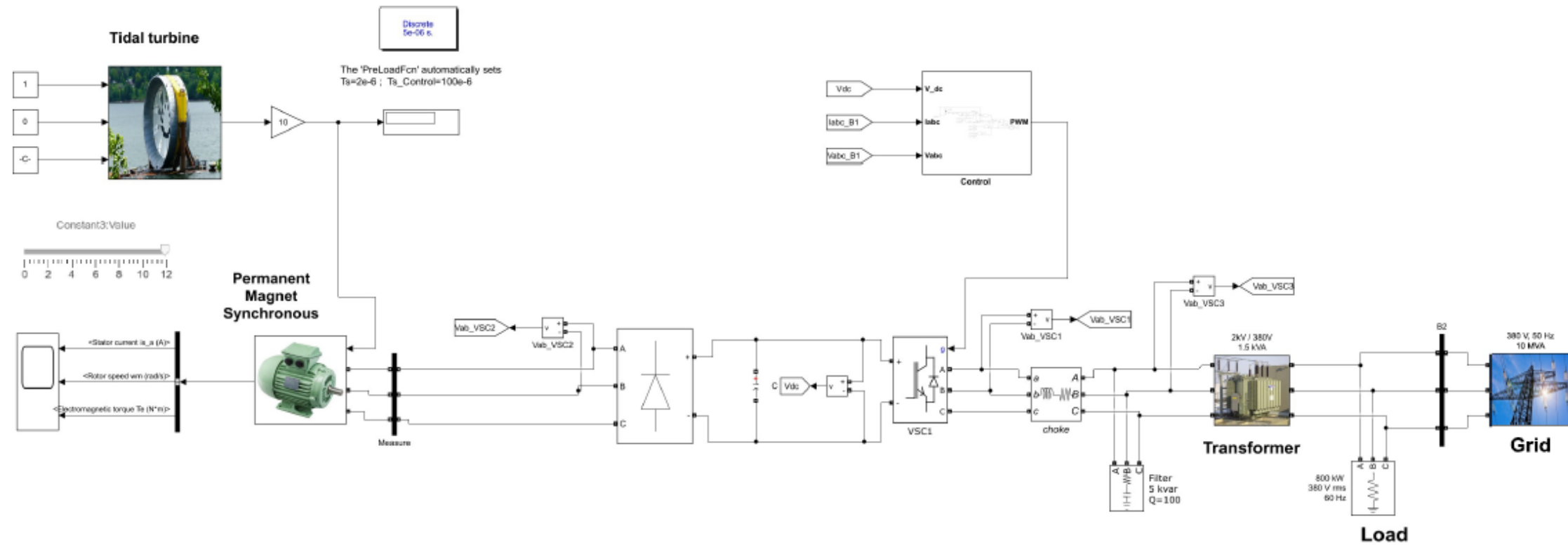
Figure 5—1: Permanent magnet synchronous tidal Generator with a PWM rectifier.

.
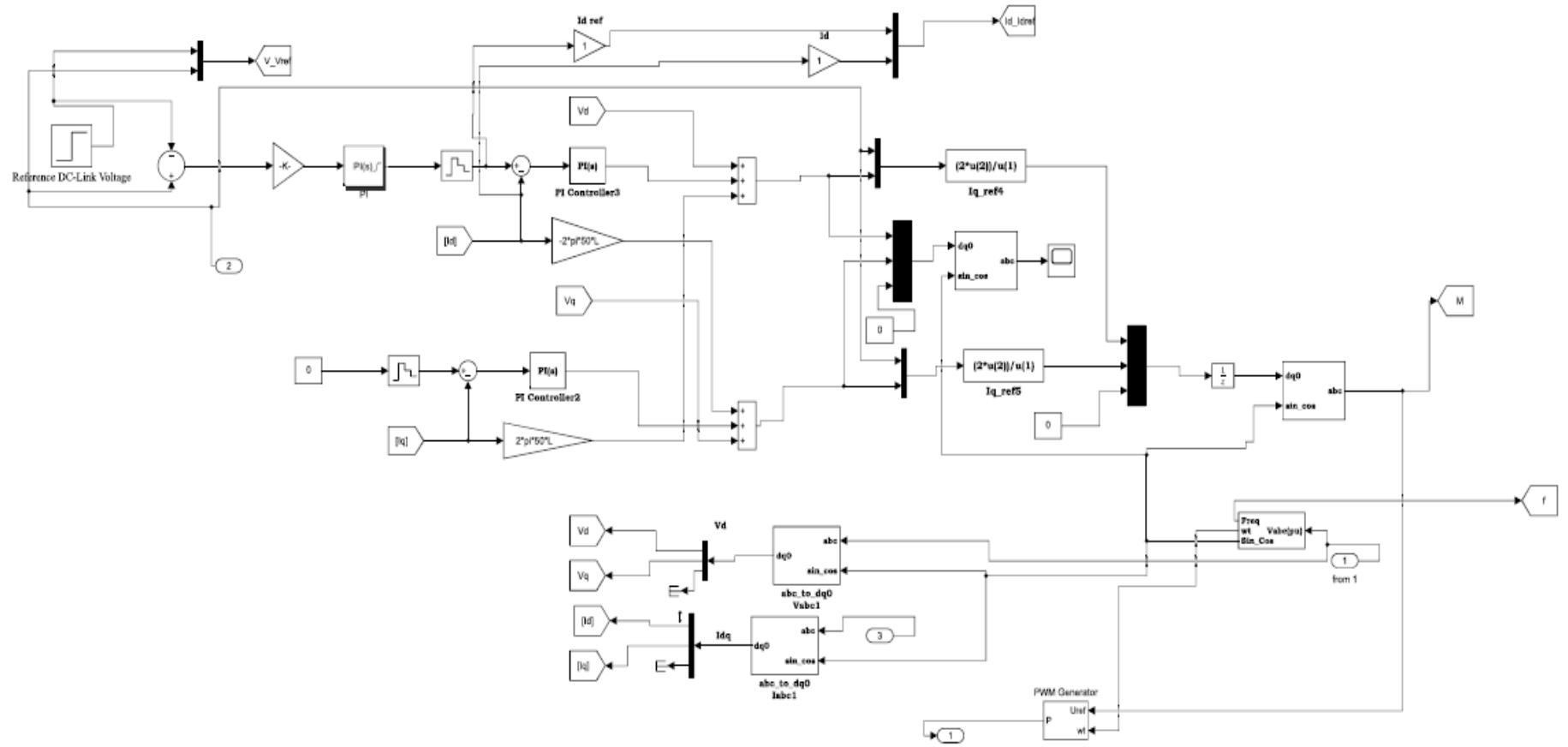
Figure 5—2: Voltage-Oriented Control Approach.

5.3. Generator-side results

The water speed to drive the tidal generator is considered constant and equal to 12 m/s. The mechanical power is used as input of the generator to obtain approximately 1.324 MW as shown in Figure 5-3, while its rotational speed is around 7.7 rad/sec. It can be observed that when the tidal current velocity increases to the rated amount of 12m/s at almost around 10s, the tidal rotor speed achieved the nominal amount of 24 r/min (Figure 4-4), and on the other hand, the generator torque achieve its maximum amount of 600 kNm (Figure 4-5). Also, it is noticed that when the current speed surplus the rated amount, the flux-weakening mechanism was activated and the rotor speed increased over the nominal speed. Figure 4-5 illustrates that at over-rated tidal currents, the mode characteristics of decreasing the generator torque for accelerating the turbine to a higher speed.
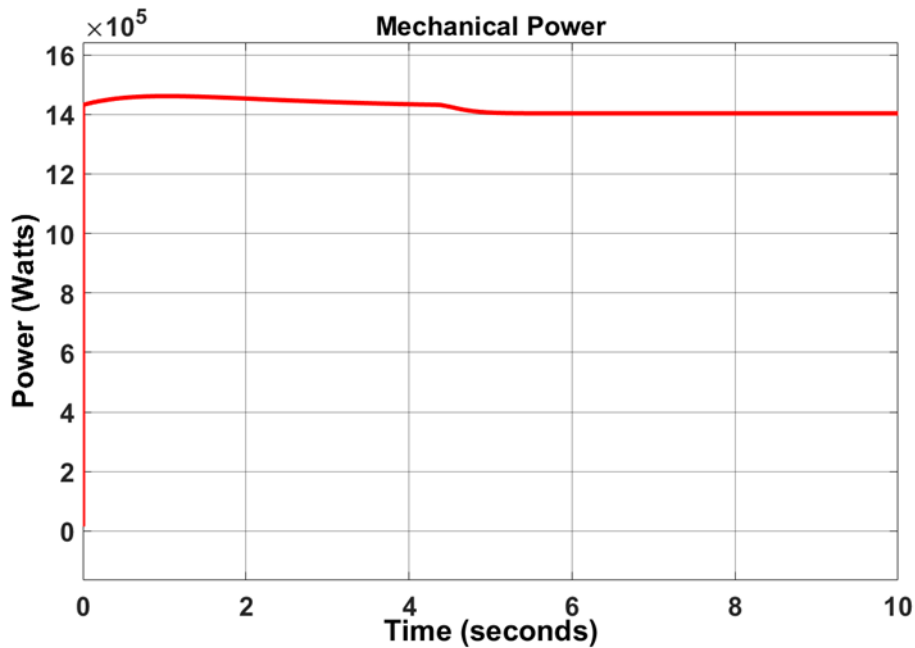
Figure 5—3: Mechanical power of the generator.

The active power produced by the tidal generator is shown in Figure 5-3; its value is about 1.324 MW. The signal displays an overshoot of 233 % at the start of the simulation, while the positive undershoot is around 1.055 % and the negative undershoot of 69.62 %. Figure 5-5 shows the reactive of the tidal generator.
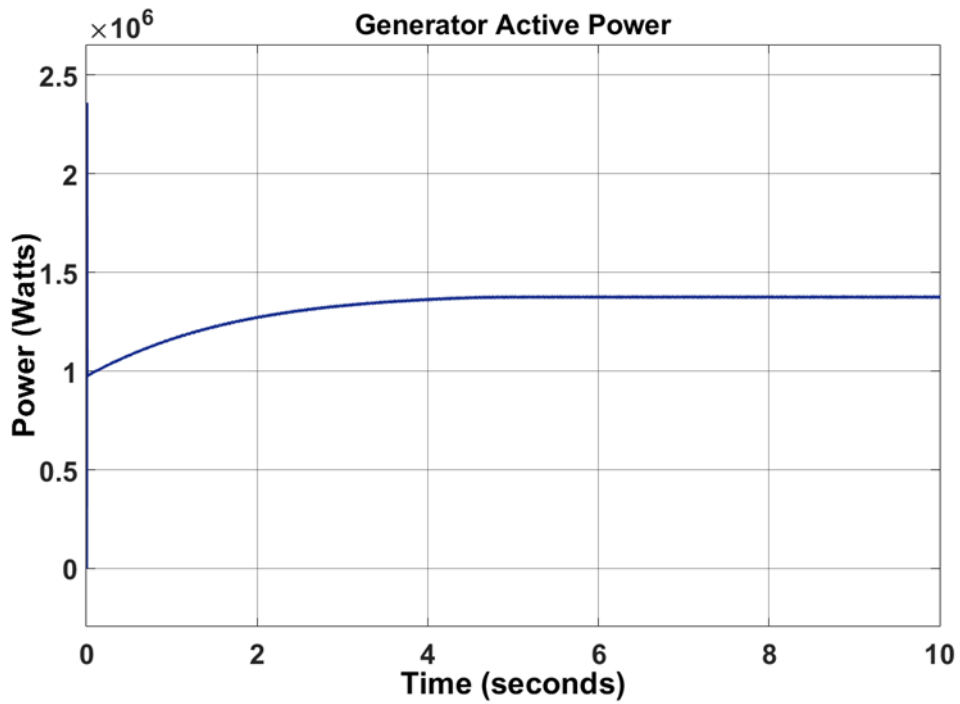
Figure 5—4: Genenrator active power.
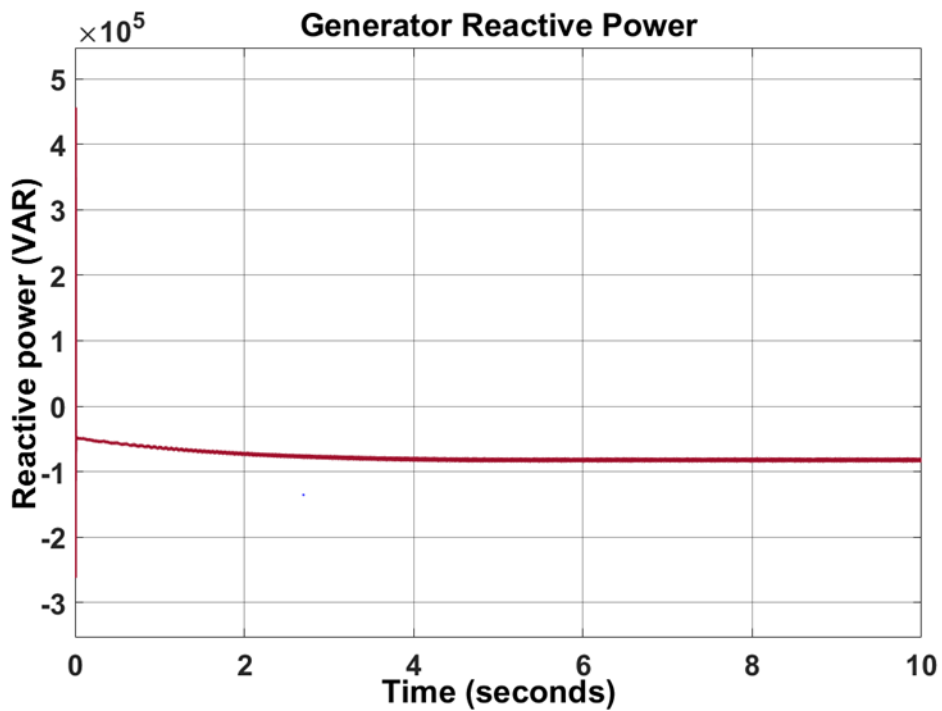
Figure 5—5: Generator reactive power.

Within 0 and 3 seconds, the simulation results indicate an overshoot and undershoot for both power signals, active and reactive respectively, as the system could not achieve its stability condition. However, after running 3 seconds, the active power and reactive power signals gained   stability .
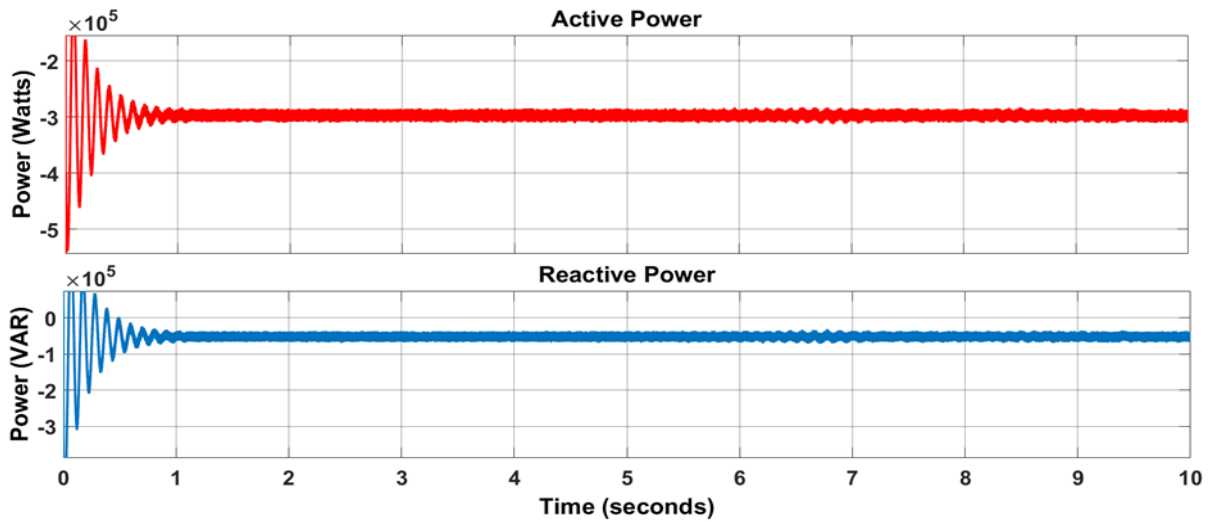
Figure 5—6:Acive and Reactive Power.

The combination of the phase to ground voltage and the phase current at the output tidal generator terminals are described in Figure 5-5. The RMS voltage amount value is about 549 V (Figure 5-8b), while the RMS of the phase-to-phase voltage is evaluated at around 951 Volts. On the other hand, this current phase of the generator is around 1082 Amps (Figure 5-6). Both signals show harmonics higher than the accepted system frequency of 50 Hz, as indicated in Figure 5-9a. It is noticed that including the rectifier and filter in the generator's output avoids very high voltage and frequency. As the high voltage and frequency can damage the load as indicated in Figure 5-10b and Figure 5-8b., The voltage at generator limits without the filter can be seen clearly that the maximum voltage is bigger than 1.2 pu of the nominal voltage, which is the admissible limit voltage when an overvoltage occurs, there is a risk of insulation breakdown, which may lead to a system failure. Previous research has obtained similar results (Meshram et al., 2013; Elbaset et al., 2017; Ben Hamad et al., 2021)**.**
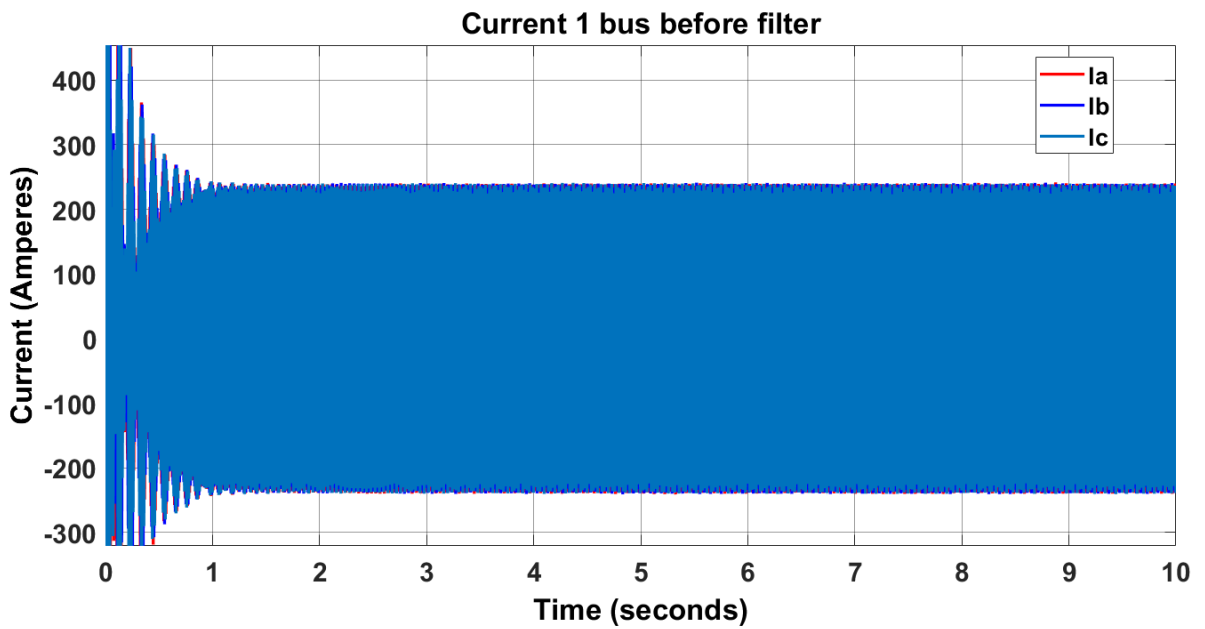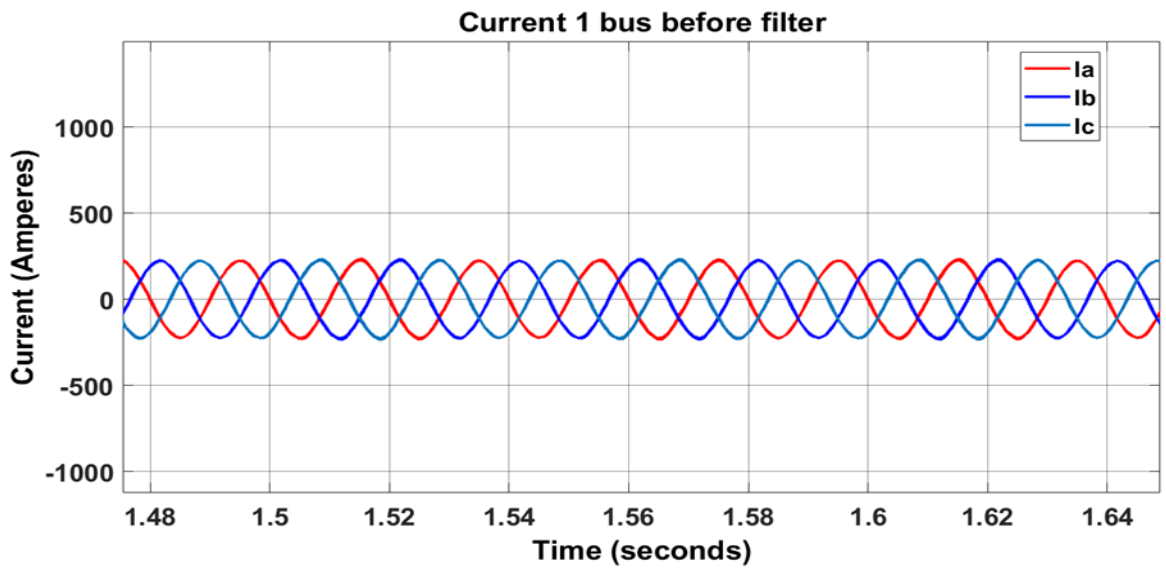
Figure 5—7a: The graphs tidal current generator.
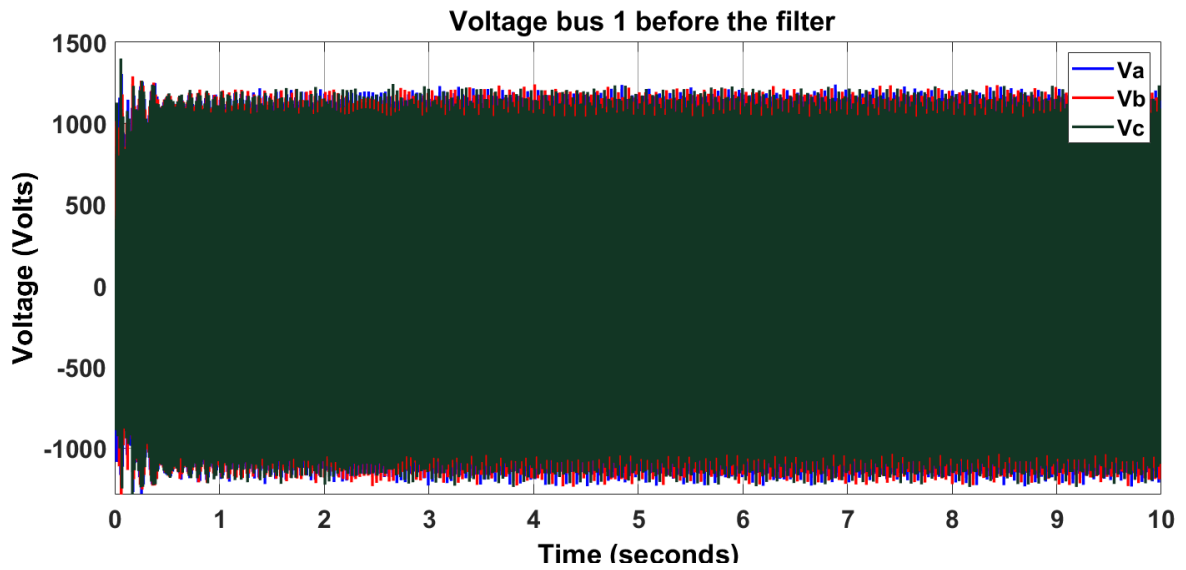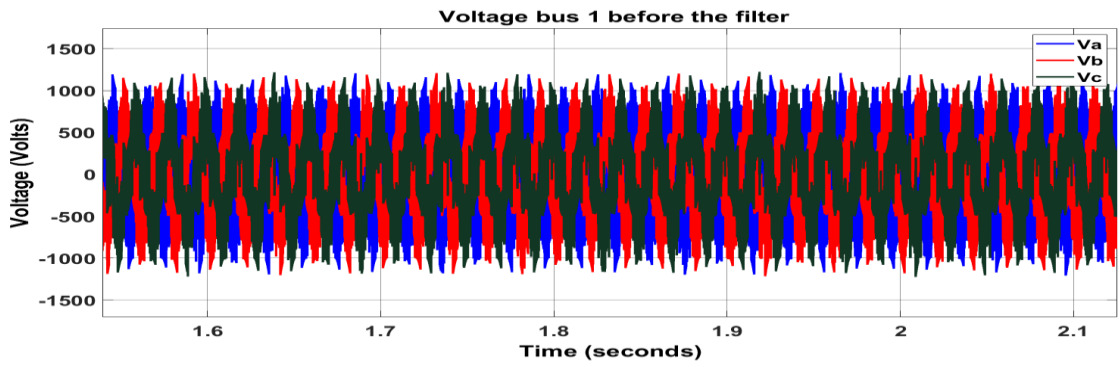
Figure 5—8b: The graphs tidal generator Voltage.

The phase to ground voltage wave has been formed with total harmonics distortion estimated around 141.38% as seen in Figure 5-8a, whereas the phase current signal presents a total harmonics distortion estimated at 13.54% (Figure 5-9b).
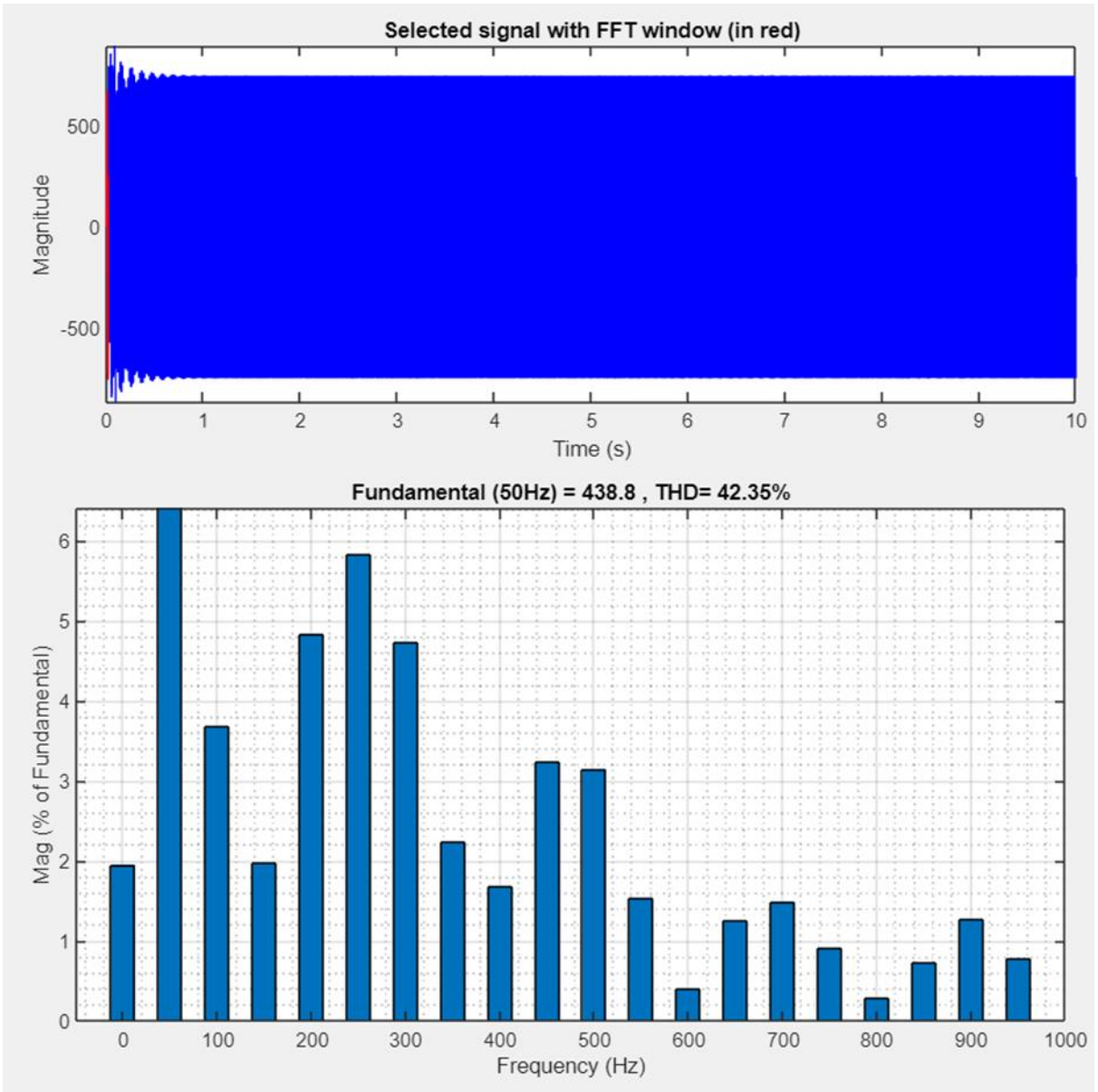
Figure 5—9a: Voltage Total Harmonics Distortion.
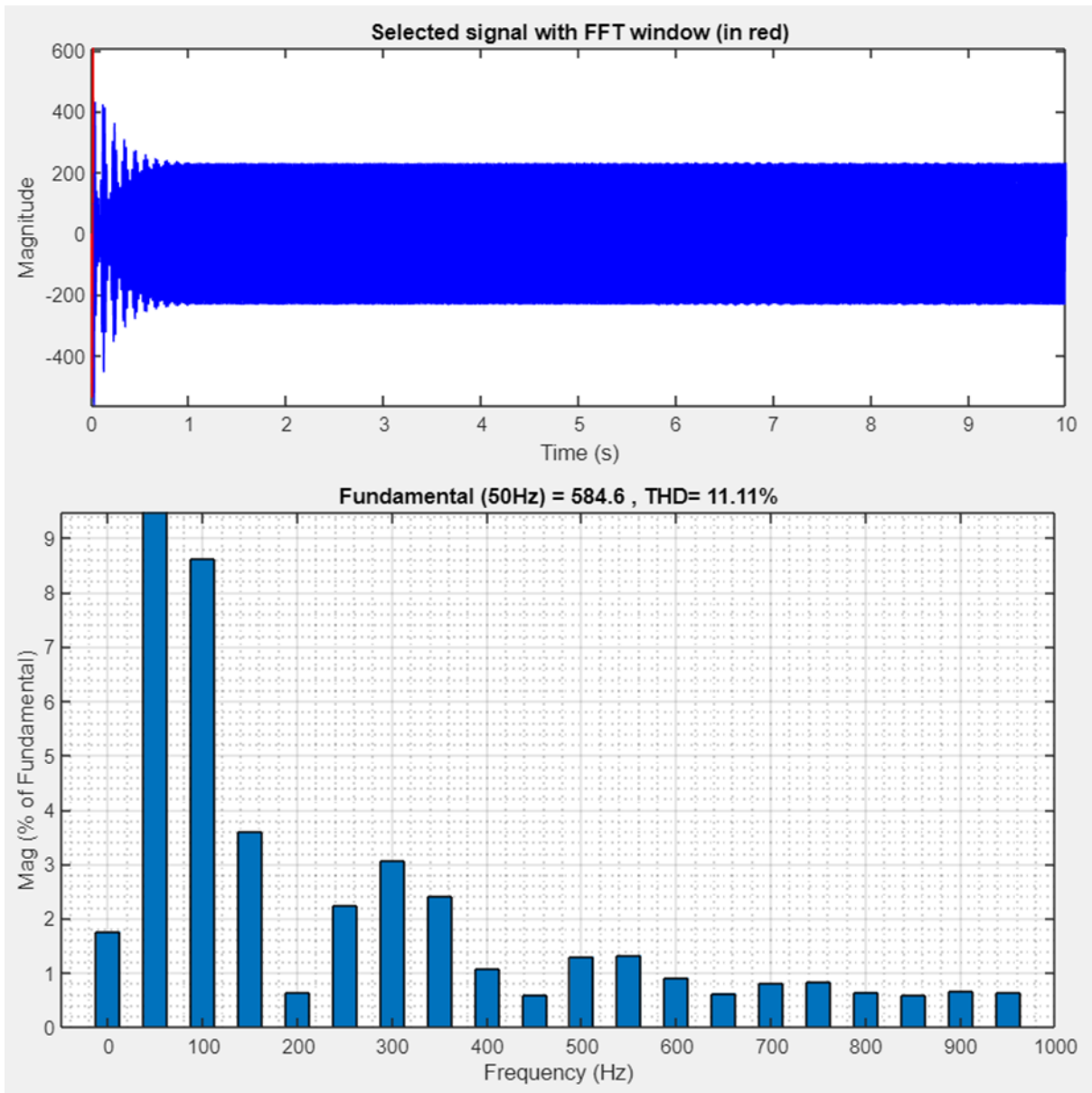
Figure 5—10b: Current Total Harmonics Distortion.

The voltage control approach stands on the principle of comparison between the DC link voltage and the reference voltage fixed to 1500V. The error which occurs after comparing it is used as input to the voltage PI controller to produce the Id reference ($\mathbf{I_{dref)}}$. It is indicated in Figure 5-13 as the actual and reference voltage of the DC link. The outcome demonstrates that the model control presents a better result as the error between both signals is nearly zero. However, overshoots occur at 14, 688 15 of 24 the simulation stater, then both voltages maintain the same amount value. The current ($\mathbf{I_d}$) and the current reference ($\mathbf{I_{dref}}$) has been compared in Figure 5-13. The error between both currents have been feeding into the current controller in the d-axis to produce the voltage ($\mathbf{V_d}$). The $\mathbf{I_{dref}}$ has been evaluated to be around 1766 Amperes with its increased time measured about 40.823 milliseconds. The overshoot and undershoot values are estimated at around 21.341% and 1.994%, respectively.

The same process of comparison has been shown by Figure 5-12 and Figure 5-13 between $\mathbf{I_q}$ and $\mathbf{I_{qreference}}$ ($\mathbf{I_{dref}}$) currents. The results from the comparison between the two currents generate the voltage (V_q) through the current PI controller in the q-axis. The Iq reference is evaluated around zero. However, the grid voltage in the dq0 frame needs to produce the voltage, which will allow determining the modulation signal. The voltage in the d-axis is 500 V, whereas that of the q-axis is zero since the grid regulates its reactive power. The voltage in the dq0 frame ($\mathbf{V_d}$and $\mathbf{V_q}$) helps to evaluate the modulation signal in the dq0 frame illustrated by Figure 5-11. Their values according to the d and q axis are evaluated around 500 V. The modulation signals results in both axes are determined by a magnitude of 0.7. Then these modulation signals are modified from the dq0 to the ABC frame, then fed into the pulse width generator to generate twelve pulses to drive the three-level inverter. The phase-locked loop (PLL) generates an output signal which depends on the input signal phase. In this study, the PLL allowed the frequency and phase of a sinusoidal three-phase signal tracking using an internal frequency oscillator. The control system regulates the internal oscillator to stabilise the phase difference to 0.Figure 5-14 indicates the frequency of the PLL, which is equal to 50 Hz. This similar frequency as well to the grid frequency and changes a bit about 50 Hz. Furthermore, the PLL determines the grid voltage and phase angle using the dq0 frame current control synchronise. The PLL features generated an accurate phase angle which facilitates the synchronisation of the inverter to the grid.
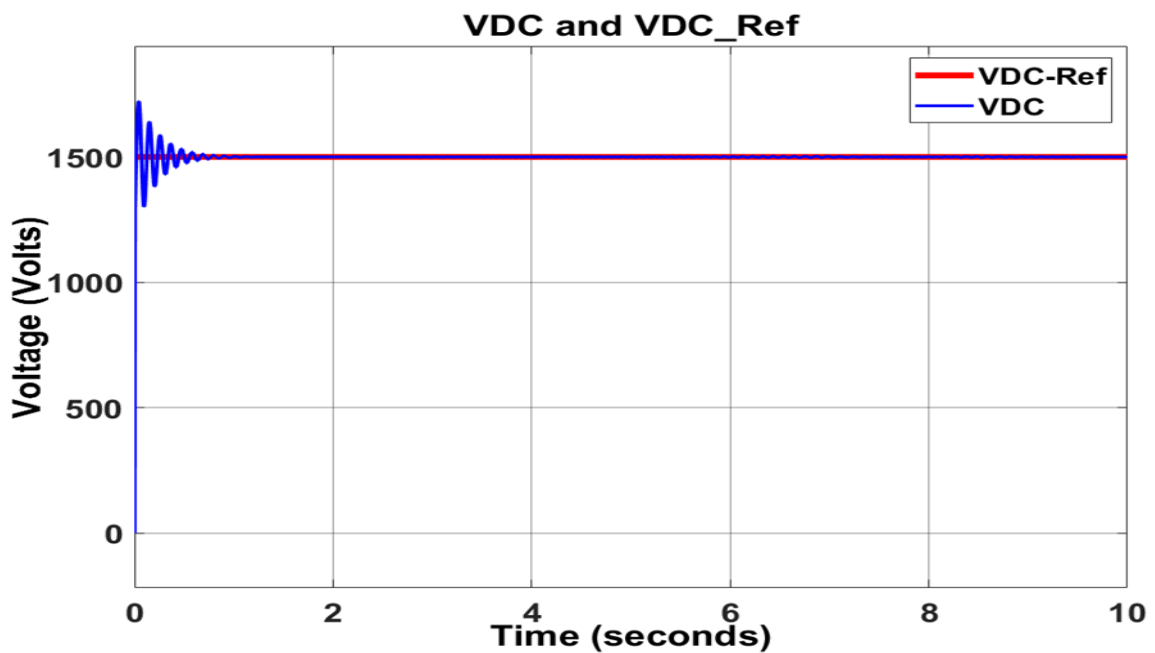
Figure 5—11: VDC and VDC reference.
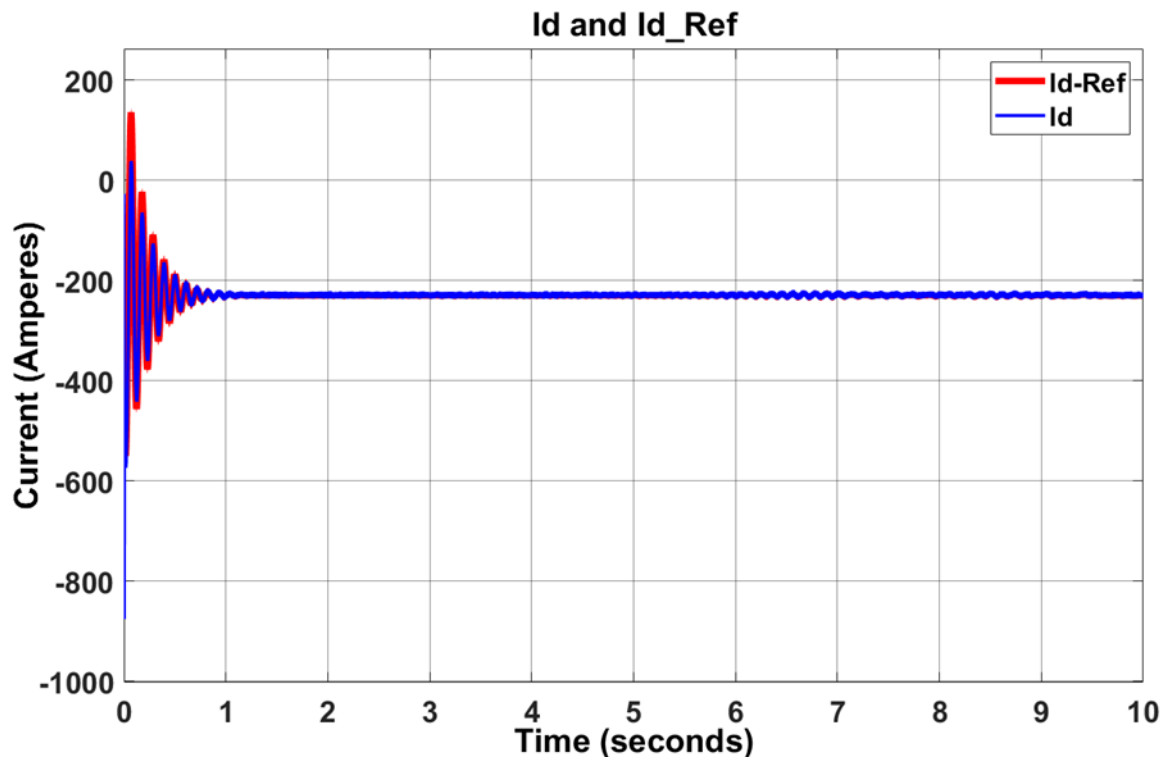
Figure 5—12: I_d and I_{dRef}.
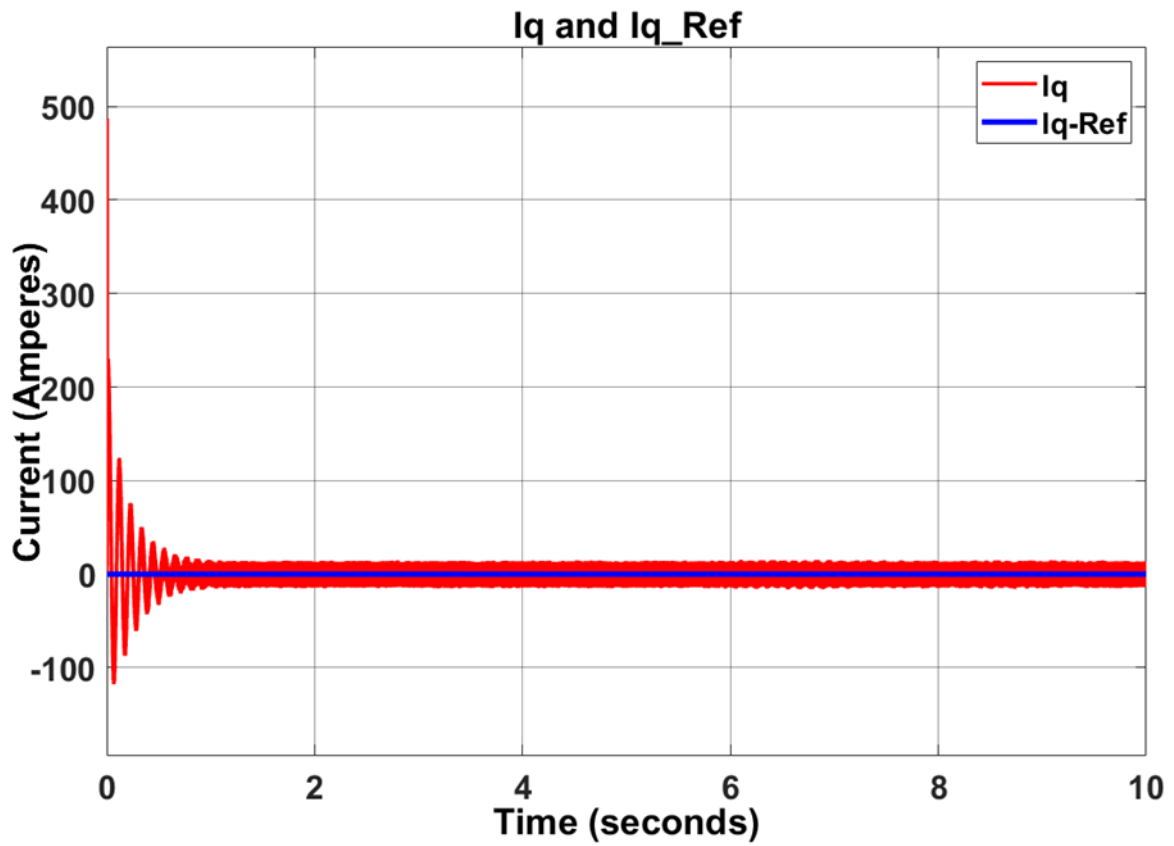
Figure 5—13: I_q and I_{qRef}.
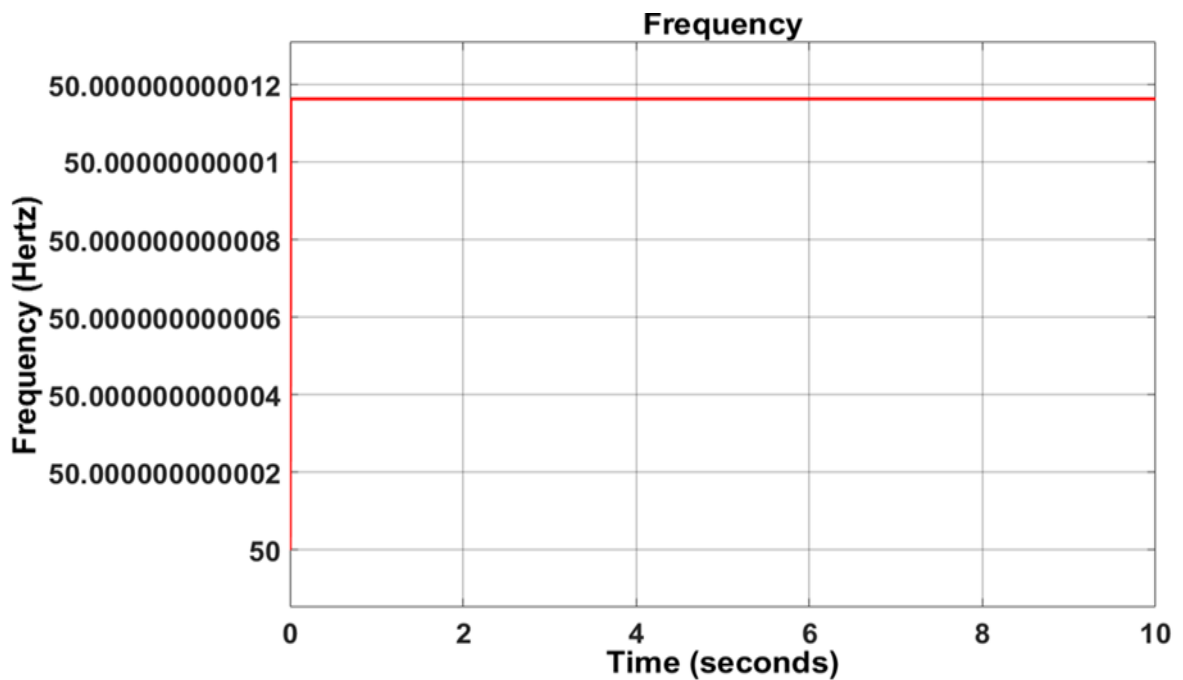
Figure 5—14:Phase-locked loop (PLL) frequency.

When the grid-tied is set into operation mode, the control design is projected to adjust the grid-tied injected current of the inverter. It is feasible to use a dual current control loop with PI controllers. The implementation of the current control is using the dq0 reference frame. While the grid-tied included with inverter frequency and phase at the common coupling (PCC) point combining the grid are into synchronisation through a PL. The investigation results demonstrate that the system response is good. The error measured between DC-link voltage and the outer loop reference voltage is approximately zero. In the same vein, the results of the inner control loop also demonstrate that the current feed into the grid is accurately adjusted and in phase combined with the voltage, then reaching a unity power factor. Whereas, when investigating the PLL it was observed that the inverter frequency is complying with the frequency at the PCC with the grid, As the capacitor voltage sags, the voltage error rises, and the voltage regulation is adjusting the current setpoint to accumulate more current from the source to raise the DC- link voltage back to the need level.

The output reaches a constant value at every shot time estimated at 0.075 seconds, including the results of the power evaluated around 84.55 kW provided by the turbine parameters and the power curve, which verified the validity of the generated Simulink model. The voltage and current also have the same frequency, which is evaluated at 50 Hz illustrate in Figure 5-13 and Figure 5-14. The configurations of harmonic at this frequency will be improved when the generator terminals are achieved. It should be noted that if the voltage has a small amount of

value at a certain specific frequency range, then the harmonic form of those frequencies will go down at the terminal generator.
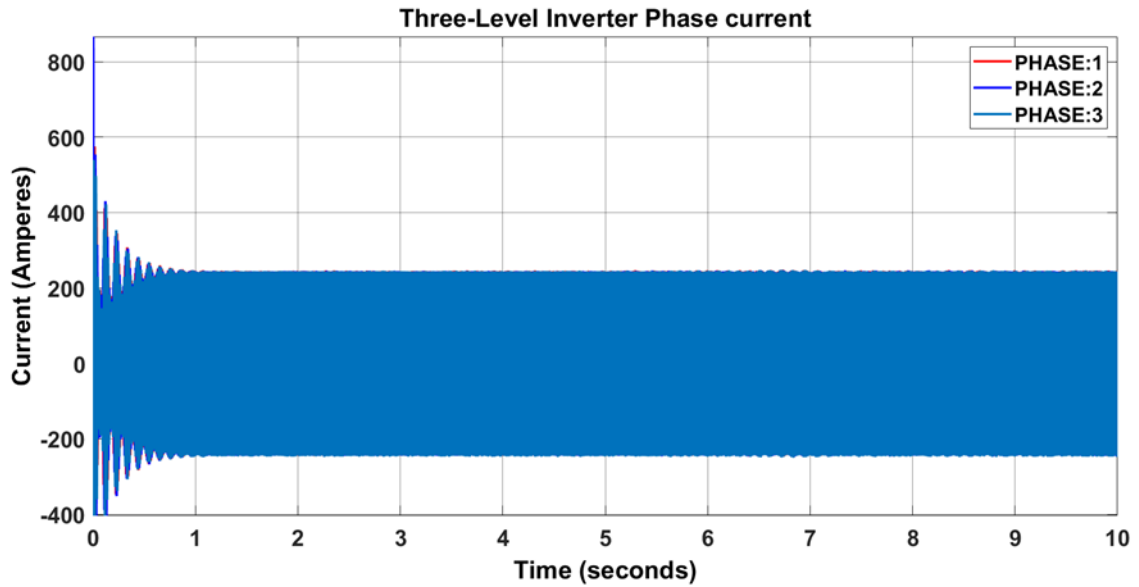
Figure 5—15: The phase-to-phase current from the three-level inverter.
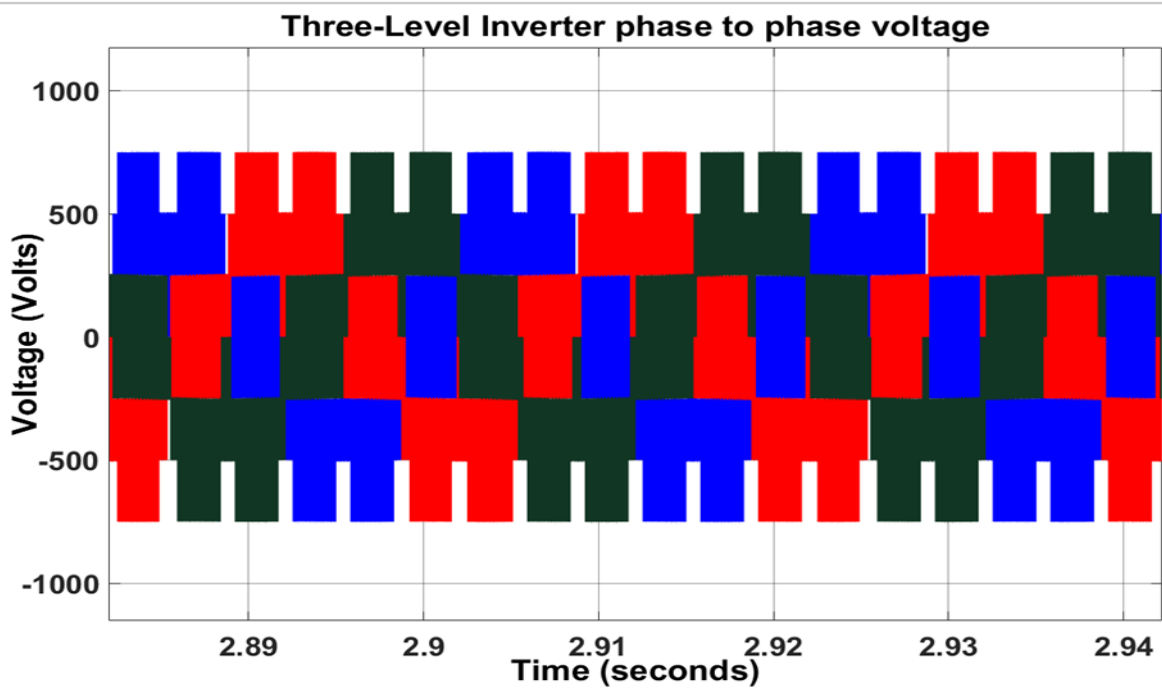
Figure 5—16: Generator terminals 3-phase voltage.
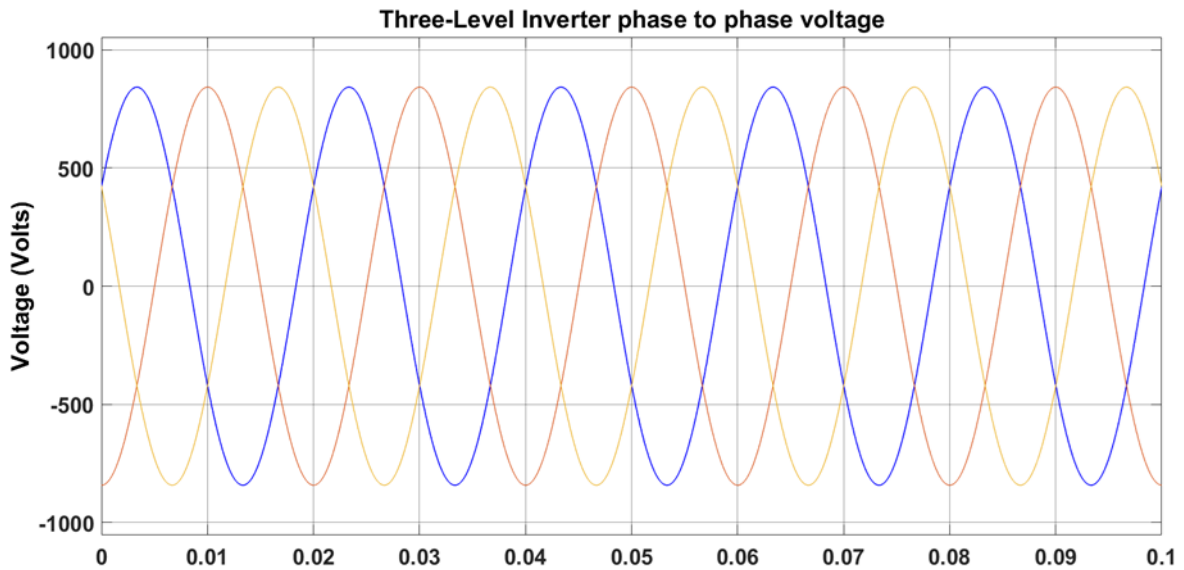
Figure 5—17: The phase-to-phase voltage from the three-level inverter

Figures 5-15 and Figure 5-16 represent the phase-to-phase voltage from the three-level inverter, including the harmonics due to the inverter's switching. These harmonics can damage the system and make it inefficient with a poor power factor and including the transient, etc. For voltages ranging from 1 to 68 kV, the total harmonic distortion of voltage must not be over 5%. Similarly, the limitation of the current harmonic distortion is higher than 1000 A, estimated at around 20%. Then the voltage total harmonic distortion is about 45.01% for frequencies up to 5 kHz. Thus, an LCL filter is situated between the inverter and the grid to minimise these harmonics. The phase-to-phase voltage at the output of the LCL filter is around 600 V, while the phase currents are around 1213 A in Figure 5-13. The phase-to-phase voltage risen period is about 5.853 milliseconds, while the fall period is around 5.837 milliseconds. The overshoot voltage and undershoot voltage are both estimated at around 0.324% and 1.985%, respectively. Similarly, the phase current increase period is estimated at around 5.819 milliseconds, while the fallen period is 5.823 milliseconds. Its overshoot and undershoot are estimated at around 1.99% and 1.99%, respectively. Figure 5-9a and Figure 5-10b describes the total harmonic distortions (THD) graph at the output of the LCL filter. The total harmonic distortions are fallen to 0.07% for the current (Figure 5-19) and 0.12% for the voltage (Figure 5-16) and (Figure 5-17), thus it shows that the grid connection standards requirement has been satisfied.

.
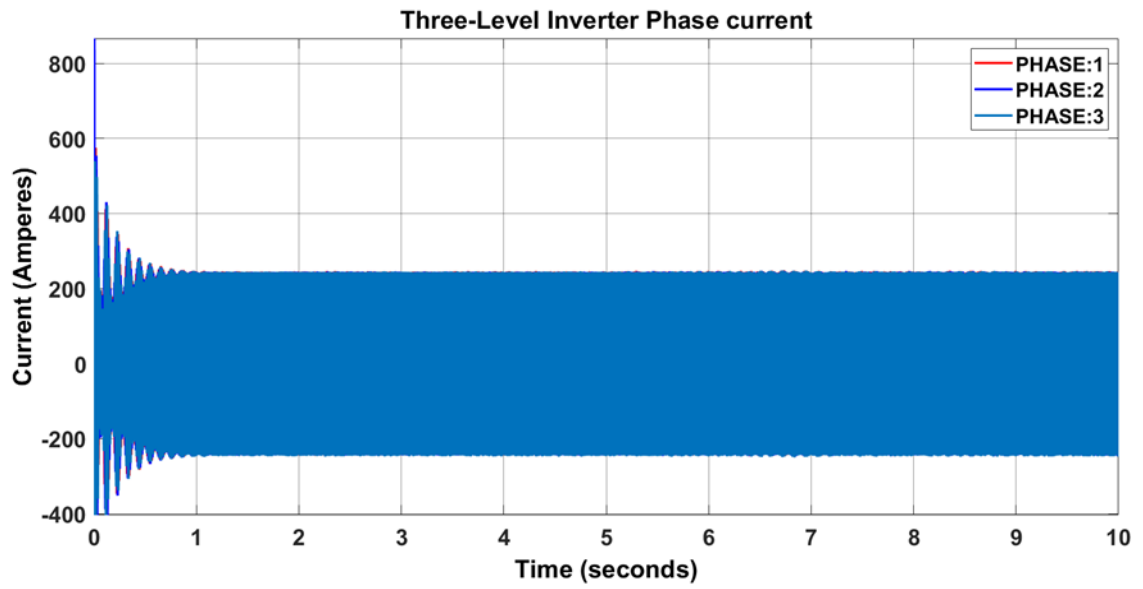
Figure 5—18: current waves at the inductance-capacitance-inductance (LCL) filter's output.
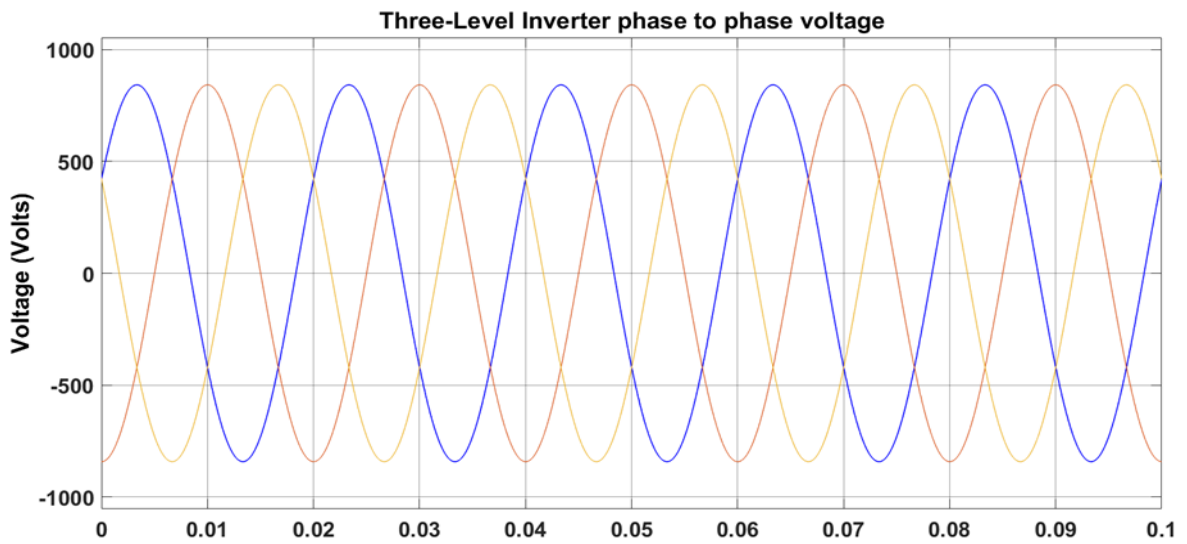
Figure 5—19: Voltage and waves at the inductance-capacitance-inductance (LCL) filter's output.
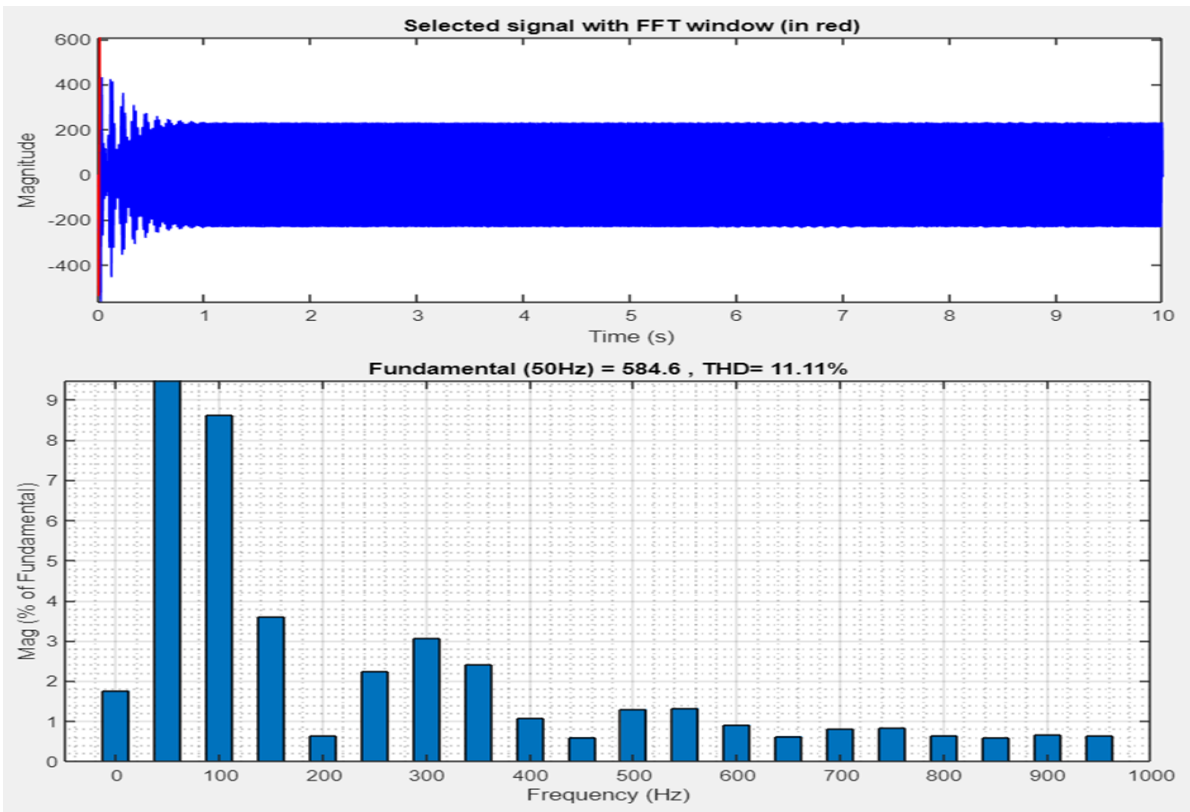
Figure 5—20: Current total harmonic distortions.
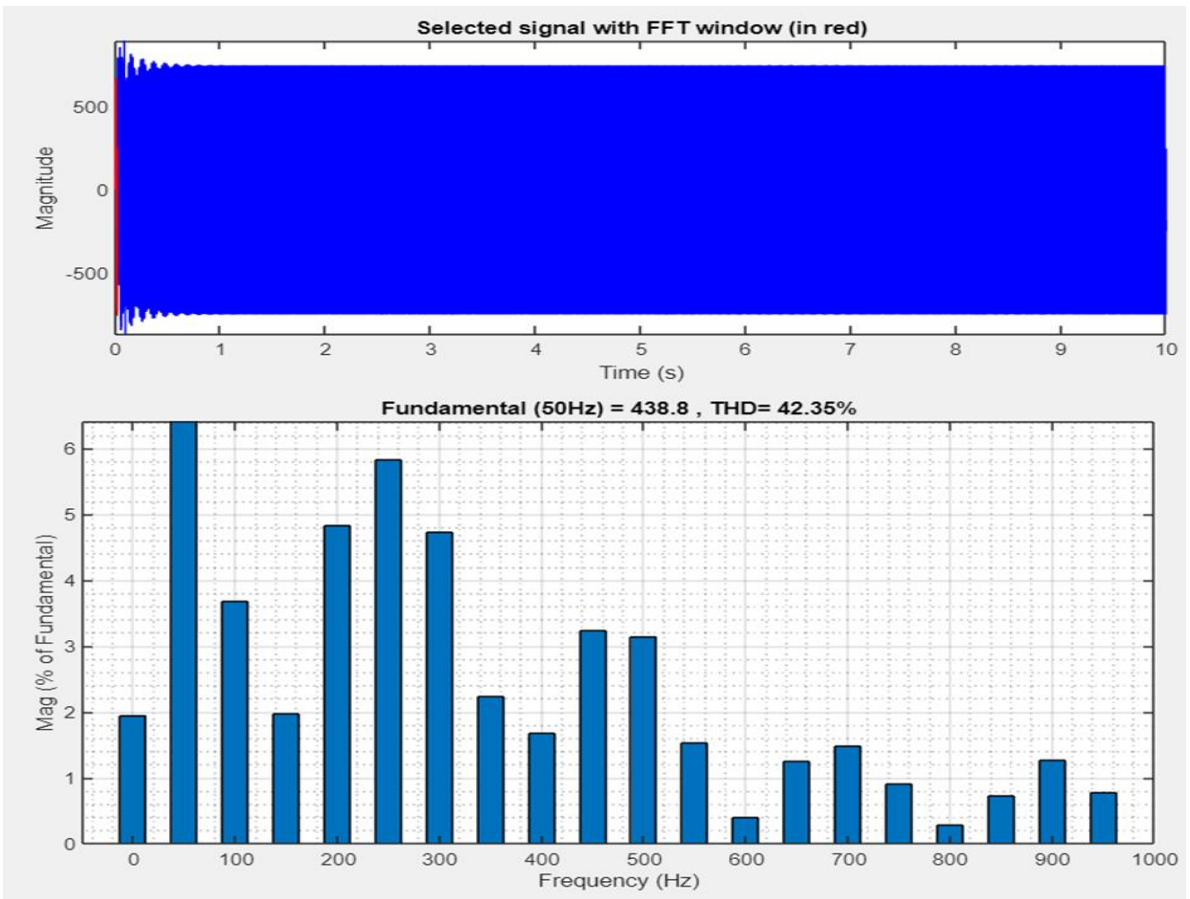
Figure 5—21: Voltage total harmonic distortions.

In this study, two scenarios were considered to determine the scheme of the operation that relies on the load amount value. The scenario comprises a load that is less than the power produced by the tidal energy generation system. This case study during tidal energy generation system used the parameters such as the active power, the reactive power, the voltage, and the current of the load and the grid.

In this case, the tidal energy system produces insufficient power, which cannot satisfy the load demand and received the shortage of power from the grid. Figure 5-21 indicates the active and reactive power which is consumed by the load. The active power is estimated at around 917 kW, while the reactive power is not stable. It shifts from 0 and 287.8 nano VAR. This active power response is formed by an overshoot estimated around 14.935% between t = 0 and t = 0.3 s and an undershoot also estimated about 2.187% between t = 0.3 and energies standard 2021, 14, 688 18 of 24 t = 0.6s.

After that, this response has been maintained to achieve the steady constant estimated at 917 kW. The active power and reactive power exported to the grid are described in Figure 5-23. The tidal energy system is importing an active power value of around 573.9 kW from the grid. On the other hand, the reactive power which comes from the grid-tied inverter is estimated to be at around 508.4 kVAR. It should be noted that the active power signal gets an increased time estimated at 61.950 milliseconds, while the overshoot is 10.92% and the undershoot is 8.35%. However, the reactive power gets an increased time evaluated at 29.842 milliseconds, corresponding to an overshoot of 55% and an undershoot of 1.986%. The phase currents and the phase-to-phase voltages at the ends of the load are illustrated in Figure 5-20 and Figure 5-10b; the signals can be observed as pure sinusoidal waves.

The voltage (RMS) is estimated at around 600 V, while the currents are evaluated at about 874.4 A. The voltage rise time is approximatively around 5.854 milliseconds, and the deceased time is around 5.858 milliseconds. Finally, the overshoot voltage and undershoot voltage are 1.983%, respectively. On the other hand, the currents rise time is about 5.858 milliseconds, while the fall time is 5.855 milliseconds. Additionally, the overshoot is 0.312%, and the currents undershoot is 1.984%, around 0.310%.
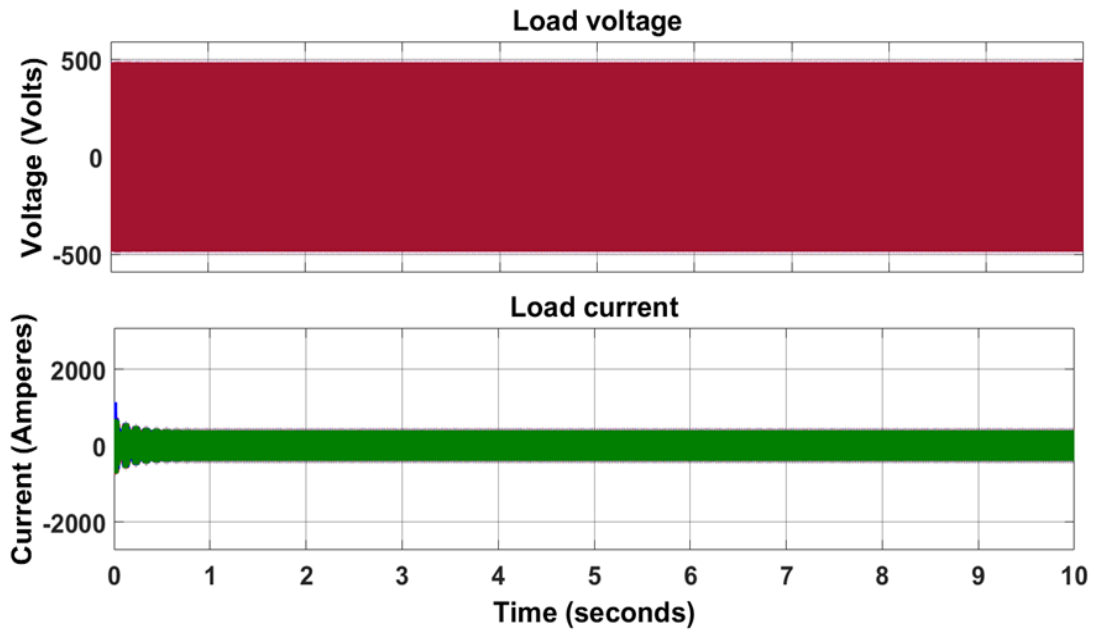
Figure 5—22: load voltage and load current.
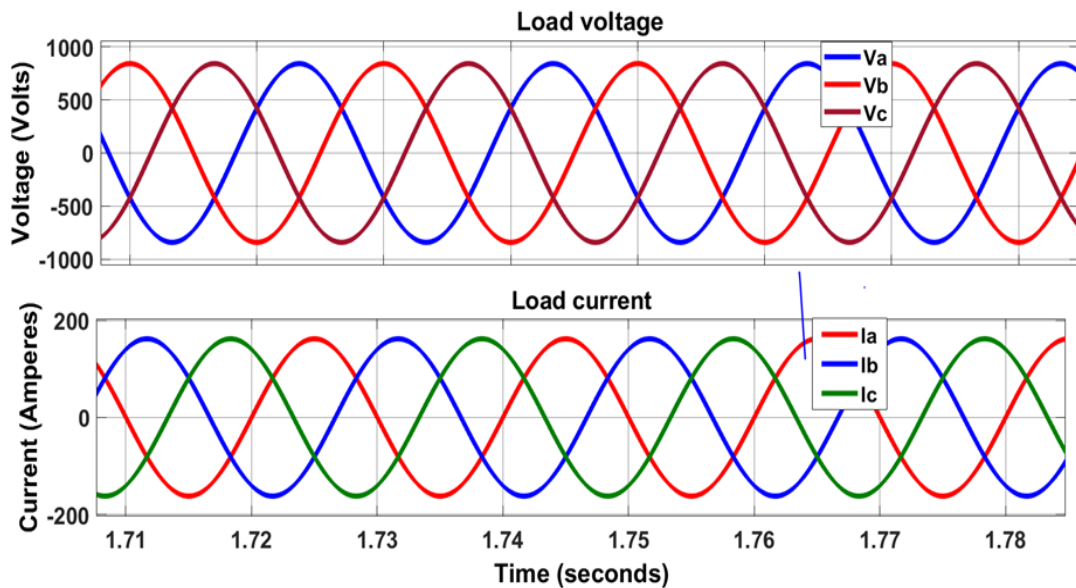
Figure 5—23: load voltage and load current.

The voltages and currents at the connection point link to the grid are shown in Figure 5-23. The measurement of RMS magnitudes of the voltages is around 600 V and measurement of RMS magnitudes of currents is 425 A. The voltage signals get an increased time of approximately 5.867 milliseconds, while the drop time is estimated at 5.866 milliseconds. It can be noted that the overshoot is 0.211%, and undershoot is evaluated at 1.987%. At the same time, the current signals get an increased period of around 5.459 milliseconds, while the

drop period is estimated at 5.381 milliseconds. Additionally, the values of other parameters such as the overshoot and undershoot have been given 6.19% and 1.983%, respectively.
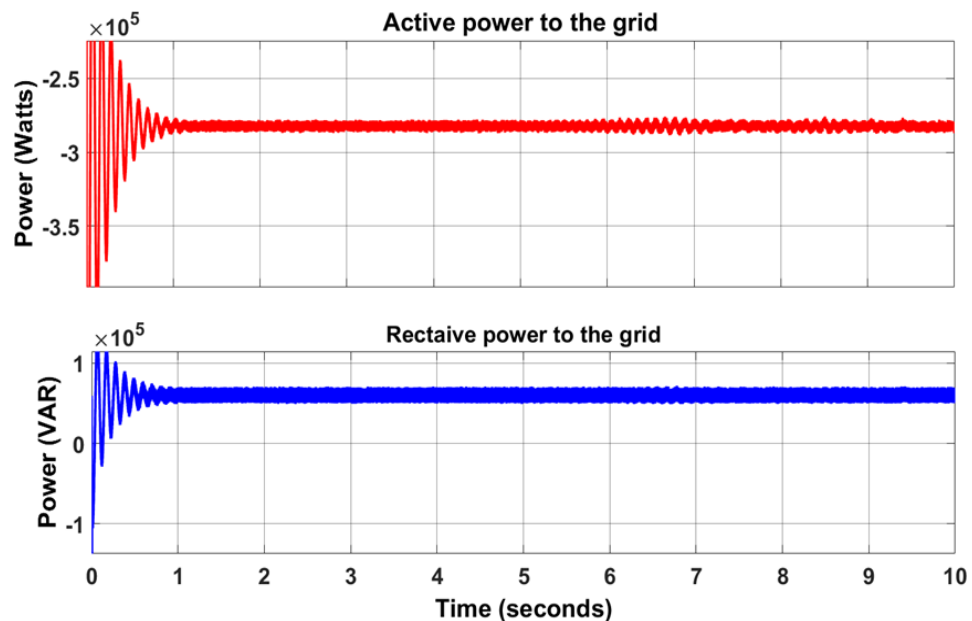
Figure 5—24: Grid active power and reactive power.

5.4. Discussion

The integration of the distribution system power unit to the utility grid presents some complex issues such as the power quality problem, Harmonics distortion (THD), which is demonstrated by the poor power quality, which can create grid disturbance and economic losses. One of the key issues in this process is that the grid-tied distributed units must match the grid codes and standards adjusting their operation. It can be noted that Harmonics Distortion (THD) was one of the parameters taken into consideration for power quality investigation.

Two organisations deal with harmonic standardisation such as IEEE, IEC standards. These standards help fix the limitation of harmonic distortion for the current and the voltage in a power system. When passive harmonic filters are added to the output of the inverter, it was observed that the terminal harmonics of the generator could be filtered. The filter can play different roles such as reducing weak harmonics and it can also change the impedance paths of the highest harmonics which escape the damping which may cause urges at the terminals of the machine due to the voltage waves reflecting in the cables. If a frequency element contains a level path with low impedance towards the filter, it would lead to this harmonic element being also filtered, but otherwise, the harmonic element will not be filtered. This situation may help in the identification of the resonant frequencies of the system to be avoided. However, the addition of a passive filter reduces the harmonics to an allowable levels for the generator side. For a

range of voltages that varies from 1 – 68 kV, the voltage THD must not exceed 5%, while the limitation of THD for currents bigger than 1000 A is 20%. However, this simulation results proved that the inverter control program successfully converted tidal DC power to AC power with total harmonic distortions estimated at 2.44% for the voltage, and the current value was 0.16%. The ripples have been minimised in the range of less than 15 mv. It is stabilised even with the variations of the generator output of either amplitude or frequency. As per IEEE Std. 1547-2003, it comes less than 5%. It was noted that the input AC voltage was exposed to a huge variation, and the generator output voltage was generating less energy than the grid voltage. In the study by Jayalakshmi et al. (2012), the q-axis reference current is designed by preferable inverter reactive power output injected to the grid. The model chosen in this study has a purely sinusoidal adjusted voltage source at the inverter terminals. This study demonstrated the importance of the generation system to be interconnected to the grid in order to minimise the harmonic distortion level. After the control and simulation, the harmonic distortion level was maintained approximatively around 3 to 3.5%, which is well within the standards. The active power wind generation system output and inverter output current diminishes. To meet the load demand, the power utility receive a shortage of power.

In the study by Reznik et al. (2012), the active and reactive power has been adjusted using the line controller. However, the PI-based controllers choose the desired reference measurements at the PCC and compare respective values with the frame. The active and reactive powers are determined using limited by the relative saturation blocks. The switching frequency ripple is reduced by the LCL filter. However, Priya,(2014) used the vector control technique to adjust the control of the MSC of the PMSG wind turbine and the GSC of the PMSG wind turbine to reach integrated control of optimal power generation, reactive power generation power, and grid voltage support control. It has been demonstrated that the direct vector control design of the PMSG system presents a good performance in diverse characteristics. Therefore, PMSG is operating with a direct current vector control structure, and the maximum power point tracking and speed control of MSC have been used to adjust the wind speed and the wind power generation. While the reactive power absorption control is reached using d- and q- axis control of GSC. The THD has resulted in estimate of around 5.78%, which corresponds to the acceptable limits range of the IEEE-519-1997 standards.

Meshram et al.(2013) assessed the Hybrid solar, hydro systems formed with a boost converter and solar inverter. The control of this power generation system used the constant current controller. It was observed that the capacitor was also connected to mitigate the high-frequency harmonics between the PV array and boost converter. However, the filter output is the control signal is related to the reference voltage. The PI controller depends on the inputs parameters for it to minimise the error. Then it has been done a comparison with the saw-tooth waveform to produce the PWM signal, which is fed as a gate signal to the IGBT switch. As it

can be observed that the voltage source converter is inverted the DC voltage to the sinusoid AC voltage waveform maintaining the unity power factor. The constant current controller is used to control the Hydro solar. The harmonics produced by the VSC is filtered by the LC filter. The Solar hydro DC power contains the harmonic distortion at the rectifier output which is filtered by the LC filter and converted to AC power by a PWM inverter. The hydro PWM inverter is also controlled using the current controller. The PWM inverter output includes the harmonics which is filtered by the LC filter, and the Voltage DC is converted into AC. The conversion of 500V constant DC voltage into 260V,50 Hz AC voltage by bridge inverter. The harmonic distortion contains in the rectifier before filtering is reduced using the passive filter to obtain the smooth DC voltage. The LC filter is also used to transform the pure sinusoidal waveform of the hybrid solar hydro inverter. According to the article by Elbaset et al.,(2017) calculated the performance of a PV grid-tied system. The inverter power output quality has been improved using an LC filter by reducing the voltage harmonic distortion up to 1.01%. In a study by Ben Hamad et al., (2021) the modelling and control of a grid-tied three-phase 3-level NPC inverter for photovoltaic systems, the combination of A 13 kW NPC inverter and LC filter resulted in less than 3% of the current THD. Ramteke & Patil, (2014) featured an LCL filter to reduce a five-level inverter's harmonics for renewable power generation. The system has demonstrated a current THD estimated of around 0.33%. The results obtained in this study show better THDs than those of previous studies in Table 5-1.

Table 5—1:Inverter control parameters.

	(Benzazah et al., 2022)	(Hassan, 2016)	(Amor & Kheldoun, 2018)	(Inverter & Ramteke, 2014)	(Amor & Kheldoun, 2018)	(Ben Hamad et al., 2021)	(Mahlooji et al., 2018)	
Source type	Renewable energy	PV	PV	PV	PV	Renewable energy	PEMFC	This study
PCU type	DC/AC	DC/AC	DC/AC	DC/AC	DC/AC	DC/AC	DC/AC	DC/AC
Multilevel	3-Level	3-Level	3-Level	3-Level	3-Level	3-Level	3-Level	3-Level
inverter	NPC	NPC	NPC	NPC	NPC	NPC	NPC	NPC
Filter type	LCL	LCL	LCL	LCL	LCL	LCL	LCL	LCL
Topology Grid-tied	Grid-tied	Grid-tied	Grid-tied	Grid-tied	Grid-tied	Grid-tied	Grid-tied	Grid-tied
DC Voltage	2200 V	500 V	_	350–850 V	800 V	400 V	1400 V	1400 V
AC Voltage	1380 V	_	_	380 V	325 V	283 V	600 V	600V
DC power	_	100 kW	_	_	9.5 kW	_	1.5 MW	1.5MW
AC Power	7 MVA		_	13 kW		5 kW	1.3 MW	1.2MW
Switching	2 kHz	5 kHz	_	5 kHz	5 kHz	10 kHz	2 kHz	2Hz
Frequency	_	_	_	97.5%	80%	_	_	_
Efficiency	_	_	88%	_	_	_	88%	_
Number of	IEEE Std	_	IEC61727	_	_	IEEE	IEEE	IEE
Standards	519-1992	_	IEEE1547	_	_	519-1992	519-2014	_
THD of	_	_	_	_	_			
Voltage	2.44%	1.01%	1.27%	_	3%	0.33%	0.12%	0,12%
THD of	_	_	_	_	_			
Current	0.16%	_	2.41%	<3%	_	_	0.07%	0,07%

5.5 Summar

This chapter evaluated the results and discussion. A simulation was conducted to assess the designed system operation in grid-tied mode. It was assumed that the tidal energy system operates at a constant water velocity of 12 m/s. The results obtained from the simulation show the system's good performance with total harmonic distortion of voltage and current meeting standards prescribed by IEEE and IEC.

CHAPTER SIX: CONCLUSION AND RECOMMENDATION

6.1. Conclusion

The purpose of this research was focused on modelling and simulating a centralised three-phase grid-tied three-level diode clamped inverter connect to a tidal power generation system. In this work, an alternative closed-loop control technique of back-to-back two-level VSC is used to regulate the DC link voltage. The power performance of direct-driven, fixed-pitch, variable-speed tidal turbines with PMSG and the mathematical model of all systems has been presented with the generation capacity of the case study of 1.5 MW PMSG. The different fundamental blocks such as rectifier, inverter, converter, have been presented with their respective mathematical modelling in detail. The all-system blocks system has been modelled using MATLAB/Simulink. Figure 5-17, Figure 5-18 and Figure 5-19 demonstrate that the tidal turbines generation algorithm has been successfully implemented.

However, Figure 5-7a indicates that the tidal power generation has some harmonics at PMSG limitations output and some with voltage sag. Then the rectifier has been used to control the frequency and voltage before connecting it to the load. The inverter was predicted to generate harmonic distortions estimated at less than 0.5%. It has been noticed that the tidal generation system has been designed to generate a power estimated around 1.5 MW/1400 VDC. On the contrary, the tidal power system presents the limit to satisfy the load demand, then the utility grid comes in to add the power shortage. It can be observed that if the controller is activated, the voltage ripples of the intermediate circuit decrease and stabilize at the set value.

Finally, the results after simulation show that the operation of the controller does not pose any problem and provides better dynamic and steady-state performance. It has been demonstrated after the simulation and control of the PMSG voltage and current output that the power output still maintains stability, which fulfils the low voltage ride-through (LVRT) requirement. Therefore, the intermediate circuit voltage and the high voltage ripple in the input line currents become unacceptable when the control system is not activated. The 1.2 MW three-level diode clamped inverter contains a nominal voltage of 600 V. It is demonstrated in this work that the Tidal energy system connected to the grid presents a good performance with a low total harmonic distortion around 0.12% for the voltage and 0.07% for the current.

6.2 Future work

Further research will focus on another aspect, as it can be noticed that the tidal generator can be required to be associated with another renewable energy system, for instance, wind power or solar so then the gap of the shortage in power generation can be reduced significantly. At the same time, it will provide ancillary services to the grid (frequency response); the validation of the development of tidal energy management system using a real-time simulator platform; the development of the power system using more advanced technique

REFERENCES

Allagui, M., Hasnaoui, O.B. & Belhadj, J. 2014. A 2MW direct drive wind turbine; Vector control and direct torque control techniques comparison. *Journal of Energy in Southern Africa*, 25(2): 117–126.

Allmark, M. 2017. *Condition Monitoring and Fault Diagnosis of Tidal Stream Turbines Subjected to Rotor Imbalance Faults* .

Amézquita-Brooks, L.A., Licéaga-Castro, J., Licéaga-Castro, E. & Ugalde-Loo, C.E. 2015. Induction Motor Control: Multivariable Analysis and Effective Decentralized Control of Stator Currents for High-Performance Applications. *IEEE Transactions on Industrial Electronics*, 62(11): 6818–6832.

Amor, Y.A. & Kheldoun, A. 2018. ISSN : 2543-3792. , (September).

Angeloudis, A. & Falconer, R.A. 2017. Sensitivity of tidal lagoon and barrage hydrodynamic impacts and energy outputs to operational characteristics. *Renewable Energy*, 114: 337–351. http://dx.doi.org/10.1016/j.renene.2016.08.033.

Angeloudis, A., Falconer, R.A., Bray, S. & Ahmadian, R. 2016. Representation and operation of tidal energy impoundments in a coastal hydrodynamic model. *Renewable Energy*, 99: 1103–1115. http://dx.doi.org/10.1016/j.renene.2016.08.004.

Angeloudis, A., Kramer, S.C. & Avdis, A. 2017. Optimising tidal range power plant operation. : 1–24.

Baker, N.J., Cawthorne, S., Hodge, E. & Spooner, E. 2014. 3D modelling of the generator for openhydro's tidal energy system. *7th IET International Conference on Power Electronics, Machines and Drives, PEMD 2014*: 17–22.

Behera, R.R. & Thakur, A.N. 2016. An overview of various grid synchronization techniques for single-phase grid integration of renewable distributed power generation systems. *International Conference on Electrical, Electronics, and Optimization Techniques, ICEEOT 2016*, (December 2017): 2876–2880.

Benelghali, S., Benbouzid, M., Charpentier, Jean Frédéric, Benelghali, S., Benbouzid, M., Frédéric, J., Marine, C., Current, T., Elghali, S.E. Ben, Member, Student, Benbouzid, M.E.H., Member, Senior & Charpentier, J F. 2010. Technology : State of the Art and Current Status To cite this version : Marine Tidal Current Electric Power Generation Technology : State of the Art and Current Status.

Benelghali, S., Benbouzid, M.E.H. & Charpentier, J.F. 2012. Generator systems for marine current turbine applications: A comparative study. *IEEE Journal of Oceanic Engineering*, 37(3): 554–563.

Benelghali, S., Benbouzid, M.E.H., Charpentier, J.F., Ahmed-Ali, T. & Munteanu, I. 2011. Experimental validation of a marine current turbine simulator: Application sliding mode control. *IEEE Transactions on Industrial Electronics*, 58(1): 118–126.

Benzazah, C., Lazrak, L. & Ait, M. 2022. Design and Performance Analysis of Energy

Conversion Chain , from Multilevel Inverter until the Grid. : 311–314.

Benzazah, C., Lazrak, L. & Lafkih, M.A. 2016. Design and performance analysis of energy conversion chain, from multilevel inverter until the grid. *Proceedings of the International Conference on Microelectronics, ICM*, 2016-March: 311–314.

Biweta, M. & Mamo, M. 2017. Closed loop control strategy of back to back PWM converter fed by PMSG using PLECS toolbox on Matlab/Simulink for wind energy application. *2017 IEEE AFRICON: Science, Technology and Innovation for Africa, AFRICON 2017*: 1313–1318.

Blaabjerg, F. & Ma, K. 2013. Future on power electronics for wind turbine systems. *IEEE Journal of Emerging and Selected Topics in Power Electronics*, 1(3): 139–152.

Borthwick, A.G.L. 2016. Marine Renewable Energy Seascape. *Engineering*, 2(1): 69–78. http://dx.doi.org/10.1016/J.ENG.2016.01.011.

Brezina, T., Hejc, T., Kovar, J. & Huzlik, R. 2011. Modeling and control of three-phase rectifier of Swirl turbine. *Mechatronics: Recent Technological and Scientific Advances*: 285–291.

Brito, R., Carvalho, A. & Gericota, M. 2015. A new three-phase voltage sourced converter laplace model. *Proceedings - 2015 9th International Conference on Compatibility and Power Electronics, CPE 2015*: 160–166.

Caixeta, D.A., Guimarães, G.C. & Chaves, M.L.R. 2014. Modeling of a wind energy conversion system for dynamic analysis using alternative transients program. *Ciencia y Engenharia/ Science and Engineering Journal*, 23(1): 37–45.

Chen, W.B., Liu, W.C. & Hsu, M.H. 2013. Modeling assessment of tidal current energy at Kinmen Island, Taiwan. *Renewable Energy*, 50: 1073–1082. http://dx.doi.org/10.1016/j.renene.2012.08.080.

Chen, Y. & Jin, X.M. 2007. Modeling and control of three-phase voltage source PWM rectifier. *Conference Proceedings - IPEMC 2006: CES/IEEE 5th International Power Electronics and Motion Control Conference*, 3: 1459–1462.

Chica, E., Ṕerez, F., Rubio-Clemente, A. & Agudelo, S. 2015. Design of a hydrokinetic turbine. *WIT Transactions on Ecology and the Environment*, 195: 137–148.

Clarke, J., Connor, G., Grant, A., Johnstone, C. & Ordonez-Sanchez, S. 2010. Analysis of a single point tensioned mooring system for station keeping of a contra-rotating marine current turbine. *IET Renewable Power Generation*, 4(6): 473–487.

Collin, A.J., Nambiar, A.J., Bould, D., Whitby, B., Moonem, M.A., Schenkman, B., Id, S.A., Chainho, P. & Kiprakis, A.E. 2017. Electrical Components for Marine Renewable Energy Arrays : A Techno-Economic Review. : 1–31.

Daborn. 2012. Conference on ocean energy conference programme.

Dong, D., Boroyevich, D., Mattavelli, P. & Cvetkovic, I. 2011. A high-performance single-phase phase-locked-loop with fast line-voltage amplitude tracking. *Conference Proceedings - IEEE Applied Power Electronics Conference and Exposition - APEC*: 1622–1628.

Eddine, S., Elghali, B., Member, Student, Balme, R., Saux, K. Le, El, M., Benbouzid, H., Member, Senior & Charpentier, J.F. 2007. Peer-Reviewed Technical Communication Harnessed by a Marine Current Turbine. *October*, 32(4): 786–797.

Elbaset, A.A., Hassan, M.S. & Ali, H. 2017. Performance analysis of grid-connected PV system. *2016 18th International Middle-East Power Systems Conference, MEPCON 2016 - Proceedings*, (1): 675–682.

Elghali, S.E. Ben, Balme, R., Le Saux, K., El Hachemi Benbouzid, M., Charpentier, J.F. & Hauville, F. 2007. A simulation model for the evaluation of the electrical power potential harnessed by a marine current turbine. *IEEE Journal of Oceanic Engineering*, 32(4): 786–797.

Elzalabani, M., H.Fahmy, F., A. Nafeh, A.E.-S. & Allam, G. 2015. Modelling and Simulation of Tidal Current Turbine with Permanent Magnet Synchronous Generator. *TELKOMNIKA Indonesian Journal of Electrical Engineering*, 13(1).

Elzalabani, M. & Nafeh, A.E.A.E. 2015. Modelling and Simulation of Tidal Current Turbine with Permanent Magnet Synchronous Generator. , (January).

Esmaeilian, H.R., Fadaeinedjad, R. & Moschopoulos, G. 2014. Dynamic operation and control of a stand-alone PEM fuel cell system. *Conference Proceedings - IEEE Applied Power Electronics Conference and Exposition - APEC*, (1): 3378–3384.

European Commission. 2019. RealTide: Advanced monitoring, simulation and control of tidal devices in unsteady, highly turbulent realistic tide environments. *2017*, (727689). https://www.realtide.eu/.

Faudot; & Dahlaung. 2011. Tidal turbine blades: Design and dynamic loads estimation using CFD and blade element momentum theory. *Proceedings of the International Conference on Offshore Mechanics and Arctic Engineering - OMAE*, 5(April 2016): 599–608.

Garcia-rosa, P.B., Bacelli, G. & Ringwood, J. V. 2015. Control-Informed Geometric Optimization of Wave Energy Converters : The Impact of Device Motion and Force Constraints. : 13672–13687.

Ghefiri;, Khaoula;, Bouallègue;, Soufiene;, Haggège;, Joseph, Ghefiri;, Khaoula;, Garrido;, Izaskun & Garrido, A.J. 2017. Modeling and MPPT control of a tidal stream generator. *2017 4th International Conference on Control, Decision and Information Technologies, CoDIT 2017*, 2017-Janua: 1003–1008.

Ghefiri, Khaoula, Bouallègue, S., Garrido, I., Garrido, A.J. & Haggège, J. 2017. Complementary power control for doubly fed induction generator-based tidal stream turbine generation plants. *Energies*, 10(7).

Ghefiri, K., Bouallègue, S. & Haggege, J. 2015. Modeling and SIL simulation of a Tidal Stream device for marine energy conversion. In *2015 6th International Renewable Energy Congress, IREC 2015*.

Ghefiri, K., Bouallègue, S., Haggège, J., Ghefiri, K., Garrido, I. & Garrido, A.J. 2017. Modeling

and MPPT control of a tidal stream generator. In *2017 4th International Conference on Control, Decision and Information Technologies, CoDIT 2017*. 1003–1008.

Goleman, D., Boyatzis, R. & Mckee, A. 2019. *Electrical Design for Tidal Energy Systems Ocean Wave and*.

Grogan, D.M., Leen, S.B., Kennedy, C.R. & Ó Brádaigh, C.M. 2013. Design of composite tidal turbine blades. *Renewable Energy*, 57: 151–162. http://dx.doi.org/10.1016/j.renene.2013.01.021.

Habibi, H., Nohooji, H.R. & Howard, I. 2017. Power maximization of variable-speed variable-pitch wind turbines using passive adaptive neural fault tolerant control. , 12(3): 377–388.

Ben Hamad, K., Luta, D.N. & Raji, A.K. 2021. A Grid-Tied Fuel Cell Multilevel Inverter with Low Harmonic Distortions. *Energies*, 14(3): 688.

Hamad, K. Ben, Taha, M.H., Almaktoof, A. & Kahn, M.T.E. 2019. Modelling and analysis of a grid-connected Megawatt Fuel Cell stack. *Proceedings of the 27th International Conference on the Domestic Use of Energy, DUE 2019*: 147–155.

Hassan, M.S. 2016. Performance Analysis of Grid-Connected PV System. , (1).

Hillis, A.J., Whitlam, C., Brask, A., Chapman, J. & Plummer, A.R. 2020. Power capture gains for the WaveSub submerged WEC using active control.

Hwang, I.S., Lee, Y.H. & Kim, S.J. 2009. Optimization of cycloidal water turbine and the performance improvement by individual blade control. *Applied Energy*, 86(9): 1532–1540. http://dx.doi.org/10.1016/j.apenergy.2008.11.009.

Ikni, D., Camara, M.S., Camara, M.B., Dakyo, B. & Gualous, H. 2014. Permanent magnet synchronous generators for large offshore wind farm connected to grid - comparative study between DC and AC configurations. *International Journal of Renewable Energy Research*, 4(2): 519–527.

Inverter, D.M. & Ramteke, R.G. 2014. Design of third order L-C-L filter for diode-clamped multi-level inverter. : 334–338.

Jahromi, M.J., Maswood, A.I. & Tseng, K.J. 2013. Design and evaluation of a tidal in-stream generator power port. *IEEE Systems Journal*, 7(4): 723–731.

Jayalakshmi, N.S., Gaonkar, D.N. & Kumar, K.S.K. 2012. Dynamic modeling and performance analysis of grid connected PMSG based variable speed wind turbines with simple power conditioning system. *PEDES 2012 - IEEE International Conference on Power Electronics, Drives and Energy Systems*.

Johnson, J.B. & Pride, D.J. 2010. River, Tidal, and Ocean Current Hydrokinetic Energy Technologies: Status and Future Opportunities in Alaska.

Khan, J., Moshref, A. & Bhuyan, G. 2009. A generic outline for dynamic modeling of ocean wave and tidal current energy conversion systems. *2009 IEEE Power and Energy Society General Meeting, PES '09*: 1–6.

Kumar; Shankar; Gauri. 2018. Quasi-oppositional harmony search algorithm based optimal

dynamic load frequency control of a hybrid tidal – diesel power generation system.

Kuschke, M., Pertzsch, S. & Strunz, K. 2012. Modeling of tidal energy conversion systems for primary response testing. In *IEEE Power and Energy Society General Meeting*.

Laws, N.D. & Epps, B.P. 2016. Hydrokinetic energy conversion: Technology, research, and outlook. *Renewable and Sustainable Energy Reviews*, 57: 1245–1259. http://dx.doi.org/10.1016/j.rser.2015.12.189.

Li, W., Zhou, H., Liu, H., Lin, Y. & Xu, Q. 2016. Review on the blade design technologies of tidal current turbine. *Renewable and Sustainable Energy Reviews*, 63: 414–422. http://dx.doi.org/10.1016/j.rser.2016.05.017.

Li, X., Li, M., McLelland, S.J., Jordan, L.B., Simmons, S.M., Amoudry, L.O., Ramirez-Mendoza, R. & Thorne, P.D. 2017. Modelling tidal stream turbines in a three-dimensional wave-current fully coupled oceanographic model. *Renewable Energy*, 114: 297–307. http://dx.doi.org/10.1016/j.renene.2017.02.033.

Lin, J., Lin, B. liang, Sun, J. & Chen, Y. ling. 2016. Modelling hydrodynamic processes in tidal stream energy extraction. *Journal of Hydrodynamics*, 28(6): 1058–1064.

Liu, H., Ma, S., Li, W., Gu, H., Lin, Y. & Sun, X. 2011. A review on the development of tidal current energy in China. *Renewable and Sustainable Energy Reviews*, 15(2): 1141–1146. http://dx.doi.org/10.1016/j.rser.2010.11.042.

Liu, J., Lin, H. & Purimitla, S.R. 2016. Wake field studies of tidal current turbines with different numerical methods. *Ocean Engineering*, 117: 383–397. http://dx.doi.org/10.1016/j.oceaneng.2016.03.061.

Loots, I., Van Dijk, M., Barta, B., Van Vuuren, S.J. & Bhagwan, J.N. 2015. A review of low head hydropower technologies and applications in a South African context. *Renewable and Sustainable Energy Reviews*, 50: 1254–1268.

Lumpkin, R. & Johnson, G.C. 2013. Global ocean surface velocities from drifters: Mean, variance, El Niño-Southern Oscillation response, and seasonal cycle. *Journal of Geophysical Research: Oceans*, 118(6): 2992–3006.

Mahamat, C., Petit, M., Costa, F., Marouani, R. & Mami, A. 2017. Optimized design of an LCL filter for grid connected photovoltaic system and analysis of the impact of neighbors' consumption on the system. *Journal of Electrical Systems*, 13(4): 618–632.

Mahlooji, M.H., Mohammadi, H.R. & Rahimi, M. 2018. A review on modeling and control of grid-connected photovoltaic inverters with LCL filter. *Renewable and Sustainable Energy Reviews*, 81(November 2016): 563–578. http://dx.doi.org/10.1016/j.rser.2017.08.002.

Melikoglu, M. 2018. Current status and future of ocean energy sources: A global review. *Ocean Engineering*, 148(November 2017): 563–573. https://doi.org/10.1016/j.oceaneng.2017.11.045.

Meshram, S., Agnihotri, G. & Gupta, S. 2013. Performance analysis of grid integrated hydro and solar based hybrid systems. *Advances in Power Electronics*, 2013.

Morris, C.E., Doherty, D.M.O., Doherty, T.O. & Mason-jones, A. 2016. Kinetic energy extraction of a tidal stream turbine and its sensitivity to structural stiffness attenuation. *Renewable Energy*, 88: 30–39. http://dx.doi.org/10.1016/j.renene.2015.10.037.

Muljadi, E., Gevorgian, V., Wright, A., Donegan, J., Marnagh, C. & McEntee, J. 2016. Electrical power conversion of river and tidal power generator. *NAPS 2016 - 48th North American Power Symposium, Proceedings*: 1–6.

Nanos, E.M., Kheirallah, N. & Campagnolo, F. 2015. Advanced Issues of Wind Turbine Modelling and Control Advanced Issues of Wind Turbine Modelling and.

Neill, S.P., Angeloudis, A., Robins, P.E., Walkington, I., Ward, S.L., Masters, I., Lewis, M.J., Piano, M., Avdis, A., Piggott, M.D., Aggidis, G., Evans, P., Adcock, T.A.A., Židonis, A., Ahmadian, R. & Falconer, R. 2018. Tidal range energy resource and optimization – Past perspectives and future challenges. *Renewable Energy*, 127: 763–778.

Ngancha, P.B., Kusakana, K. & Markus, E. 2017. Modelling and simulation of a power converter for variable speed hydrokinetic systems. *Proceedings of the 25th Conference on the Domestic Use of Energy, DUE 2017*: 227–232.

Nguyen, T., Yoo, H. & Kim, H. 2015. A Flywheel Energy Storage System Based on a Doubly Fed Induction Machine and Battery for Microgrid Control. : 5074–5089.

Odedele, N., Olmi, C. & Charpentier, J.F. 2014. Power extraction strategy of a robust kW range marine tidal turbine based on permanent magnet synchronous generators and passive rectifiers. *IET Conference Publications*, 2014(CP651): 1–6.

Odgaard, P.F. & Stoustrup, J. 2015. A benchmark evaluation of fault tolerant wind turbine control concepts. *IEEE Transactions on Control Systems Technology*, 23(3): 1221–1228.

Paz, F. 2020. Advanced Monitoring and Control of Distributed DC Systems. , (February).

Pegels, A. 2010. Renewable energy in South Africa: Potentials, barriers and options for support. *Energy Policy*, 38(9): 4945–4954. http://dx.doi.org/10.1016/j.enpol.2010.03.077.

Priya, G.J. 2014. Modelling and Performance Analysis of Grid Connected PMSG Based Wind Turbine. *Ijareeie*, 3(2): 155–165.

Rafiei, M., Salvatore, F. & Capponi, F.G. 2019. Generator Topologies for Horizontal Axis Tidal Turbine. , (May): 21–26.

Ramteke, R.G. & Patil, U. V. 2014. Design of third order L-C-L filter for diode-clamped multi-level inverter. *2014 International Conference on Circuits, Power and Computing Technologies, ICCPCT 2014*: 334–338.

Rassooll, R. 2014. Why are there two CDs. : 14. https://cosmosmagazine.com/geoscience/why-are-there-two-tides-day 31 October 2019.

Reinecke, J. 2013. *Assessment of the Ocean Energy Resources off the South African Coast*.

Reznik, A., Simoes, M.G., Al-Durra, A. & Muyeen, S.M. 2014. LCL Filter design and performance analysis for grid-interconnected systems. *IEEE Transactions on Industry Applications*, 50(2): 1225–1232.

Reznik, A., Simões, M.G., Al-Durra, A. & Muyeen, S.M. 2012. LCL filter design and performance analysis for small wind turbine systems. *PEMWA 2012 - 2012 IEEE Power Electronics and Machines in Wind Applications*: 1–7.

Rourke, F.O., Boyle, F. & Reynolds, A. 2010. Marine current energy devices: Current status and possible future applications in Ireland. *Renewable and Sustainable Energy Reviews*, 14(3): 1026–1036.

Sanjuan, S.L. 2010. *Voltage Oriented Control of Three - Phase Boost PWM Converters Voltage Oriented Control of Three - Phase Boost PWM Converters*.

Schumann, E. 2013a. Oceans and Coasts Resource Valuation Programme An Assessment of the Potential of Ocean Based Renewable Energy to the South African Economy. , (October).

Schumann, E. 2013b. *Oceans and Coasts Resource Valuation Programme An Assessment of the Potential of Ocean Based Renewable Energy to the South African Economy*.

Schumann, E.H., Fiona MacKay, C. & Strydom, N.A. 2019. *Nurdle drifters around South Africa as indicators of ocean structures and dispersion*.

Sen, S., Yenduri, K. & Sensarma, P. 2014. Step-by-step design and control of LCL filter based three phase grid-connected inverter. *Proceedings of the IEEE International Conference on Industrial Technology*: 503–508.

Sousounis, M.C. 2018. Electro-Mechanical Modelling of Tidal Arrays. : 250. http://hdl.handle.net/1842/31089.

Sousounis, M.C. & Shek, J.K.H. 2019. Assessment of pulsating torque mitigation control strategy through tidal turbine emulation. *The Journal of Engineering*, 2019(18): 5059–5063.

Sousounis, M.C. & Shek, J.K.H. 2017. Mitigation of Torque Pulsations in Variable Pitch Tidal Current Turbines Using Speed Control. *Proceedings of the 12th European Wave and Tidal Energy Conference*, (March): 1146-1–9.

Sousounis, Marios C, Shek, J.K.H. & Mueller, M.A. 2016. Filter Design for Cable Overvoltage and Power Loss Minimization in a Tidal Energy System With Onshore Converters. , 7(1): 400–408.

Sousounis, M.C., Shek, J.K.H. & Mueller, M.A. 2016. Modelling, control and frequency domain analysis of a tidal current conversion system with onshore converters. *IET Renewable Power Generation*, 10(2): 158–165.

Sousounis, M.C., Shek, J.K.H. & Mueller, M.A. 2014. Modelling and control of tidal energy conversion systems with long distance converters. *7th IET International Conference on Power Electronics, Machines and Drives, PEMD 2014*.

Sousounis, M.C., Shek, J.K.H. & Sellar, B.G. 2019. The effect of supercapacitors in a tidal current conversion system using a torque pulsation mitigation strategy. *Journal of Energy Storage*, 21(December 2017): 445–459. https://doi.org/10.1016/j.est.2018.11.032.

Tarafdar, S., Abroshan, M., Mirsalim, M. & Member, S. 2013. Permanent Magnet Linear Synchronous Generator for an Oscillating Hydrofoil in a Tidal Current Regime. , (January 2016).

Tarasantisuk, C., Suyata, T., Tarateeraseth, V. & Witheephanich, K. 2016. Active and reactive power control for three-phase grid inverters with proportional resonant control strategies. *2016 13th International Conference on Electrical Engineering/Electronics, Computer, Telecommunications and Information Technology, ECTI-CON 2016*.

Teodorescu, R., Liserre, M. & Rodriguez, P. 2011. *Grid Converters for Photovoltaic and Wind Power Systems Chapter 10 Control of Grid Converters under Grid Faults*.

Tiwari, R. & Babu, N.R. 2016. Recent developments of control strategies for wind energy conversion system. *Renewable and Sustainable Energy Reviews*, 66: 268–285. http://dx.doi.org/10.1016/j.rser.2016.08.005.

Tripura, P. 2019. Power Maximization and Control of PMSG Wind Energy System without Wind Speed Sensors. , (January 2016).

Ugalde-Loo, C.E., Amézquita-Brooks, L.A., Licéaga-Castro, E. & Licéaga-Castro, J. 2014. Analysis and efficient control design for generator-side converters of PMSG-based wind and tidal stream turbines. *Proceedings - 2014 Power Systems Computation Conference, PSCC 2014*.

Wang, R., Wu, Y., He, G., Lv, Y., Du, J. & Li, Y. 2018. Impedance modeling and stability analysis for cascade system of three-phase PWM rectifier and LLC resonant converter. *Energies*, 11(11).

Zanette, J., Imbault, D. & Tourabi, A. 2010. A design methodology for cross flow water turbines. *Renewable Energy*, 35(5): 997–1009. http://dx.doi.org/10.1016/j.renene.2009.09.014.

Zhang, J., Moreau, L., Machmoum, M. & Guillerm, P.-E. 2014. State of the art in tidal current energy extracting technologies. In *2014 1st International Conference on Green Energy, ICGE 2014*. 1–7.

Zhang, Jian, Moreau, L., Machmoum, M. & Guillerm, P.E. 2014. State of the art in tidal current energy extracting technologies. *2014 1st International Conference on Green Energy, ICGE 2014*: 1–7.

Zhou, Z., Scuiller, F., Charpentier, J.F., El Hachemi Benbouzid, M. & Tang, T. 2015. Power Control of a Nonpitchable PMSG-Based Marine Current Turbine at Overrated Current Speed with Flux-Weakening Strategy. *IEEE Journal of Oceanic Engineering*, 40(3): 536–545.